KfK 4896
Oktober 1992

KfK-Analysis of the SUPER-PHENIX-1 Control Rod Experiments Part 2: Rod Worth Calculations

H. Giese
Institut für Neutronenphysik und Reaktortechnik
Projekt Nukleare Sicherheitsforschung

Kernforschungszentrum Karlsruhe

KERNFORSCHUNGSZENTRUM KARLSRUHE

Institut für Neutronenphysik und Reaktortechnik
Projekt Nukleare Sicherheitsforschung

KfK 4896

KfK Analysis of the SUPER-PHENIX-1 Control Rod Experiments
Part 2: Rod Worth Calculations

H. Giese

Kernforschungszentrum Karlsruhe GmbH, Karlsruhe

Kernforschungszentrum Karlsruhe GmbH
Postfach 3640, 7500 Karlsruhe 1

ISSN 0303-4003

KfK Analysis of the SUPER-PHENIX-1 Control Rod Experiments
Part 2: Rod Worth Calculations

Abstract

The present report forms the second part of the documentation covering the KfK analysis of the SUPER-PHENIX-1 (SPX-1) control rod experiments. While the first part described the determination of experimental control rod reactivities from the recorded count rates, the subcriticality of calibration states derived by kinetic methods, and the calculated MSM correction factors, the present report is exclusively devoted to control rod worth calculations.

These calculations started at KfK in 1986 and were performed in close cooperation with Belgonucléaire; later also with GRS (Gesellschaft für Reaktorsicherheit) in Munich. Using standard data and codes, this first analysis campaign led to results that drastically overestimated measured control rod worths with C/E ratios ranging from 1.17 to 1.28. These findings were in sharp contrast to the results of the majority of earlier control rod experiments in zero-power facilities, where C/E ratios were usually comprised between 1.0 and 1.1. Investigations were then launched to identify the origin of this discrepancy. By comparison with the calculation methods employed by the other working groups engaging in the analysis of the SPX-1 experiments it was found that the principal problem arose from the KfK/BN-procedure used for the homogenization of control rod absorber cross sections. The specific failure of this standard procedure in the case of the SPX-1 analysis is ascribed to the extremely heterogeneous structure of the SPX-1 control rods.

In an attempt to improve on this point, a new method for the production of homogenized absorber cross sections was developed and applied to the SPX-1 analysis.

The report concludes with a description of this method and a survey of the results obtained for SPX-1. It is found that this revised analysis leads to a significantly improved agreement of measured and calculated control rod worths and to a better consistency with the results of earlier control rod experiments in zero-power facilities.

Die KfK Auswertung von SUPER-PHENIX-1 Kontrollstabexperimenten
Teil 1: Die experimentellen Resultate

Zusammenfassung

Der vorliegende Bericht repräsentiert den zweiten Teil einer Dokumentation über die KfK-Auswertung der in SUPER-PHENIX-1 (SPX-1) durchgeführten Kontrollstabexperimente. Während im ersten Teil beschrieben wurde, wie die experimentellen Kontrollstabreaktivitäten aus den registrierten Detektorzählraten, den kinetisch ermittelten Unterkritikalitäten von Eichkonfigurationen und den gerechneten MSM-Korrekturfaktoren bestimmt wurden, widmet sich der jetzige Bericht ausschließlich den Nachrechnungen der Reaktivitätswerte.

Diese Nachrechnungen wurden im KfK im Jahre 1986 begonnen und in enger Zusammenarbeit mit Belgonucléaire, später auch mit GRS (Gesellschaft für Reaktorsicherheit) in München durchgeführt. Bei Benutzung von Standarddaten und -Rechenmethoden wurden in dieser Erstauswertung Resultate gefunden, welche die gemessenen Kontrollstab-Reaktivitätswerte drastisch überschätzten, wobei die C/E Werte im Bereich von 1.17 bis 1.28 lagen. Dieses Ergebnis stand in krassem Widerspruch zu den Resultaten von KfK- Auswertungen früherer Kontrollstabexperimente in Nullenergie-Anlagen, bei denen die Mehrzahl der C/E Werte zwischen 1.0 und 1.1 lagen. Detaillierte Untersuchen wurden hieraufhin gestartet, um die Ursache dieser Diskrepanz zu klären. Durch Vergleich mit den von anderen mit der SPX-1 Analyse beschäftigten Arbeitsgruppen verwendeten Rechenverfahren wurde festgestellt, daß das wesentliche Problem in der bei KfK/BN verwendeten Methode zur Homogenisierung von Kontrollstab-Absorberquerschnitten lag. Das spezifische Versagen dieser Standardmethode im Fall der SPX-1 Analyse wird der extrem heterogenen Struktur der SPX-1 Kontrollstäbe zugeschrieben.

Um diesen Schwachpunkt der KfK/BN Analyse zu beseitigen, wurde eine neue Methode zur Produktion homogenisierter Absorberquerschnitte entwickelt und versuchsweise auf die SPX-1 Auswertung angewandt.

Der Bericht schließt mit einer Beschreibung dieser Methode und einer Übersicht der mit den neuen Rechnungen erhaltenen Resultate. Es zeigt sich, daß die nunmehr berechneten Reaktivitätswerte sehr viel besser mit den experimentellen Werten übereinstimmen und somit auch die Konsistenz mit den Resultaten früherer Kontrollstabexperimente in Nullenergie-Anlagen deutlich verbessert wurde.

Table of contents

		Page
I	**Introduction**	**1**
II	**Description of the SUPER-PHENIX-1 core**	**5**
III	**The first phase of the KfK analysis calculations**	**7**
III.1	Historical points	7
III.2	The initial (BN) cross section production	7
III.2.1	Core cells	8
III.2.2	Control rod absorbers	8
III.2.3	Control rod sodium-followers	9
III.2.4	Other components	10
III.3	Cross section condensation	10
III.4	Cross section dilution for 2D calculations	11
III.5	Basic analysis calculations and corrections	12
III.6	Results of the first phase of the KfK analysis	14
III.6.1	Control rod worths in CMP	14
III.6.2	Control rod worths in C1D	18
III.6.3	Core excess reactivity and criticality prediction for CMP and C1D	20
IV	**The second phase of the KfK analysis calculations**	**22**
IV.1	Residual errors in the first cross section production	22
IV.2	Results of the second phase of the KfK analysis	22
IV.2.1	Control rod worths in CMP and C1D	22
IV.2.2	Core excess reactivity and criticality prediction for CMP and C1D	24

V Attempts to explain the aberrant results of the first two analysis campaigns 26

V.1 Comparison with the techniques and results of other groups 26

INTERATOM 26
AEA Great Britain 27
CEA 28

V.2 Supplementary studies on the cross section production for SCP 31

VI The third phase of the KfK analysis calculations 33

VI.1 The novel cross section production for control rod absorbers 33

VI.1.1 The general strategy 33

VI.1.2 The 'Reference' calculations 34

VI.1.3 Homogeneous cross section production 36

VI.1.4 The 'Homogeneous' calculations 37

VI.2 Rod worth predictions obtained with the new absorber cross sections 38

VI.3 Core excess reactivity and criticality prediction for CMP and CID 40

VI.4 Supplementary investigations concerning the reliability of the 'Reference' calculations 41

VII Conclusions 42

Acknowledgements 44

References 45

Appendix 1 : 49

Appendix 2 : 55

Appendix 3 : 65

Appendix 4 : 79

Appendix 5 : 91

Appendix 6 : 97

Figures of the main part of this report 107

List of Figures Page

Figure 1 Core loading of SUPER-PHENIX-1, core version C1D 109

Figure 2 Core loading of SUPER-PHENIX-1, core version CMP 110

Figure 3 Layout of an SCP absorber 111

Figure 4 Schematic construction of a SAC absorber assembly 112

Figure 5 Layout of the SAC absorbers 113

Figure 6 Axial position of the B_4C column of SCP control rods with respect to the fissile loading at 180°C 114

Figure 7 Axial position of the B_4C column of SAC control rods with respect to the fissile loading at 180°C 115

Figure 8 KAPER4 models used for the cross section production for SPX-1 control rod absorbers in the first BN/KfK analysis campaign 116

Figure 9 Axial models used for core and control elements in KfK D3E calculations 117

Figure 10 Cylindricalized models of SPX-1 control rod absorbers as used in IA MONTE CARLO calculations 118

Figure 11 Cylindricalized model of an SCP absorber as used in the AEA analysis 119

Figure 12 Cylindricalized and detailed XY geometry models of SPX-1 control rod absorbers as used in the CEA analysis 120

Figure 13 RΘ models of SCP and SAC as used in the third BN/KfK analysis campaign 121

Figure 14 Refined RΘ models of SAC absorbers 122

I Introduction

The analysis of the SUPER-PHENIX-1 (SPX-1) start-up experiments was performed jointly by an international task force, presided by a task force kernel at the CEN/Cadarache. The different external working groups were located within the AEA, the ENEA, Belgonucléaire (BN), Interatom (IA) and the Kernforschungszentrum/Karlsruhe (KfK).

The focus of the activities at BN and KfK within this task force was placed on the analysis of the control rod experiments, the critical mass prediction and fission rate distributions. Concerning the control rod experiments in particular, the work performed at KfK falls into two categories:

1. The interpretation of subcritical detector count rates allowing the assessment of corrected experimental reactivities for the different control rod arrays established.

2. The prediction of core reactivity levels and of control rod worths using KfK calculation strategies and data.

While the first task, involving mainly the production of correction factors for the modified source multiplication experiments was recently completed / 1 /, the second task forms the subject of the present report.

The history of these KfK calculations is rather complex, since in the course of this work initial errors in data and models were progressively eliminated and finally even the strategy used for control rod cross section production was revised. It is for this reason that in the conferences and meetings held over the entire period of this analysis, distinctly different calculated results were stated by KfK, each one corresponding to the 'state of the art' of that time. As for those readers who are not familiar with the details of the SPX-1 analysis, this 'fluctuation' of the calculated results must be utterly confusing, it was decided to structure the present report in historical order, stating explicitely the various stages of data and model changes and the associated calculated results. For those who are interested only in the latest stage of the KfK analysis, the information given in Sec. VI will suffice.

In a global view, 3 phases can be distinguished in the KfK analysis calculations:

The first phase started towards the end of 1986. At that time, BN had already published a first technical note / 2 / on the SPX-1 analysis, quoting a comparison between measured rod worths and critical mass and the corresponding calculated values obtained when using the synthesis code KASY / 3 /. The cross section preparation of BN was - as usual - based on the 26 energy group adjusted nuclear data library KFKINR001 / 4 /, i.e. on the library, that is also commonly used at KfK for this type of analysis. For reasons of consistency between the BN and KfK analyses it was considered both useful and time saving to simply take over the cross section set already available at BN.

KfK calculations of the first analysis phase thus employed the first BN cross section set without major modifications (only the cross sections for the dummy subassemblies and for the SAC control rods were somewhat improved) and used - again for reasons of consistency - the same geometrical calculation model as BN. In contrast to the BN analysis, however, KfK used the finite difference diffusion code D3E

/ 5 /, while BN had used synthesis diffusion. It was found that the results of the KfK and BN analyses agreed very closely, but that the prediction of control rod worths was unsatisfactory with C/E ratios for bank insertion peaking at 1.20. Accordingly poor was the k_{eff} prediction for the critical core containing approximately half inserted control rods / 6,7 /.

These results were in sharp contrast to the experience made in numerous experiments performed in the critical assemblies SNEAK, ZEBRA and MASURCA. Using the same methods and data, the analysis of control rod experiments in these assemblies had produced C/E ratios in the range of 0.95 to 1.10 / 8,9 /. Selecting the experiments performed in assemblies whose core sizes resembled those of conventional prototype breeders, the C/E ratios covered an even smaller range between 1.00 and 1.10.

The second phase of the analysis started with the discovery of errors both in the first cross section preparation and in the geometrical model used up to then by BN and KfK. Apart from some minor modifications which are largely irrelevant in the present context, these errors concerned the fuel age and the insertion levels of the SCP control rods. Although these errors had already been discovered in the first half of 1987, a revision of the cross section preparation and of the calculation geometry had to await the publication of a CEA note stating officially the updated parameters. This note was available at the beginning of 1988 and BN produced a revised cross section set which was received at KfK mid 1988.

Some of the analysis calculations were then re-run by BN and KfK using the revised cross section set and geometrical model, but apart from a general increase in k_{eff} values of the order of 300 to 350 pcm, due predominantly to the use of a corrected reference date for the $^{241}Pu \rightarrow {}^{241}Am$ decay in the fuel, the results were not significantly improved / 10 /. In particular the prediction of control rod worths was still unsatisfactory.

Since geometrical and compositional data of the reactor components were now considered to be correct, and the treatment of control rod sodium followers was believed to be sufficiently accurate through the use of adequate diffusion coefficients, it was concluded that the principal source of error had to lie in the cross section preparation for the control rod absorbers. This point was further supported by the results of the IA analysis of the SPX-1 control rod experiments. Using the same cross section library as KfK/BN (KFKINR001), MONTE CARLO calculations produced C/E ratios close to unity and thus only somewhat higher than previous transport theory analyses of criticals that had given a corresponding average C/E ratio of 0.94 / 7 /. As global transport effects on SPX-1 control rod worths were found to explain only 5% within the $\simeq$17% difference in C/E ratios (1.00 / 1.20 $\simeq$0.83) when passing from the KfK/BN to the IA analysis, the different treatment of control rod absorbers seemed to be the only possible explanation:

Since the MONTE CARLO code employed by IA allows to use different geometry options within one calculation, the control rod absorbers could be represented as subassemblies with cylindrical internal structures, while the rest of the core was treated in hexagonal geometry. In contrast, the finite difference codes employed by KfK and BN do not allow any representation of absorber substructures in the whole core calculations but demand the use of homogenized cross sections over the full radial extention of the control rod subassemblies. These homogenized cross sections are produced via flux-volume weighting of the individual cross sections of the internal absorber structures. The required neutron fluxes are obtained from an integral transport 'Supercell' calculation in which the absorber is surrounded by a 'core-sea' with 'white' outer boundary condition. The basic difficulty encountered in this context is in that the collision probability code KAPER4 which is used at KfK/BN for

this type of cross section production only permits a 1D representation of the absorbers. The cross section production is therefore not based on the original absorber geometry, but on a simplified cylindrical model leading to the loss of azimuthal details.

Although the INTERATOM calculations too used cylindrical absorber models and thus in principle suffered from the same type of simplification, there were two important differences: (i) IA had used different, and apparently more adequate radial subdivisions in their cylindrical absorber models than the KfK/BN analysis, and (ii) the cylindrical absorbers were directly implanted in the whole core reactor calculation so that the intermediate step of creating averaged absorber cross sections was avoided. Concerning the first point, test calculations run at IA showed that their C/E ratios for the main control system would have been $\simeq$6 % higher, had they used the KfK/BN cylindrical model. Transport effects and differences in absorber modelling thus explained already about 2/3 of the discrepancy between IA and KfK/BN results! The remaining 6% difference were therefore caused by the type of cross section homogenisation employed by BN and KfK.

The production of adequate homogenized absorber cross sections was thus finally identified to be the principal problem of the present analysis. Although in literature more elaborate and reliable methods for the homogenization of cross sections are proposed / 11,12,13,14 / than the one employed up to this point by KfK/BN, they all have certain (partially common) disadvantages: (i) They usually still rely on the correct choice of a 1D cylindrical absorber model and (ii) they all require the use of special calculating modules that are presently not available at BN and KfK. The latter point is also true for the more advanced schemes like pin cluster codes which allow a correct treatment of internal absorber structures in 2D geometry.

For the third phase of the KfK/BN analysis it was therefore decided to tentatively use a novel approximate method for the production of more reliable homogenized control rod absorber cross sections on the basis of readily available calculating modules. This novel approach was still based on flux-volume weighting of the subregion cross sections of a 1D cylinder model of the absorber, but the radial subdivisions and isotopic contents of the different annuli were now adequately adjusted so that a use of the resulting homogenized cross sections in a diffusion theory calculation resembling those used for whole core calculations reproduced the absorber worth found in a detailed transport theory calculation in RΘ geometry. This work started in the first half of 1989 and was carried out in parallel at BN and KfK. While BN concentrated on the cross section improvement for the SCP control rods, KfK in cooperation with the GRS [1] - Munich was in charge of the SAC rods. Using these new cross sections, not only the prediction of control rod worths was drastically improved, giving C/E ratios much closer to unity (and thus consistent with earlier analyses of critical assemblies) but also the prediction of the critical mass and of the power distribution. The results of these latest analysis activities were published in internal notes / 15,16,31 / and at the PHYSOR conference / 17,18 /.

For easier reference, the present report starts off with a description of the SPX-1 core, which was simply taken over from / 1 /.

This is followed by a description of the different analysis phases at KfK in historical order.

---

[1] GRS = Gesellschaft für Reaktorsicherheit

II Description of the SPX-1 core

Cross section views of the fissile loading of the first critical core C1D with minimum excess reactivity and of the fully loaded core CMP are shown in Figures 1 and 2. The reactor comprises a two zone plutonium fuelled conventional core, surrounded axially and radially by uranium blankets and steel reflectors and has a 120° periodicity. At 20°C, the hexagonal element pitch over the flats is 17.9 cm, resulting in an average area per subassembly of 277.4832 cm^2. The nominal core height is 100 cm. As the control rod experiments to which the present analysis refers were performed at the standard handling temperature of 180°C it appears useful to also indicate the dimensions corresponding to this temperature.

With axial and radial linear expansion factors of 1.00114 and 1.00269 / 19 / for the transition from 20°C to 180°C the dimensions at 180°C become:

Pitch:	17.9482 cm
Area per subassembly:	278.9781 cm^2
Core height:	100.1140 cm

The core region comprises 190 inner core subassemblies and 168 outer core subassemblies with corresponding enrichments of about 16 at.% and 19 at.% Pu/Pu+U. Cylindricalised core radii at 180°C are 133.932 cm for the inner zone and 188.468 cm for the outer zone.

The following singularity types are present in the core region:

- 18 diluent assemblies.
- 33 dummy fuel elements present only in the first critical core C1D. These elements were all located in the inner core zone.
- 21 SCP control rods representing the main control system.
  (SCP = 'système de commande principale')
- 3 SAC control rods representing the secondary shut down system.
  (SAC = 'système d'arrêt complementaire')

The internal structure of the SCP and SAC control rod absorbers is presented in Figures 3 to 5.

SCP control rods (Fig.3) comprise an outer hexagonal and an inner cylindrical steel tube, the latter containing a cluster of 31 pins consisting of boroncarbide of 90 at.% ^{10}B enrichment canned in steel. The gaps between this cluster and the surrounding cylindrical steel tube are filled with 8 steel pins of adequate shape. The gaps between all pins and between inner and outer steel tube are filled with sodium.

The length of an SCP absorber from the first to the last boroncarbide pellet is 114.5 cm at 20°C, and expands to 114.63 cm at 180°C.

SAC control rods comprise a train of three individual absorber units running in a hexagonal outer steel tube. These absorber units, the upper two of which are identical, are connected to each other and to the driving mechanism by universal joints. A schematic drawing of the absorber assembly is shown in Figure 4.

The length of the upper and central absorber unit at 20°C is 30 cm, that of the lower unit is 16.8 cm.

The upper and central units contain 4 absorber pins each. At 20°C, the diameter of the boroncarbide pellets over the lower 25 cm of these pins is 4.7 cm. Over the remaining 5 cm at the top of each pin it is 4.5 cm (Figures 4 and 5).
The lower unit contains 8 absorber pins. At 20°C, the diameter of the boroncarbide pellets in these pins is 2.2 cm over the lower 11.8 cm and 2.0 cm over the top 5 cm (Figures 4 and 5).
The corresponding dimensions at 180°C can be derived by using the axial and radial expansion factors quoted above.
As for the SCP control rods, boroncarbide is used as an absorber with a ^{10}B enrichment of 90 at.%.

Figures 6 and 7 show the axial location of the absorber parts of SCP and SAC with respect to the fissile core region when the control rods are said to be fully raised and fully inserted. The dimensions given in Figures 6 and 7 refer to the realistic temperature at the time of the experiments, i.e. 180°C.

When SCP is said to be fully raised (abbreviated as $SCP^{\uparrow}$), its lower end (i.e. the bottom of its lowest boroncarbide pellet) is located 0.2 cm above the upper core/blanket interface, and when the rod is fully inserted ($SCP^{\downarrow}$), the lower end is 1.4 cm below the lower core/blanket interface.
The SCP insertion levels ('Cotes') found in documention have to be interpreted as the distance in [mm] by which the absorber has been raised from full insertion. The indication SCP 542 or SCP^{542} (critical insertion in CMP) therefore means that the lower absorber end is located 52.8 cm above the lower core boundary or that the absorber is inserted into the core by 47.3 cm.

The overall length of a SAC absorber is 97.08 cm (from the first to the last boroncarbide pellet) and thus less than the core height.
When the rod is fully raised ($SAC^{\uparrow}$), the lower end of the absorber is located 6.8 cm above the upper core/blanket interface to avoid excessive burnup during plant operation, and when the rod is fully inserted ($SAC^{\downarrow}$), its lower end is located 1.06 cm above the lower core/blanket interface.

The neutron flux can be monitored by:

- The reactor operation instrumentation consisting of three clusters of under-vessel detectors located in the positions marked GDN (GDN = 'guide des neutrons', see Figures 1 and 2). Each cluster comprises two ^{3}He detectors, two ^{235}U fission chambers and one BF_3 ionisation chamber.

- Three ^{235}U fission chambers of 12 cm length located at 3 axial positions in a central channel of the core centre subassembly. To provide sufficient space for this channel, 19 fissile pins had been removed from this subassembly and replaced by a cylindrical steel tube. The mechanical setup that was inserted into the central channel to hold the chambers at the desired axial position is normally referred to as the 'BOUPHY' (BOUPHY = 'bouchon physique').

  During the majority of the experiments, two chambers 'touched' the core/axial breeder interface from the core side, while the third chamber was centered on the core midplane.

III The first phase of the KfK analysis calculations

III.1 Historical points

In 1986 Belgonucléaire (BN) and KfK agreed to perform the analysis of the SPX-1 neutronics start-up experiments in close cooperation. To avoid unnecessary doubling of work, it had in particular been decided to use the same cross section set and geometrical calculation models, but that concerning the calculations themselves, BN would put the emphasis on the use of the synthesis code KASY and lateron on the coarse mesh code DEGEN, while KfK would employ its standard finite difference code D3E. By mid 1986 BN had completed the production of the cross sections and commenced the analysis calculations. About 6 months later, analysis work on SPX-1 started at KfK and the cross sections and geometrical calculation model could be taken over from BN. The only exception from this parallel use of input data in the BN and KfK calculations formed the cross sections of the so-called 'FAUXCOMB' dummy fuel subassemblies, loaded only in the first critical core C1D, and those for the SAC control rods. The reason for this exception was in that shortly after the completion of the BN cross section production it was discovered that the specification of these two subassembly types in earlier CEA documentation, on which the BN work had been based, was erroneous. A revised production of these cross sections for the KfK analysis seemed therefore useful, although this led to a minor inconsistency between the initial KfK and BN analyses. A description of the models and data used in this cross section revision is given in Appendix 1.

III.2 The initial (BN) cross section production

Since a detailed description of the BN cross section preparation was presented in / 2 /, only a brief review of the main points will be given hereafter.

Both, KfK and BN analyses of the SPX-1 experiments were based on finite difference codes, and thus demanded the production of cell averaged or homogenized nuclear cross sections. In power reactor analysis it is common practice to extend the homogenization over the full radial extension of one subassembly[2] and to use these homogenized cross sections over the axial range of constant cell structure and composition.

Depending on the subassembly/cell type in view, homogenized cross sections for the SPX-1 analysis were produced using the standard cross section processing code for homogeneous cells GRUCAL / 20 / or the 1D collision probability code KAPER4 / 21 / or a combination of the two. The individual procedure chosen will be described in the appropriate context.

All cross section productions were based on the 26 energy group adjusted cross section library KFKINR001 / 4 /.

---

[2] This point is stressed, as in whole core analysis calculations for critical facilities internal structures of subassemblies were occasionally to some extent resolved / 8 /. The lateral homogenization was then not performed over the full radial extension of the subassembly but only over the appropriate internal components. In the analysis of large power reactors such as SPX-1, a resolution of internal subassembly structures is hardly possible as the deterministic codes in use require an extension of the fine mesh grid, basically necessary only for the spatial resolution of the subassembly in view, to the whole reactor, leading to intolerable computer space and time requirements. This undesired high spatial resolution in regions where it is largely irrelevant could only be avoided by application of specially tailored codes.

III.2.1 Core cells

For the inner and outer core fissile subassemblies, the cross section preparation followed a standardized path:

In a first step, the heterogeneous and the homogeneous option of KAPER4 were used alternatively to prepare cell averaged cross sections for a simplified heterogeneous 1D model of the fissile cell and for the equivalent homogeneous cell, respectively. In the heterogeneous cell calculation, a fuel pin was surrounded by 1/271 part of a homogeneous mixture of the pin environment including the subassembly sheath. (There are 271 fissile pins in one subassembly)

The difference between these two sets of cross sections, which is indicative of the degree of cell heterogeneity (in the simplified model used) was then added to homogeneous cross sections produced for the same cell using the code GRUCAL.

In symbolic writing, the heterogeneity corrected, cell averaged cross sections for the core cells were thus obtained from:

$$\Sigma_{het} = \Sigma_{hom}^{GRUCAL} + (\Sigma_{het}^{KAPER} - \Sigma_{hom}^{KAPER}) \qquad (1)$$

The purpose of running through this procedure rather than using the cell averaged cross sections from the heterogeneous KAPER4 run directly in the analysis calculations is in that the f-factor concepts in KAPER4 and GRUCAL are somewhat different. To avoid the risk of inconsistencies between the cross sections prepared for the different cell types, it was once decided to normalize all cross section productions for fissile and fertile cells to the GRUCAL f-factor concept. In those cases where one intends to account for the heterogeneous cell structure and where one is consequently obliged to use KAPER4, this normalization is achieved by employing the procedure described above.

It should be noted that cross sections were prepared only for the average inner and outer core cell compositions and not for the individual isotopic composition of each of the 358 fissile subassemblies which might vary considerably (SPX-1 uses fuel originating from both, light-water and gas-graphite reactors). Due to the adequate choice of the average fissile composition for the cross section preparation, this simplification is known to have relatively little influence on global parameters like the calculated core reactivity. It has the obvious disadvantage, however, that asymmetries e.g. in the power distribution and control rod worths originating from local changes in fissile element composition could not be reproduced by the BN and KfK analysis calculations.

III.2.2 Control rod absorbers

Cross sections for control rod absorbers were produced using the so-called 'Supercell'-mode of KAPER4. It is recalled that the basic idea of the Supercell method is to improve the quality of homogenized cross sections for such non-fissile subassemblies for which simple volume weighting of the subcomponent cross sections is considered inadequate. This is the case, for example, for subassemblies with strongly heterogeneous internal structures that lead to pronounced local flux gradients. The general strategy of such Supercell runs is that the subassembly for which homogenized cross sections are to be produced is modelled in as much detail as possible and is surrounded by an annulus of fissile material with 'white' outer boundary condition - preferably the same material in which the subassembly is located in the reactor. For this arrangement a direct flux calculation is performed and the resulting

neutron fluxes are used to average the subcomponent cross sections by flux/volume weighting.

In the present case the inner core cell was always used for the fissile annulus and its thickness was chosen as 20 cm.

The principal difficulty of this procedure lies in the fact that the degree of detail to which the subassemblies can be modelled in such a Supercell calculation is limited by the number of dimensions available in the code in use. Since the collision probability code KAPER4 employed at BN/KfK only allows to treat onedimensional geometries (as do most other codes of this type), the real geometries of the SPX-1 control rods had to be transformed into adequate cylindrical geometries, and that without -as far as possible - changing the neutronic properties of these subassemblies. In the case of the SPX-1 analysis this task proved particularly difficult because of the complicated radial and axial structures of the control rods.

After a number of exploratory studies it was decided to use the same cylindricalised absorber models as CEA in its pre-experiment calculations / 7,13,23 / :

For the SCP absorbers a 2 zone model was chosen. As shown in Figure 8, the inner zone comprised the absorber pins, the steel filling pins, the interpin sodium and the cylindrical inner steel tube. The outer zone included the sodium located between the cylindrical tube and the hexagonal wrapper and the wrapper itself.

As a sideremark it is noted that IA, AEA and CEA (in their final analysis) used models that differed from the one shown in Figure 8 in as far as the absorbing region covered a smaller area (see also Sec. V.I). It will be seen later that even relatively small variations of this parameter have a substantial influence on calculated rod worths.

For the SAC absorbers the situation was more complicated as they consist of a train of three absorber units, the upper two being identical (Figures 4 and 5). KAPER4 was therefore run separately for each of the two absorber types. Following the results of the preceding investigations, for the upper/central absorber, a 2 zone model was considered sufficient while for the lower absorber a 3 zone model was believed to be more adequate (Figure 8).

Comparing these simplified models used in the first analysis phase with the actual geometries of the SCP and SAC absorbers, it seemed rather obvious that surface to volume ratios of the absorber constituents had not been preserved and that therefore the radial attenuation of the neutron flux obtained with these models would deviate appreciably from the real flux distribution. Apart from other factors which will be discussed later, it was thus the poor quality of the fluxes used for the subcomponent cross section weighting that led to the unsatifactory results of the first KfK analysis phase: see Sec. III.6. Although this 'weakness' of the models was appreciated in an early state of the analysis, they were nevertheless employed to guarantee consistency with the CEA analysis, and thus to simplify the explanation of potential discrepancies in the results obtained by the different groups.

III.2.3 Control rod sodium-followers

A special feature of the Supercell mode of KAPER4 is the production of so-called effective diffusion coefficients for subassemblies with extremely low material density such as control rod sodium followers. This special mode was also used to produce cross sections for the sodium followers of SPX-1. The use of these effective diffusion coefficients in place of the usual values $D = 1/3\Sigma_{tr}$ leads to a substantial improvement in the treatment of axial neutron leakage in subsequent whole core diffusion theory calculations / 23 /.

In this context it seems further worth noting that the diffusion coefficients of the low density regions are modified in such a way that the enhanced axial leakage in the core region surrounding this subassembly is included. In the whole core calculations, standard diffusion coefficients can therefore be used for all fissile subassemblies - even for those in the proximity of control rod positions - without the risk of a faulty axial leakage treatment.

III.2.4 Other components

The Supercell mode of KAPER4 was also used for the following subassembly/cell types (Region Nos. in control rods refer to Figure 9):

- Dummy fuel assemblies
  (present in the first critical core 'C1D', i.e.'coeur de 1ère divergence', only)
- Diluent subassemblies
- Transition zone between SCP absorber and sodium follower (Region No.5)
- Inter-absorber-articulations in the SAC control rods (Region No.11)

For the remaining cell types, simple homogeneous cross sections were prepared using GRUCAL. This was the case for the following subassembly types and components:

- Radial and axial blanket
- Radial and axial shielding
- Neutron guide tubes
  (used to direct neutrons from the core mid-plane to the under-vessel operation instrumentation)
- Top and bottom structural parts of the main control system rods SCP (Region Nos.7,8,9 in Fig.9). Not for the absorber, the absorber/follower transition zone and the sodium follower!
- Top and bottom structural parts of secondary shut down system rods SAC (Region Nos.14,15,16 in Fig.9). Not for the three absorber units, the inter-absorber-articulations and the sodium follower!

III.3 Cross section condensation

The cross sections prepared by BN were available at KfK in 26 energy groups. Since part of the analysis calculations was intented to be run with a reduced number of energy groups, the cross sections were condensed to 4 and 1 energy group(s), respectively, using flux spectra from a 3D calculation of SPX-1 in 26 energy groups with the SCP control rod absorbers half inserted.

III.4 Cross section 'dilution' for 2D calculations

In order to economize on computing costs, a considerable number of calculations of the first analysis phase - notably those that served to assess radial mesh and condensation corrections - were run in 2D geometry. A well-known difficulty encountered with such calculations is in that partial absorber insertion, i.e. the typical operating situation of a reactor cannot be directly represented. In analogy to the first CEA analysis of SPX-1, the first KfK analysis also tentatively tackled this problem by employing so-called 'diluted' absorber cross sections. These diluted absorber cross sections were produced by mixing absorber and sodium-follower cross sections in different proportions. It should be mentioned that this was done only for the SCP absorbers, as the SAC control rods were always either fully raised or fully inserted. A law of equivalence between an actual absorber insertion and the diluted absorber cross sections to be employed to simulate this insertion in a 2D calculation was then established by comparing rod worths obtained from calculations in RZ and in 1D (radial) geometry. The detailed results of the calculations run in this context are found in Appendix 2.

Though very useful at first sight, some clarifying comments concerning the applicability of this equivalence relationship are necessary:

- The relationship does only apply to the complete SCP system and not to partial insertion of smaller rod groups or even of single rods.

- The relationship is to be understood as an appriximate tool only. One of its main weaknesses lies in the fact that although reactivity differences between rod insertions might correctly reproduce values obtained in 3D calculations, this is rarely true for the flux distortions caused by such rod movements. This deficiency becomes very apparent when radial mesh corrections on rod worths (Sec. III.5) are derived by mesh refinement in 2D and in the radial direction of 3D calculations, respectively. CEA calculations / 24 / had shown that these corrections can differ by more than 50%.

- At the end of the first analysis phase it was found that rod worths were substantially overestimated and that this was a consequence of faulty absorber cross sections. Since the same cross sections were used to produce the equivalence relationship, the usefulness of the latter now appeared questionable. In a later phase of the KfK analysis the absorber cross sections were improved, and one could have obviously produced a new set of diluted cross sections and re-established the equivalence model. But in the meantime the calculation strategy had been changed and so this was not considered necessary.

- Nevertheless, the diluted absorber cross sections produced in this first phase of the KfK analysis were extensively used, but without taking reference to the equivalence relationship. This was the case in the analysis of the MSM experiments where numerous 2D calculations were run. In these calculations the diluted cross sections were not chosen according to the equivalence relationship but in such a way that experimental reactivity levels were best reproduced / 1 /.

III.5 Basic analysis calculations and corrections

The standard strategy, widely employed for the prediction of critical mass, control rod worths etc. starts off by running - depending on the objective - one or several so-called 'basic'-calculations in threedimensional geometry. For reasons of computer economy these calculations mostly use diffusion theory, a reduced number of energy groups and a relatively coarse mesh grid. Adequate corrections are then applied to the results found with these basic calculations to obtain the same critical mass or rod-worth prediction as one would have obtained from hypothetical calculations in 3D geometry using 26 energy groups and infinitely small meshes. This 'target' calculation level will in the following be referred to as '26 groups/M∞'. Concerning the application of the corrections, different paths can be chosen, depending on the parameter to be determined and to a certain extent on the preference of the evaluator:

1. If the k_{eff} or the associated reactivity value $\rho = 1 - 1/k_{eff}$ of a given reactor configuration is the parameter of interest, additive corrections will be applied to the result found in the basic calculation. A typical example is found in the core excess reactivity and criticality prediction of Sec. III.6.3.

2. If only reactivity differences rather than individual reactivities levels are of interest, the corrections can be applied directly as relative corrections. A typical example are the control rod worth predictions of Sec. III.6.1. Control rod worths, obtained from the basic calculations as $\Delta\rho = 1/k_{eff,1} - 1/k_{eff,2} = \rho_1 - \rho_2$, with ρ_1 belonging to the state with all absorbers fully raised (all-follower state) and ρ_2 to the absorber configuration of interest, are thus directly corrected without going back to the individual ρ-values.

3. For configurations with inserted control rods, a combination of additive and relative corrections can be applied in place of a pure relative correction.
   In a first step, an additive correction is determined for the situation in which all control rod absorbers are fully raised. This first correction is thus core inherent.
   In a second step, a relative correction is applied to the control rod worth obtained from the basic calculations. The absolute difference between the corrected and uncorrected rod worth is then added to the 'core-inherent' correction and the sum of the two is used to correct the k_{eff} or ρ value of the basic calculation. The additive correction is thus synthesized from two components which are considered to be independent of oneanother.

In the first phase of the KfK analysis the majority of the basic calculations used the standard threedimensional diffusion theory code D3E / 5 / in 26 energy groups and with a radial mesh M2, i.e. 19 points per subassembly, corresponding to an average of 12 points in an infinitely extended grid. Axial meshes ranged from about 2 to 13 cm. A survey of how the different types of subassemblies were represented in the basic calculation and of the location of axial meshes is presented in Figure 9:

A fissile subassembly consists simply of a central fissile zone containing the homogenized cross sections of either the inner or outer core cell, and is surrounded axially by regions containing the cross sections of the upper and lower axial breeder and reflector.

For SCP control rods, Figure 9 shows the representation of four different states of insertion: 'Fully raised' ($SCP^{\uparrow}$), critical insertion for the first critical core C1D (SCP^{929}), critical insertion for the fully loaded core CMP (SCP^{542}), and 'fully inserted' ($SCP^{\downarrow}$).

For SAC rods only the states 'fully raised' ($SAC^{\uparrow}$) and 'fully inserted' ($SAC^{\downarrow}$) are shown, as only those were of interest in the context of the start-up experiments.

To cut down on the number of axial meshes, two simplifications were introduced, concerning the SCP insertion levels $SCP^{\uparrow}$ and $SCP^{\downarrow}$. As can be seen in Figure 9, the calculations assumed that for these two cases the lower end of the SCP- absorber is exactly level with either the upper or the lower core/breeder interface. In reality, the absorber was in the first case located 0.2 cm above, and in the second case 1.4 cm below the core/breeder interface. In the context of the present investigations these small deviations can be considered irrelevant.

Radial breeder and reflector subassemblies were not shown in Figure 9, as their axial loading is simply deduced from that of the core subassembly by replacing either only the fissile loading by the axial breeder cell or by replacing both, fissile and axial breeder loading by axial reflector.

Diluent, dummy fuel and neutron guide tube subassemblies are represented by a uniform loading over the entire reactor height.

While for those control rod configurations that did not affect the intrinsic $2\pi/3$ periodicity of the core, these basic calculations could be restricted to a 120° sector of the reactor, the investigation of isolated control rods demanded a full core representation.[3] As in such cases computing costs for '26 group/mesh M2' calculations on the then used M7890 processor would have been prohibitive, the basic calculations were run in 4 energy groups with a radial mesh M1, i.e. 7 points per subassembly, corresponding to an average of 3 points per subassembly in an infinitely extended grid.

Depending on the type of basic calculation used, therefore either only mesh corrections ('CM') or both mesh and condensation corrections ('CC') had to be applied. While condensation corrections were simply determined by comparing the results of corresponding calculations in 4 and 26 energy groups, mesh corrections demanded as a first step an extrapolation of the k_{eff} values found with M1 and M2 mesh grid to an infinitely fine mesh grid M∞. Since in mesh-edged codes like D3E the k_{eff} value varies linearly with the square of the average point distance / 37 /, this extrapolation can be easily made by using the relationship:

$$k_{eff}^{M\infty} = \frac{4k_{eff}^{M2} - k_{eff}^{M1}}{3} \qquad (1)$$

The mesh corrections were then determined by comparing the extrapolated result for mesh M∞ with the results found for mesh M1 or mesh M2.

Finally it should be mentioned that for reasons of computing economy, condensation and mesh corrections were on some occasions assessed separately for the radial and axial direction and simply summed up to give the corresponding total correction. Experience has shown that errors introduced by this assumption of the separability of radial and axial contributions are small.

Details on which of the different correction strategies were used in a particular case and on these corrections were derived will be found in the appropriate sections.

---

[3] In reality the 120° periodicity of the core is violated by the presence of a neutron guide tube 'GDN' in reactor position 37/17. (Figs. 1&2) Located in the first radial blanket row, the influence of these positions on core reactivity is small. To allow calculations to be run for a 120° sector of the core one simply assumed this 'GDN' to be located in a position symmetrical to those of the other two 'GDN', i.e. in reactor position 36/17.

III.6 Results of the first phase of the KfK analysis

III.6.1 Control rod worths in CMP

The discussion starts with the results obtained for the fully loaded power core 'CMP', to which most of the analysis work had been devoted.

The results of the basic control rod worth calculations performed in the first analysis campaign are listed in Tables 1 and 2.

Configuration	3D Diffusion 26 energy groups, M2		3D Diffusion 4 energy groups, M2	
	k_{eff}	$\rho[pcm]$	k_{eff}	$\rho[pcm]$
$SCP^{\uparrow}$ $SAC^{\uparrow}$	1.04001	+3847.1	1.04116	+3953.3
$SCP^{\uparrow}$ $SAC^{\downarrow}$	1.02759	+2684.9	1.02833	+2755.0
SCP^{540} $SAC^{\uparrow}$	0.99168	-839.0	0.99162	-845.1
SCP^{540} $SAC^{\downarrow}$	0.97930	-2113.8	0.97898	-2147.1
$SCP^{\downarrow}$ $SAC^{\uparrow}$	0.94144	-6220.3	0.94002	-6380.7
$SCP^{\downarrow}$ $SAC^{\downarrow}$	0.92902	-7640.3	0.92748	-7819.0
SCP^{520} $SAC^{\uparrow}$			0.98847	-1166.4
$SCP^{625.6}$ $SAC^{\uparrow}$	0.99203	-803.4	0.99195	-811.5

Table 1. **First KfK analysis of CMP:** The superscripts '↑' and '↓' signify a fully raised and a fully inserted rod, respectively. The meaning of intermediate SCP insertion levels like '540' had been explained in Sec. II.

Configuration	3D Diffusion 26 energy groups, M1		3D Diffusion 4 energy groups, M1	
	k_{eff}	$\rho[pcm]$	k_{eff}	$\rho[pcm]$
$SCP^{\uparrow}$ $SAC^{\uparrow}$			1.03966	+3814.7
SCP^{540} $SAC^{\uparrow}$			0.98742	-1274.0
SCP^{520} $SAC^{\uparrow}$			0.98405	-1620.9
SCP^{520} $B4^{\uparrow}$ $SAC^{\uparrow}$			0.98825	-1189.0
SCP^{520} $B4^{\downarrow}$ $SAC^{\uparrow}$			0.98144	-1891.1

Table 2. **First KfK analysis of CMP.**

For configurations with $2\pi/3$ periodicity basic calculations were run both in 26 and in 4 energy groups (Table 1). Although those run in 26 groups would have obviously sufficed for the intended rod worth predictions, 4 group calculations were added to

get some information on the condensation corrections to be applied to the results of the 4 group calculations for the non-periodic configurations found in the last two lines of Table 2.

Furthermore, the 4 group calculations in Table 1 offered the possibility to compare condensation corrections obtained from 3D calculations with those that were tentatively synthesized from 2D centre plane and a combination of RZ and 1D (radial) calculations. The motivation for these side-studies arose with the intention to economize on computing expenses by running future basic calculations in few energy groups. The conclusion drawn from these studies, the detailed results of which are given in Appendix 3, was that for the relatively small number of configurations investigated here, condensation corrections could be reliably synthesized from simpler calculations in 1D and 2D geometry with an accuracy of better than 1% on rod worth. It should be added, however, that in the course of the KfK analysis little practical use was made of this possibility as later calculations followed a different strategy. (see Sec. IV and VI)

Configuration	**Calculated rod worths relative to $SCP^{\uparrow}$ $SAC^{\uparrow}$ $\Delta\rho^{calc.}[pcm]$**		**CC [%]**	**Resulting calculated SAC worth $\Delta\rho^{calc.}_{SAC}[pcm]$**		**CC [%]**
	26 groups	4 groups		26 gr.	4 gr.	
$SCP^{\uparrow}$ $SAC^{\uparrow}$	0	0		1162.2	1198.3	-3.01
$SCP^{\uparrow}$ $SAC^{\downarrow}$	-1162.2	-1198.3	-3.01			
SCP^{540} $SAC^{\uparrow}$	-4686.1	-4798.4	-2.34	1274.8	1302.0	-2.09
SCP^{540} $SAC^{\downarrow}$	-5960.9	-6100.4	-2.29			
$SCP^{\downarrow}$ $SAC^{\uparrow}$	-10067.4	-10334.0	-2.58	1420.0	1438.3	-1.27
$SCP^{\downarrow}$ $SAC^{\downarrow}$	-11487.4	-11772.3	-2.42			
SCP^{520} $SAC^{\uparrow}$		-5119.7				
$SCP^{625.6}$ $SAC^{\uparrow}$	-4650.5	-4764.8	-2.40			

Table 3. First KfK analysis of CMP. 3D calculations, radial mesh M2

Configuration	**Calculated rod worths relative to $SCP^{\uparrow}$ $SAC^{\uparrow}$ $\Delta\rho^{calc.}[pcm]$**		**CC [%]**	**Resulting calculated B4 worth $\Delta\rho^{calc.}_{B4}[pcm]$**	
	26 groups	4 groups		26 gr.	4 gr.
$SCP^{\uparrow}$ $SAC^{\uparrow}$		0			
SCP^{540} $SAC^{\uparrow}$		-5088.7			
SCP^{520} $SAC^{\uparrow}$		-5435.6			
SCP^{520} $B4^{\uparrow}$ $SAC^{\uparrow}$		-5003.7			702.1
SCP^{520} $B4^{\downarrow}$ $SAC^{\uparrow}$		-5705.8			

Table 4. First KfK analysis of CMP. 3D calculations, radial mesh M1

Tables 3 and 4 present control rod worths $\Delta\rho^{calc.}$ in pcm, i.e. units of $10^{-5}\Delta(1/k)$, and condensation corrections derived from the results of the basic calculations in Tables 1 and 2. In a first step so-called direct control rod worths are always taken relative to the 'clean' situation with all control rods fully raised, i.e. $SCP^{\uparrow}\,SAC^{\uparrow}$. In the present context fully raised means that the lower end of the absorbing portions of the control rods is level with the upper core/axial breeder interface.

In a second step, the worths of single rods or certain rod groups like SAC are then extracted as the difference between the appropriate direct worths. Condensation corrections for direct rod worths are of the order of 2 to 3%, those on SAC worths vary between 1 and 3%.

Table 4 gives the direct rod worths for 4 group M1 calculations and the resulting worth of the single rod B4.

Based on Tables 3 and 4, the final rod worth predictions corresponding to a calculation level '26 groups/mesh M∞' were produced in the following way:

For predictions based on Table 3, only mesh corrections were necessary to perform the transition M2→M∞. Following past experience these corrections can be derived separately for the radial and axial direction and simply added up to give the total correction.

- Radial mesh corrections were obtained from the same series of 2D diffusion theory calculations of the SPX-1 centerplane that served for the investigation of condensation corrections, the results of which are discussed in Appendix 3. It was found that for the investigated configurations, the M2→M∞ corrections were all comprised between -1 and -3%. Considering the small range of dispersion of the corrections and with the relatively poor results of the first analysis campaign already in view, it was not considered worth the effort to apply configuration dependent mesh corrections. For simplicity, a global radial mesh correction of -2% was therefore used for all control rod groups.

- Axial mesh corrections were not explicitely calculated at KfK, since corresponding investigations had already been made at BN / 2 /. There it was found that with the relatively fine axial meshes used in the basic calculations, these corrections were very small ($\simeq$-0.3%). It was therefore decided to simply neglect the axial mesh corrections and only apply the above mentioned radial mesh correction of -2%.

More complicated was the situation for the prediction of the worth of B4, based on the '4 group/mesh M1' results of Table 4.

- Condensation corrections: Table 3 had shown that for the transition from configuration $SCP^{540}\,SAC^{\uparrow}$ to $SCP^{625.6}\,SAC^{\uparrow}$ the condensation correction changed very little from 2.34 to 2.40%. It was therefore assumed that the correction found for $SCP^{540}\,SAC^{\uparrow}$ could also be used with sufficient confidence for the two arrays with B4 fully raised and fully inserted, respectively.

- Mesh corrections were tentatively derived in two independent ways.

  1. In Table A3.13 of Appendix 3 we find radial mesh corrections for the transition M1→M∞ of -5.37 and -5.67% when B4 is raised and of -5.95 and 6.24% when B4 is fully inserted. Two values are given for each case, since the 2D calculations were run for 2 different SCP absorber dilutions approximating the real SCP insertion level '520' from the higher and from the lower side of the reactivity scale. (see also Sec. III.4 for details)

2. Alternatively the cross sections were condensed to 1 energy group using the same flux spectra as for the 4 group condensation. 3D diffusion theory calculations in mesh M1 and M2 were then run for the configurations in question and gave mesh corrections for the transition M1→M∞ of -5.50 and -6.09%. These values compare very well with the results of the 2D calculations if these are linearly interpolated for the correct SCP level '520': -5.54 and -6.11% ! The corrections that were finally used for the analysis were those found with the 3D 1 group calculations.

The final worth prediction of B4 was thus established on the basis of the $\Delta\rho^{calc.}$ values of Table 4 relative to $SCP^{\uparrow}$ $SAC^{\uparrow}$ and the following corrections:

SCP^{520} $B4^{\uparrow}$: $\Delta\rho$ = -5003.7pcm CC = -2.34% CM = -5.50% → $\rho^{corr.}$ = -4617.8pcm

SCP^{520} $B4^{\downarrow}$: $\Delta\rho$ = -5705.8pcm CC = -2.34% CM = -6.09% → $\rho^{corr.}$ = -5232.9pcm

The reactivity difference between these two configurations which represents the worth of B4 is found as 615.1 pcm. Had one used the mesh corrections from the 2D calculations interpolated for SCP^{520} the predicted worth of B4 would have been 615.9 pcm.

A comparison between the predicted rod worths of various SCP and SAC insertions as obtained in the first analysis campaign with the corresponding measured worths from / 1 / is given in Table 5.

Control rod group	Insertion state of the remaining rods	Rod worths [pcm]		C/E
		$\Delta\rho^{calc.}$	$\Delta\rho^{meas..}$	
$SCP^{\uparrow\rightarrow 540}$	$SAC^{\uparrow}$	4592.4	3732.0	1.231
$SCP^{540\rightarrow\downarrow}$	$SAC^{\uparrow}$	5273.7	4381.0	1.204
$SCP^{\uparrow\rightarrow\downarrow}$	$SAC^{\uparrow}$	9866.0	8113.0	1.216
$SCP^{\uparrow\rightarrow 625.6}$ $SAC^{\uparrow\rightarrow\downarrow}$	-	4557.5	3732.0	1.221
$SAC^{\uparrow\rightarrow\downarrow}$	SCP^{540}	1249.3	1039.0	1.202
$SAC^{\uparrow\rightarrow\downarrow}$	$SCP^{\downarrow}$	1391.6	1191.0	1.168
$SCP^{540\rightarrow\downarrow}$ $SAC^{\uparrow\rightarrow\downarrow}$	-	6665.3	5572.6	1.196
$SCP^{\uparrow\rightarrow\downarrow}$ $SAC^{\uparrow\rightarrow\downarrow}$	-	11257.6	9304.0	1.210
$B4^{\uparrow\rightarrow\downarrow}$	SCP^{520} $SAC^{\uparrow}$	615.1	478.5	1.285

Table 5. **First KfK analysis of CMP. 3D Diffusion, 26 groups, M∞:** Comparison of calculated and measured rod worths. With the exception of the individual rod B4, calculated rod worths quoted here were obtained from those given in Table 3 by applying a global mesh correction of -2%. Other than in / 7 / where the measured worth of B4 was assumed to be identical to that of its homologeous rod B2 (488.1pcm), the present table uses the correct worth of B4 based on / 1 /.

A horizontal arrow '→', as e.g. in $SCP^{\uparrow\rightarrow 540}$, symbolizes a transition from one insertion state to another.

One observes that for bankwise insertions of SCP and SAC, rod worths were significantly overpredicted between 17 and 22% and that this misprediction was even aggravated in the case of the individual rod B4. The latter result was comprehensible in as far as the worth of B4 was known to depend strongly on the insertion state and on the worth of the remaining SCP rods. Parametric studies using 2D calculations, the detailed results of which are given in Appendix 4, have indicated that if one had predicted the worth of the remaining SCP rods properly, the overprediction of the B4 worth would have been similar to those of the other configurations of Table 5. The extremely high C/E ratio of B4 is thus the consequence of a superposition of two effects: the overprediction of the reactivity worth of B4 itself and the overprediction of the worth of the remaining SCP rods enhancing the worth of B4.

In conclusion one could state that these results were in sharp contrast to the experience made in critical assemblies, where for core sizes close to those of prototype breeders, control rod C/E ratios ranged from 1.00 to 1.10 / 8 /. Before investigations were launched to identify the origin of this discrepancy, it seemed interesting to run some calculations for the first critical core 'C1D'. The particular purpose of this campaign was to see whether rod worths would be similarly overpredicted as for the fully loaded core 'CMP' or whether the more complicated loading of the first critical core including 33 dummy subassemblies in the inner core zone would further deteriorate the results.

For completeness it should be mentioned that BN obtained very similar results with the use of KASY synthesis calculations. This also applies to the rod worth predictions for the the first critical core and to the predictions of core excess reactivity and criticality described hereafter.

III.6.2 Control rod worths in C1D

The sequence of calculations corresponded exactly to that employed in the CMP analysis so that no further comments are necessary on this subject.

Table 6 quotes the results of the basic calculations (3D diffusion, 26 energy groups, mesh M2), Table 7 the resulting direct and SAC rod worths and Table 8 compares the corrected calculated rod worths with the corresponding measured results.

Configuration	3D Diffusion 26 energy groups, M2		3D Diffusion 4 energy groups, M2	
	k_{eff}	$\rho[pcm]$	k_{eff}	$\rho[pcm]$
$SCP^{\uparrow}$ $SAC^{\uparrow}$	1.00196	+195.9	1.00234	+233.5
$SCP^{\uparrow}$ $SAC^{\downarrow}$	0.99080	-928.0		
SCP^{929} $SAC^{\uparrow}$	0.99794	-206.2	0.99824	-176.4
SCP^{929} $SAC^{\downarrow}$	0.98699	-1317.9	0.98691	-1326.2
SCP^{600} $SAC^{\uparrow}$	0.96307	-3834.6		
SCP^{600} $SAC^{\downarrow}$	0.95340	-4887.8		
$SCP^{\downarrow}$ $SAC^{\uparrow}$	0.90702	-10251.3	0.90537	-10452.4
$SCP^{\downarrow}$ $SAC^{\downarrow}$	0.90081	-11011.5	0.89925	-11204.4

Table 6. First KfK analysis of C1D / Results of basic calculations.

Configuration	Calculated rod worths relative to $SCP^{\uparrow}$ $SAC^{\uparrow}$ $\Delta\rho^{calc.}[pcm]$		CC [%]	Resulting calculated SAC worth $\Delta\rho^{calc.}_{SAC}[pcm]$		CC [%]
	26 groups	4 groups		26 gr.	4 gr.	
$SCP^{\uparrow}$ $SAC^{\uparrow}$	0	0		1123.9		
$SCP^{\uparrow}$ $SAC^{\downarrow}$	-1123.9					
SCP^{929} $SAC^{\uparrow}$	-402.1	-409.9	-1.90	1111.7	1149.8	-3.31
SCP^{929} $SAC^{\downarrow}$	-1513.8	-1559.7	-2.94			
SCP^{600} $SAC^{\uparrow}$	-4030.5			1053.2		
SCP^{600} $SAC^{\downarrow}$	-5083.7					
$SCP^{\downarrow}$ $SAC^{\uparrow}$	-10447.2	-10685.9	-2.23	760.2	752.0	+1.09
$SCP^{\downarrow}$ $SAC^{\downarrow}$	-11207.4	-11437.9	-2.02			

Table 7. **First KfK analysis of C1D / Rod worths 3D, mesh M2.**

Control rod group	Insertion state of the remaining rods	Rod worths [pcm]		C/E
		$\Delta\rho^{calc.}$	$\Delta\rho^{meas.}$	
$SCP^{\uparrow\rightarrow 929}$	$SAC^{\uparrow}$	394.0	321.8	1.224
$SCP^{929\rightarrow\downarrow}$	$SAC^{\uparrow}$	9844.2	7747.0	1.271
$SCP^{\uparrow\rightarrow\downarrow}$	$SAC^{\uparrow}$	10238.3	8068.8	1.269
$SAC^{\uparrow\rightarrow\downarrow}$	SCP^{929}	1089.4	895.0	1.217
$SAC^{\uparrow\rightarrow\downarrow}$	$SCP^{\downarrow}$	745.0	705.0	1.057
$SCP^{929\rightarrow\downarrow}$ $SAC^{\uparrow\rightarrow\downarrow}$	-	10589.2	8452.0	1.253
$SCP^{\uparrow\rightarrow\downarrow}$ $SAC^{\uparrow\rightarrow\downarrow}$	-	10983.3	8773.8	1.252

Table 8. **First KfK analysis of C1D. 3D calculations, extrapolated to M_{∞}:** Comparison of calculated and measured rod worths. Calculated rod worths quoted here were obtained from those given in Table 7 by applying a global mesh correction 'CM' of -2%.

One finds that the overprediction is even more pronounced than in CMP. Inconsistent with this general trend seems the surprisingly good prediction of the SAC worth with SCP fully inserted. It is believed, however, that this result was fortuitous. This scepticism is based on the fact that severe difficulties had been encountered in the interpretation of the subcritical count rates recorded for configurations $SCP^{\downarrow}$ $SAC^{\uparrow}$ and $SCP^{\downarrow}$ $SAC^{\downarrow}$. As a consequence of these difficulties, the experimental uncertainties quoted in the related CEA documents was significantly greater than those quoted for other configurations and in particular greater than for the corresponding experiments in CMP. These increased uncertainties led to a cumulative uncertainty for the SAC worth of $\pm$17.3%. The corresponding value in the CMP analysis was $\pm$8.2% / 1 /. The low C/E ratio for SAC with SCP fully inserted is therefore affected by a very large uncertainty!

III.6.3 Core excess reactivity and criticality prediction for CMP and C1D

In the light of the results discussed above, it seemed also interesting to look at k_{eff} predictions for the core loading versions CMP and C1D and to quantify the deteriorating influence of the poor rod worth predictions on this parameter.

From earlier studies / 25 / the expected (C-E) bias for an unperturbed core with a clean (SNEAK - type) plutonium vector and when using calculations in diffusion theory, 26 energy groups and a mesh size of about 2.65 cm was $+70\pm320$ pcm.

As the isotopic contents of ^{240}Pu and ^{241}Pu is significantly higher in SPX-1 than in SNEAK-fuel on which the (C-E) prediction was based, a correction of $+300\pm200$ pcm was found necessary to be added to the initial bias giving a final expected (C-E) value for SPX-1 of $+370\pm520$ pcm.

Selected for the present investigations were two configurations:

1. All SCP and SAC control rods fully raised ($SCP^{\uparrow}\ SAC^{\uparrow}$), where the control rod absorbers are located in the upper axial blanket and thus have relatively little influence on k_{eff}.

2. The experimentally critical situations $SCP^{929}\ SAC^{\uparrow}$ in C1D and $SCP^{540}\ SAC^{\uparrow}$ in CMP.

The choice of these two configurations allows to distiguish (at least to some good approximation) between error contributions arising from faulty control rod cross sections and those originating from the rest of the core.

The results of these investigations are given in Tables 9 and 10.

While the basic calculations were identical to those used in the control rod worth predictions (3D diffusion, 26 groups, radial mesh M2, cf. Tables 1 and 6), mesh corrections had to be derived differently as now they had to be applied directly to the ρ-value of a given configuration rather than to $\Delta\rho$-values as in rod worth predictions (see Sec. III.5).

Radial mesh corrections were obtained from 2D centreplane calculations in 26 energy groups, as demonstrated in Table A3.2 of Appendix 3.

Axial mesh corrections were taken over from the BN analysis. They had been deduced from KASY synthesis calculations run alternatively with an axial mesh of 10 and of 5 cm.

The reason for which the column 'Aging correction' was left void in Tables 9 and 10 is the following:

This column should normally state a correction taking into account the decay of ^{241}Pu into ^{241}Am in the reactor fuel between the reference date for which the cross section preparation had been performed and the date of the experiment. In the first analysis no such correction was applied as at that time there was some uncertainty concerning the fuel age quoted in CEA documentation. It was therefore preferred to leave this point open, and to take the results quoted in Tables 9 and 10 as a more general first information. In the second analysis phase this point was clarified and a correct aging correction was included.

To avoid confusion, it should be mentioned that the 'Final $\rho^{calc.}$' values quoted here differ somewhat from those published in / 6 / which also referrred to the first analysis. The reason for these differences is in that on one hand the basic calculations used for publication / 6 / were not yet fully converged and that on the other hand some very minor errors of the order of a few pcm were a-posteriori discovered in the mesh corrections. In the present tables, both errors were corrected.

Conf.	Basic Calc.	Corrections [pcm]			Final $\rho^{calc.}$	$\rho^{meas.}$	C-E
	3D Diff 26gr M2	CM^{rad}	CM^{ax}	Aging			
	ρ^{basic}[pcm]				[pcm]	[pcm]	[pcm]
$SCP^{\uparrow}$ $SAC^{\uparrow}$	+3847.1	+26	+35	-	+3908	+3732	+176
SCP^{540} $SAC^{\uparrow}$	-839.0	+94	+56	-	-689	0	-689

Table 9. **First KfK analysis of CMP:** Reactivity predictions for the core with all rods fully raised and for the critical core and comparison with the associated measured reactivities
Radial mesh size corrections for the transition from M2 to M_∞ were taken from 2D calculations, axial corrections from BN KASY calculations

Conf.	Basic Calc.	Corrections [pcm]			Final $\rho^{calc.}$	$\rho^{meas.}$	C-E
	3D Diff 26gr M2	CM^{rad}	CM^{ax}	Aging			
	ρ^{basic}[pcm]				[pcm]	[pcm]	[pcm]
$SCP^{\uparrow}$ $SAC^{\uparrow}$	+195.9	+52	+35	-	+283	+321	-38
SCP^{929} $SAC^{\uparrow}$	-206.2	+52	+37	-	-117	0	-117

Table 10. **First KfK analysis of C1D.:** Reactivity predictions for the core with all rods fully raised and for the critical core

Comparing the (C-E) values of Tables 9 and 10 with the expected value of +370±520 pcm one observes that:

1. The best prediction is found for the excess reactivity of the CMP core with all rods fully raised. The calculated value of +176 pcm is well within the error bars of the predicted bias of +370 pcm.

2. As could be anticipated, the k_{eff}-value of the critical CMP core with approximately half inserted SCP rods is largely underpredicted as a consequence of rod worth overestimation.

3. In the first critical core, even the core excess reactivity with all rods fully raised is poorly predicted. As the core loading of C1D differs from that of CMP only by the presence of 33 dummies in the place of fuel subassemblies, the (C-E) error must be attributed to these dummy elements. Since the composition data of the so-called FAUXCOMB dummy elements are believed to be correct, the source of error is suspected to lie either in faulty cross section data for iron in the KFKINR001 cross section data library or in the KAPER4 supercell run used to produce cell averaged cross sections or is a combination of the two. To date this problem has still not been solved.

4. In the critical core of C1D the misprediction of (C-E) appears to be less dramatic than in CMP :-117 pcm vs. -689 pcm. This is obviously misleading as the SCP

reactivity inserted to achieve criticality was much smaller than in CMP: -321 pcm vs. -3732 pcm. In reality the (C-E) shift of 79 pcm (-38 to -117 pcm) for an inserted SCP reactivity of -321 pcm reflects an even poorer rod worth prediction than in CMP, which was already seen in Table 8.

IV The second phase of the KfK analysis calculations

IV.1 Residual errors in the first cross section production

Apart from the faulty specifications of the 'FAUXCOMB' and SAC absorber subassemblies in earlier CEA documentation that had already been corrected before the KfK calculations commenced (Appendix 1), two more errors were eliminated in the course of the second analysis phase.

1. BN repeated the cross section production for the fissile cells, now referring to an agreed reference date, the 01/09/1985, and issued a new complete set of cross sections for the SPX-1 analysis. This new set also included a revision of the cross sections for the 'FAUXCOMB' and SAC subassemblies.

2. Part of the SCP insertion levels used in the first analysis campaign were erroneous:

   a. The critical insertion level of SCP in the CMP loading was initially assumed to be '540' (see Tables 1 through 9) instead of the correct value '542' which was used from here onwards.

   b. When SCP was completely inserted, its lower absorber end was initially assumed to be located 17 mm below the lower core blanket interface. This value was now revised to 14 ± 9 mm.

IV.2 Results of the second phase of the KfK analysis

In the second phase of the analysis, only a relatively small number of calculations was run to test the influence of the latest cross section and geometry revisions.

IV.2.1 Control rod worths in CMP and C1D

As major changes in rod worth predictions were not to be expected, rod worth calculations were now run only in 4 energy groups. k_{eff} and corresponding ρ values of the basic calculations (3D diffusion, 4 energy groups, mesh M2) are shown in Tables 11 and 12, the resulting rod worths in Tables 13 and 14. Comparing the calculated rod worths of the latter two tables with the corresponding values of the first analysis campaign (Tables 3 and 7) one observes - as expected - only minor changes of the order of 1 to 2%. The problem of the substantial overestimation of rod worths thus remained unresolved.

IV.2.2 Core excess reactivity and criticality prediction for CMP and C1D

The strategy of the calculations used for these predictions in the second analysis phase was somewhat different from those of the first analysis:

- The basic calculations, identical to those of the rod worth predictions, were performed in 4 energy groups.

Configuration	3D Diffusion 4 energy groups, M2	
	k_{eff}	$\rho[pcm]$
$SCP^{\uparrow}$ $SAC^{\uparrow}$	1.04576	+4376.1
SCP^{542} $SAC^{\uparrow}$	0.99646	-355.1
SCP^{542} $SAC^{\downarrow}$	0.98400	-1625.8
$SCP^{\downarrow}$ $SAC^{\uparrow}$	0.94340	-5999.7
$SCP^{\downarrow}$ $SAC^{\downarrow}$	0.93105	-7406.1

Table 11. Second KfK analysis of CMP. 3D calculations, radial mesh M2.

Configuration	3D Diffusion 4 energy groups, M2	
	k_{eff}	$\rho[pcm]$
$SCP^{\uparrow}$ $SAC^{\uparrow}$	1.00595	+591.9
SCP^{929} $SAC^{\uparrow}$	1.00181	+181.0
SCP^{929} $SAC^{\downarrow}$	0.99041	-968.2
$SCP^{\downarrow}$ $SAC^{\uparrow}$	0.90874	-10042.0
$SCP^{\downarrow}$ $SAC^{\downarrow}$	0.90268	-10780.6

Table 12. Second KfK analysis of C1D. 3D calculations, radial mesh M2.

Configuration	Calculated rod worths relative to $SCP^{\uparrow}$ $SAC^{\uparrow}$ $\Delta\rho^{calc.}[pcm]$	Resulting calculated SAC worth $\Delta\rho^{calc.}_{SAC}[pcm]$
	4 groups	4 groups
$SCP^{\uparrow}$ $SAC^{\uparrow}$	0	
SCP^{542} $SAC^{\uparrow}$	-4731.2	1270.7
SCP^{542} $SAC^{\downarrow}$	-6001.9	
$SCP^{\downarrow}$ $SAC^{\uparrow}$	-10375.8	1406.4
$SCP^{\downarrow}$ $SAC^{\downarrow}$	-11782.2	

Table 13. Second KfK analysis of CMP. 3D calculations, radial mesh M2: Rod worths relative to $SCP^{\uparrow}$ $SAC^{\uparrow}$ and SAC worths

Configuration	Calculated rod worths relative to $SCP^{\uparrow}$ $SAC^{\uparrow}$ $\Delta\rho^{calc.}[pcm]$	Resulting calculated SAC worth $\Delta\rho^{calc.}_{SAC}[pcm]$
	4 groups	4 groups
$SCP^{\uparrow}$ $SAC^{\uparrow}$	0	
SCP^{929} $SAC^{\uparrow}$	-410.9	1149.2
SCP^{929} $SAC^{\downarrow}$	-1560.1	
$SCP^{\downarrow}$ $SAC^{\uparrow}$	-10633.9	738.6
$SCP^{\downarrow}$ $SAC^{\downarrow}$	-11372.5	

Table 14. Second KfK analysis of C1D. 3D calculations, radial mesh M2: Rod worths relative to $SCP^{\uparrow}$ $SAC^{\uparrow}$ and SAC worths

- Unlike the k_{eff} predictions of the first analysis, mesh corrections were now not synthesized from the results of 2D centre plane and KASY calculations, but directly assessed with 3D calculations. The detailed procedure used for this purpose is described in Appendix 5.

- As the cross section condensation to 4 energy groups had already been performed at BN, the condensation corrections were also supplied from there. They were given as -224 pcm for the core with all rods fully raised and as -3.8% on the worth of the SCP rods determined by the basic calculation for an insertion to the critical level. The same corrections were used for C1D and for CMP.

- Although relatively small, the introduction of aging corrections was considered useful. While in the revised BN cross section preparation, the ^{241}Pu content was updated to 01/09/1985, the critical C1D experiment was carried out on the 08/09/1985, and the critical CMP experiment on 04/10/1985. The corresponding reactivity loss of the core with respect to the calculation reference date was -5 pcm for the C1D and -21 pcm for the CMP loading.

The complete results of the second phase predictions are given in Tables 15 and 16 below:

Conf.	Basic Calc.	Corrections [pcm]			Final $\rho^{calc.}$	$\rho^{meas.}$	C-E
	3D Diff 4gr M2	CM^{rad}	CM^{ax}	Aging			
	ρ^{basic}[pcm]				[pcm]	[pcm]	[pcm]
$SCP^{\uparrow}$ $SAC^{\uparrow}$	+4376.1	+73	-224	-21	+4204	+3732	+472
SCP^{542} $SAC^{\uparrow}$	-355.1	+207	-44	-21	-213	0	-213

Table 15. **Second KfK analysis of CMP.:** Reactivity predictions for the core with all rods fully raised and for the critical core.

Conf.	Basic Calc.	Corrections [pcm]			Final $\rho^{calc.}$	$\rho^{meas.}$	C-E
	3D Diff 4gr M2	CM^{rad}	CM^{ax}	Aging			
	ρ^{basic}[pcm]				[pcm]	[pcm]	[pcm]
$SCP^{\uparrow}$ $SAC^{\uparrow}$	+591.9	+108	-224	-5	+471	+321	+150
SCP^{929} $SAC^{\uparrow}$	+181.0	+122	-208	-5	+90	0	+90

Table 16. **Second KfK analysis of C1D.:** Reactivity predictions for the core with all rods fully raised and for the critical core.

One observes that with respect to the first analysis campaign, all (C-E) values are shifted towards more positive values, leading to a generally better agreement with the predicted (C-E) value of +370 pcm. The poor control rod worth prediction, however, is still reflected in the different (C-E) values found for the experimentally critical state and the state with all rods fully raised.

V Attempts to explain the aberrant results of the first two analysis campaigns

V.1 Comparison with the techniques and results of other groups

Having found that after the elimination of all trivial data errors the prediction of control rod worths was still unsatisfactory and largely different from the experience made in earlier experiments at zero-power facilities, the investigations concentrated on the methodology of the cross section production for control rods itself. First of all, a comparison seemed advisable with the analysis strategies of the other task-force working groups which had found less discrepant results in their analysis of the SPX-1 experiments.

INTERATOM

One of the first surprising points in this context was that despite the use of the same cross section library as KfK/BN (KFKINR001), the INTERATOM analysis of the SPX-1 control rod experiments had produced rod worth C/E ratios in the range of 1.00 ± 0.05 and very consistent with earlier analyses of zero power reactor experiments. However, some essential differences existed between the INTERATOM and KfK analysis calculations:

- IA used MONTE CARLO calculations, while the KfK analysis was based on finite difference diffusion codes. Apart from the advantage of treating neutron propagation in transport theory, these MONTE CARLO calculations have the additional merit of allowing the use of different geometry options within one calculation. In the case of the control rod absorbers, for instance, IA was therefore not obliged to produce homogenized cross sections over the full radial extention of a control rod subassembly - as was the case in the KfK analysis - but a cylindricalized model of the absorber (Figure 10) could be directly implanted into the otherwise hexagonal whole core calculation.

- The cylindrical model used for the SCP absorbers differed from that used in the KfK Supercell cross section production (Figure 8) in as far, as the innermost region did not include the steel filling pins and the cylindrical inner steel tube (see Sec. III.2) but only the absorber pins with their cladding and the interpin sodium. The resulting inner zone radius used by IA was 6.861 cm (@ 180°C) instead of 7.47 cm as used by KfK/BN and CEA.

As supplementary studies had shown that global transport effects on SPX-1 control rod worths could only explain about 5% of the difference between the IA and KfK results, the major fraction of this difference had to originate from the modelling and the cross section production used for the control rod absorbers.

In this context it proved very helpful that IA had repeated part of its analysis calculations using the SCP model of BN/KfK/CEA. It was found that with respect to the IA model, calculated rod worths increased by $\simeq 6$ % leading to a range of C/E ratios from 1.04 to 1.09. A combination of the 5% transport correction with the effect of 6% due to the different absorber modelling explains already a major fraction (about 2/3) of the C/E difference observed between the IA and the KfK analyses. The residual difference had therefore to be attributed to the KfK/BN cross sections homogenisation via flux-volume weighting. The subsequent comparison with the analysis techniques used by the other groups confirmed this conclusion.

AEA Great Britain

As KfK and BN, AEA also uses finite difference codes and is thus also obliged to produce homogenized absorber cross sections / 26,27 /. The method used by this group is the well known 'Rowlands method' / 11 /. As a detailed description of this method is found in literature, only the essential points are highlighted hereafter:

The basic idea of the Rowlands method is to treat the transition from an actual heterogeneous control rod geometry to an equivalent homogeneous geometry using perturbation theory. The original heterogeneous geometry is considered to be the unperturbed situation, the homogenized geometry as the perturbed situation. A set of cross sections are sought in the perturbed (homogeneous) geometry such that the reactivity of the heterogeneous geometry is preserved. The above reactivity equivalence is established using the exact transport theory perturbation expression for the difference in reactivity between the unperturbed and perturbed geometries. In operator writing:

$$\delta\rho = 1/N \int \Phi_u(\overline{\Sigma} - \Sigma_r)\Phi_p^+ dV \equiv 0 \qquad (2)$$

and thus

$$\overline{\Sigma} = \int \Phi_u \Sigma_r \Phi_p^+ dV / \int \Phi_u \Phi_p^+ dV \qquad (3)$$

for all reaction types and energy groups.

Φ and Φ^+ are the real and adjoint neutron fluxes with suffix 'u' identifying the unperturbed (heterogeneous) geometry and suffix 'p' the perturbed (homogeneous) geometry. Σ_r are the regionwise cross sections of the heterogeneous geometry, $\overline{\Sigma}$ the searched homogenized cross sections, and N is the normalization integral. Since the use of the so produced homogenized cross sections $\overline{\Sigma}$ produces the same reactivity effect as the heterogeneous absorber model, they will in the following be referred to as '**homogeneous equivalent**' cross sections and be abbreviated by the symbol '$\mathcal{HE}$'.

Since the homogenized cross sections are a-priori unknown, the adjoint flux distribution Φ_p^+ of the homogeneous geometry required in the weighting procedure cannot be directly determined. The problem is solved by producing a 'first-guess' set of homogenized cross sections via simple flux weighting of the regionwise cross sections Σ_r of the heterogenous model and by subsequent iterative improvement via cyclic recalculation of the adjoint fluxes and homogeneous cross sections.

It is important to emphasize, that this whole procedure is carried out in a one-dimensional cell model and that therefore the heterogeous geometry of the control rod used above as the unperturbed reference situation does not really represent the original layout of the absorber. As in the KAPER4 supercell runs of the KfK/BN analysis, the realistic absorber geometries need to be transformed into suitable cylindrical models with the consequence that the results of the Rowlands method too are influenced by the - to a certain extent - arbitrary choice of the cylindricalized absorber model.

In agreement with the KfK/BN method, the first step of the AEA production of homogenized absorber cross sections consisted in a supercell flux calculation using the collision probability code MURAL, in which the cylindricalized heterogeneous absorber model was immersed into a 'fuel-sea' of 40 cm thickness with an external reflective boundary condition. Different from the analyses of the other groups was

the very detailed cylindrical model chosen for SCP which is shown in Figure 11 and the fact that the innermost, boron carbide containing region had a smaller radius. Other than the analyses of the other groups whose one-dimensional models were more directed by the question whether the cylindrical guide tube should be included in the innermost region or not, the AEA approach was much stricter in that it was based on a 'unit-cell' definition. Attributing to each of the 31 absorber pins the same hexagonal unit-cell such that the bulk of the absorber is filled without gaps, the cumulative area of all 31 unit cells leads to a cylindricalized radius of r = 6.67 cm (@ 180°C). The radius used here for the absorbing portion of the control rod was thus even smaller than that used in the IA analysis.

The neutron flux solution Φ_r of this supercell calculation is used to produce a first set of homogenized cross sections by simple flux weighting of the cross sections of the cylindrical subregions. Up to this point, the procedure thus corresponds to the KfK/BN analysis. In the Rowlands method, however, these cross sections only represent the first iteration for the production of the desired $\mathscr{H}\mathfrak{E}$ cross sections.

A second supercell calculation is then performed in which the initially heterogeneous central control rod is replaced by a homogeneous rod for which the above produced 'first-guess' homogenized cross sections are used. The adjoint flux solution from this calculation is then used together with the direct flux solution of the heterogeneous cell to produce according to Eq. 3 a first set of improved homogenized cross sections, which again are used in another homogeneous cell calculation to produce the next improved adjoint flux distribution. This procedure is continued until convergence is reached, i.e. until Eq. 3 is fullfilled to a specified accuracy.

A point of particular importance in the AEA analysis, which was confirmed by the studies conducted at the CEA was the following: Although the $\mathscr{H}\mathfrak{E}$ cross sections had in principle been derived for use in transport theory calculations, they can also be employed with confidence in diffusion theory calculations / 27 /.

To date, AEA has produced $\mathscr{H}\mathfrak{E}$ cross sections for the SCP control rods only. They gave very satisfactory results with rod worth C/E ratios close to unity and thus consistent with analyses of earlier experiments in critical facilities / 8 /.

CEA

The CEA cross section homogenization for control rod absorbers followed the basic idea of the Rowlands method, i.e. the production of $\mathscr{H}\mathfrak{E}$ cross sections via recursive weighting of the subregion cross sections of a cylindrical absorber model with Φ of the heterogeneous cell model and Φ^+ of its homogenized equivalent / 12,13,18 /. There were several points, however, in which the CEA analysis differed from the approach chosen by AEA:

- Instead of using a supercell model with the control rod immersed in a clean core-sea, initial CEA work was based on a cylindrical 1D model resembling the layout of SPX-1 with two control rod annuli and with the control rod absorber in view implanted into the core centre. Two arguments led to this approach: The control rod in view was located in a more 'realistic' spectral environment than in a 'clean' supercell, and the presence of the control rod annuli offered the possibility to produce $\mathscr{H}\mathfrak{E}$ cross sections also for off-centre control rods. Without going into the details of the results, it was found that the cross section homogenization for the off-centre positions proved little successful.

  Lateron, the calculation model was truncated to an outer radius of 50 cm, the control rod annuli were omitted and a reflective outer boundary condition was

imposed. The model thus agreed largely with the Rowlands model. Tests using this truncated model, which at a later stage was planned to be implemented in the standard cross section preparation routines, showed that the resulting $\mathscr{HE}$ cross sections for the central control rod agreed closely with those found for the complete 1D reactor model used initially.

- Neutron flux and adjoint solutions were not obtained from a collision probability code but from S_N transport theory calculations.

- Unlike the 'Rowlands' procedure, the first guess homogenized cross sections were not obtained by weighting the subregion cross sections Σ_r of the heterogeneous reference model with the corresponding direct flux solution Φ_u , but by simple volume weighting of the subregion cross sections. Although this different choice somewhat slowed down the speed of convergence of the iteration procedure, it obviously had no influence on the final results.

More important than these minor differences between the CEA and AEA analyses is the fact that for SCP control rods (only those were so far investigated by AEA) the two groups used substantially different absorber models. While in the AEA analysis, the absorbing region extended to a radius of 6.66 cm, the CEA analysis used a much more diluted absorber extending to a radius of 7.47 cm.[4]

The results of this first CEA analysis showed that rod worths were significantly overpredicted with C/E ratios ranging from 1.10 to 1.25 (only one case) with the majority centred around 1.15. / 18,22,28 /. This was in sharp contradiction to the results found in measurements in critical assemblies. Control rod experiments in PRE-RACINE had given a C/E ratio of 1.06 / 29 /, in RACINE-1D between 1.07 and 1.10 / 29 /, and in RACINE-1E of 1.01 to 1.03 / 30 /. Systematic studies were thus launched at CEA to identify the origin of this SPX-1 specific overprediction. In the course of these studies, a new approach was tentatively employed for the definition of the different zone radii to be used in the 1D absorber models on which the cross section homogenisation was based:

The first step of this new approach was to set up a quarter plan XY-model (XY-geometry enforced by the transport code used later) consisting of a central singularity to be specified hereafter, and a surrounding clean core zone of about 125 cm thickness.

The central singularity was filled alternatively with the following insets:

1. A sodium follower

2. The three different absorber types encountered in SPX-1 (SCP, upper SAC, lower SAC) using alternatively

   a. homogeneous cross sections, which were produced by simple volume weighting of the absorber component cross sections, and which therefore not contain any information of the absorber heterogeneity,

   b. the $\mathscr{HE}$ cross sections used for these absorbers throughout the first CEA analysis, i.e. those that had been produced according to Rowlands' proposal by $\Phi\Phi^+$-weighting of the annular subregion cross sections of cylindrical absorber models,

---

[4] It is recalled that up to this point, this CEA absorber model was also used in the KfK/BN analysis; see Sec. III.2.2.

c. very detailed models of the different absorbers in which the internal structures of the absorbers were well resolved. The use of XY-geometry obviously limited the possible resolution to some extent. See Figure 12 and / 18 /.

The k_{eff} values of these arrangements were determined using transport theory S_n calculations (BISTRO) with a uniform axial buckling.[5] Three types of absorber worths could thus be determined relative to the sodium follower:

1. $\Delta\rho_{hom}$ corresponding to absorber type (a) of the preceding list,

2. $\Delta\rho_{\mathcal{H}\mathcal{E}}$ corresponding to absorber type (b), and

3. $\Delta\rho_{detailed}$ corresponding to absorber type (c)

To see how well the $\mathcal{H}\mathcal{E}$ cross sections of the first analysis had taken into account the reactivity effects of the different heterogeneous absorber structures, the following 'heterogeneity factors' (or 'heterogeneity corrections') were compared with eachother:

$$F_{\mathcal{H}\mathcal{E}} = \frac{\Delta\rho_{\mathcal{H}\mathcal{E}} - \Delta\rho_{hom}}{\Delta\rho_{hom}}\,[\%] \qquad F_{detailed} = \frac{\Delta\rho_{detailed} - \Delta\rho_{hom}}{\Delta\rho_{hom}}\,[\%]$$

These factors indicate the percentage reduction observed in calculated rod worths when homogeneous absorber cross section are replaced by those that account for the heterogeneous structure of the control rods.

Surprisingly, the factors found for the detailed absorber representation differed substantially from those found for the $\mathcal{H}\mathcal{E}$ absorbers. The most significant difference was observed in the case of the SCP absorber, where a correction of -14.5% was observed for the detailed XY model and of only -9.0% for the $\mathcal{H}\mathcal{E}$ cross sections of the first CEA analysis. In comparison, the upper and lower SAC absorbers showed corresponding heterogeneity corrections of -13.2 vs. -12.9% and -12.3 vs. -11.4%. In these cases, the use of $\mathcal{H}\mathcal{E}$ cross sections had apparently been more adequate. The first analysis had thus - in particular in the case of the SCP rods - used $\mathcal{H}\mathcal{E}$ absorber cross sections that did not sufficiently well account for the absorber heterogeneity and, as heterogeneity corrections have a negative sign, was predestined to overestimate control rod worths.

The next step of the CEA investigations was to repeat the cross section preparation for the SCP and the lower SAC absorber; the formerly used $\mathcal{H}\mathcal{E}$ cross sections for the upper SAC were considered sufficiently accurate and no more effort was made to further improve these. The repetition of the cross section preparation followed in principle the lines as the original analysis, i.e. a $\Phi\Phi^+$ weighting of the subregion cross sections of a 1D cylindrical absorber model, but with the following new feature: Individually for each of the two absorber types, the area of the B_4C containing region was progressively reduced - under preservation of the B_4C mass - and for each step of this process new $\mathcal{H}\mathcal{E}$ cross sections were produced.

In the case of SCP, this shrinking of the B_4C containing area was made be stepwise reduction of the radius of the inner zone (see Figure 8) from the initial value of 7.47 cm down to 6.2 cm.

In the case of the lower SAC absorber the original analysis had used a 1D model in which the absorbing area was represented by an annunlus of $\simeq$2.2 cm thickness

---

[5] Concerning potential problems arising with the use of a uniform buckling for the sodium follower configuration, see Sec. VI.4.

and with a mean radius of ≃4.8 cm from the subassembly centre. Maintaining the former mean radius, the inner and outer radius of the annulus were now synchroniously shifted towards the mean radius, leading to a progressively thinner annunlus.

The $\mathscr{HE}$ cross sections obtained in this process of stepwise absorber surface reduction - or B_4C density increase - were used to determine for each of the two absorbers a set of heterogeneity factors $F_{\mathscr{HE}}$. By comparison with the corresponding heterogeneity factors $F_{detailed}$ found before, one was now able to define the optimum 1D absorber models for which $F_{\mathscr{HE}}$ was identical to $F_{detailed}$.

For the SCP absorber this was the case for an inner zone radius of 6.28 cm, for the SAC absorber for an annulus thickness of 1.72 cm.

Whole core control rod worth calculations were then repeated with the new adjusted $\mathscr{HE}$ cross sections and C/E ratios were found to have improved significantly; for SCP rods, e.g. C/E ratios were reduced by 6-7%. This finding confirmed the results obtained at IA when in MONTE CARLO calculations the standard IA model of SCP with an outer absorber radius of 6.861 cm was replaced by the initial CEA model (cf. beginning of this section).

The resulting situation at CEA was an overprediction of control rod worths of the order of 5 to 11%, attributed predominantly to basic data uncertainties in the cross section library CARNAVAL-IV. The fact that this overprediction was much less pronounced in the majority of the measurements in critical assemblies is ascribed to different sensitivities of flux and adjoint profiles in these compared with real size power reactors / 38 /.

Although without direct relevance to the present problem it should be mentioned that further activities were launched at CEA with the aim to not only integrate heterogeneity effects but also transport and mesh size effects into the homogenized cross sections of control rod absorbers and other non-fissile assemblies. This procedure, usually referred to as the 'MONSTRE' method, was found to largely simplify design level calculations without introducing impermissable errors / 12 /.

V.2 Supplementary studies on the cross section production for SCP

Having found that all other groups of the task force - at least in their revised analyses - used cylindrical models for the absorbers in which the absorbing portions covered much smaller areas and that these were subdivided into finer meshes than in the KfK models, and that C/E ratios were substantially lowered by this modification, it appeared interesting to launch corresponding studies also at KfK.

The following investigations were performed only for SCP control rods:

1. The standard cross section preparation for SCP used a 1D(radial) KAPER4 supercell model (see Figure 8) with only two meshes for the whole control rod absorber (1 mesh from 0.0 to 7.47 cm, and 1 mesh from 7.47 to the control surface at 9.424 cm). To see the influence of mesh refinement, the supercell calculation was repeated using 5 meshes of 1.4942 cm between 0.0 and 7.47 cm and two meshes of 0.9765 cm to pass from 7.47 to 9.424 cm. (These dimensions referred to 180°C.)

   Subsequent rod worth calculations indicated a reduction of C/E ratios with respect to the original KfK analysis by ≃2% .

2. In the second step, the original radial subdivision with the absorbing area extending to 7.47 cm was abandoned and two different new models were established, both using fine meshes of 1.1 to 1.6 cm within the absorber.

   a. The first model was called the 'unit-cell-model' and corresponded to the one used at AEA. As mentioned before, the outer radius of the absorbing region in this model was chosen to 6.673 cm (@ 180°C) and was derived from the area of the unit cell surrounding each absorber pin, scaled by the number (31) of these pins. Details on the cross section preparation for the unit-cell-model are found in Appendix 6.

      Using these cross sections instead of those of the first two KfK analysis campaigns, rod worth C/E ratios dropped by $\simeq$8.5 %.

   b. The second model was called the 'envelope-model'. The outer radius used for the absorbing region was now only 6.37 cm (@ 180°C) and was based on the area enlosed by a line that enclosed all absorber pins and joined one absorber pin with its neighbour via the the shortest distance. More details on this model and on the associated cross section production are also found in Appendix 6.

      Using the so produced SCP absorber cross sections, C/E ratios dropped by even $\simeq$10.2% with respect to the original cross sections.

In agreement with the experience made at CEA and at IA, these investigations have shown that KfK C/E ratios could be lowered substantially - for SCP to below 1.10 - by using for the preparation of homogenized absorber cross sections, cylindrical models in which the absorbers cover a smaller area. Such C/E ratios approach those found in the conventional BIZET assemblies containing the largest cores analysed so far at KfK / 8 /.

The problem of rod worths overprediction in the KfK analysis could have therefore been solved - at least to its better part - by simply changing the models used for the absorber cross section production. The negative aspect that was seen in such a manipulation was that the choice of the cylindrical absorber model would always remain an arbitrary parameter (cf. the radii of 6.67 and 6.30 cm used by AEA and CEA, respectively, for the absorbing area of SCP).

Apart from the difficulty of the arbitrary choice of the absorber model, KfK/BN were confronted with another, more practical problem:

The Rowlands method for the production of $\mathscr{H}\mathfrak{E}$ cross sections could not be applied as the module performing the recursive $\Phi\Phi^+$ weighting of the cylindrical subregion cross sections was not available.

It was therefore decided to develop a novel method for the production of $\mathscr{H}\mathfrak{E}$ cross sections, based on realistic absorber models and not requiring any new computer modules. This method will be described in the next section. Its application represents the third and final phase of the KfK/BN analysis calculations.

VI The third phase of the KfK analysis calculations

VI.1 The novel cross section production for control rod absorbers

VI.1.1 The General Strategy

The initial analysis efforts of KfK and BN had shown that in the case of very voluminous absorbers with a strongly heterogeneous structure and with highly enriched absorber material, substantial errors could be introduced into homogenized absorber cross sections when these were produced on the basis of a simplified 1D model of the absorber, where the thickness and contents of the subregions were fixed following plausibility considerations i.e. in a more or less arbitrary way. The errors could be enhanced by inadequate weighting of the subregion cross sections of the 1D model.

To avoid the difficulties arising in this context, a completely different approach was now chosen:

The basic idea behind this new approach was to adhere to the old method of cross section averaging using KAPER4 fluxes of a 1D absorber model but to adjust the dimensions and/or the contents of the absorber zone of this 1D model in such a way that later use of these homogenized cross sections would produce the same reactivity worth against a sodium follower as obtained in a calculation representing the detailed absorber geometry. The strategy thus resembles the one chosen by CEA in its re-analysis of the experiments (see Sec. V.1), where the radii of the 1D absorber models had been adjusted to give cross sections that reproduced rod worths found with detailed XY-models.

Globally, the new cross section production thus involved the following steps:

1. A set of so-called *'reference'* calculations in transport theory comprising a detailed description of the absorber heterogeneity. Comparing the k_{eff} values obtained for the different absorbers with that obtained for a sodium follower yielded *'reference absorber worths'*.

2. The production of homogenized cross sections which were due to be tuned.

3. A set of calculations, later on referred to as *'homogeneous'* calculations, in which the absorbers were represented by homogeneous cross sections which were first taken from (2.) but then iteratively tuned until the corresponding *'reference absorber worths'* were reproduced.

Concerning the level of the *'homogeneous'* calculations, different routes are possible. If only the transition from a heterogeneous to a homogeneous absorber description is intended to be accounted for in the adjustment of the homogenized cross sections, *homogeneous* and *reference* calculations will be run on the same level, i.e. in transport theory and with the same mesh width and number of energy groups. Consequently, whole core analysis calculations run for the prediction of control rod worth would then have to be run in transport theory too, as the cross section adjustment had been done on that calculation level. Correction for the use of a coarse mesh and, if applicable, for the use of a reduced number of energy groups, would have to be applied a-posteriori.

Lacking transport theory codes that would allow to perform whole core calculations in 3D geometry at moderate computer expense, the standard computational tool for whole core calculations has become diffusion theory. This leads to the con-

clusion that it would be more convenient and logical if the above equivalence included not only the transition from the original heterogeneous to the homogeneous geometry / cross sections, but also the transition from transport to diffusion theory.

Following the same line of reasoning, the so-called 'MONSTRE' method / 12 /, developed at the CEA/CEN Cadarache, extends the equivalence even further. The idea behind this method was simply that the overall procedure of predicting control rod worths could be substantially facilitated, if the *homogeneous* calculation was performed directly on the level of the later envisaged whole core calculations. In view of reducing computer costs for the frequently substantial number of control rod configurations to be analysed, it is obviously attractive to run these calculations on a relatively low level, e.g. in few-group diffusion theory with coarse meshes. If the *homogeneous* calculation is run on this level, the adjustment of the homogenized absorber cross sections will thus not only account for the transition from a heterogeneous to a homogeneous absorber representation and from a transport to diffusion theory treatment, but also for the transition to a reduced number of energy groups and to coarse meshes. Rod worth predictions later obtained from few-group diffusion theory calculations using these cross sections will therefore only require minor - if any - a-posteriori condensation, mesh and transport corrections which refer to the core itself rather than to effects provoked by the presence of the absorbers.

A similar 'multi-equivalence' strategy as proposed by the MONSTRE method was followed in the present BN/KfK cross section production. While BN focussed its work on the SCP absorbers, KfK in cooperation with GRS-Munich [6] concentrated on the two types of SAC absorbers.

Since the whole subject of the new cross section production is already discussed at length in individual reports / 15,16,31 / only a relatively concise description will be given in the present report.

An important point that should be stressed in this context is that the approach presented here is not to be considered a firmly established method but rather a study that could help to render future rod worth predictions more reliable.

VI.1.2 The 'Reference' Calculations

These calculations play a key role in the present approach to cross section production, as the absorber worths obtained with their help will serve as a basis for the subsequent cross section adjustment. It would therefore seem desirable to perform these calculations with the highest degree of sophistication presently possible within the constraints of the computer codes and data available, i.e. in transport theory, 26 energy groups and using very fine meshing to allow a satisfactory resolution of the internal absorber structures.

Concerning the geometry in which these reference calculations should be performed, one might consider whole core geometry the optimum choice to make sure that the absorbers are exposed to a spectral and flux shape environment typical of the realistic reactor situation. For several reasons, however, this is hardly possible:

- Apart from the fact that presently no suitable transport code in 3D geometry, as required for a whole core description, is available at KfK, computing costs would be intolerable, in particular with a view to the extremely fine meshes that have to be used to resolve the internal structures of the absorber rods.

---

[6] GRS = Gesellschaft fuer Reaktorsicherheit

- The spectral and flux shape environment of a control rod changes with the overall configuration of all control rods, and consequently a whole variety of reference calculations would have to be performed to include all situations encountered, giving an impractical multitude of configuration dependent cross sections for the different absorbers.

The idea of a determination of the *reference absorber worths* in a realistic environment had therefore to be abandoned and the choice fell on a clean fuel environment, neclecting perturbations invoked by the presence of other control rods, and of zone boundaries etc. This type of arrangement is frequently referred to as a *macrocell.* The sodium follower or one of the SPX-1 absorbers were placed into the centre of an annular core 'sea' with reflective outer boundary. Using 2D cylindrical plane geometry with RΘ coordinates, the k_{eff} values of these arrangements were determined using the 2D transport codes DOT-IV / 32 / for the SCP studies at BN and TWODANT / 33 / for the SAC studies at KfK/GRS.

Apart from the different codes, BN and KfK/GRS also used somewhat different modelling schemes, cross sections and axial bucklings. These differences were obviously not intentional but rather a consequence of the separate exploratory studies conducted by BN and KfK/GRS.

SCP control rods and their sodium follower:

The upper part of Figure 13 shows the detailed model used by BN to assess the *'reference worth'* of an SCP absorber. The absorber was surrounded by 18 inner core fuel subassemblies (i.e. 2 element rows) resulting in a fuel annulus thickness of about 32 cm. A global buckling of 5.8 m^{-2} was imposed to shift k_{eff} values close to unity. The azimuthal geometry of the SCP absorber allowed to reduce the calculation to a 30° sector.

Concerning the modelling of the individual absorber pins, it should be mentioned that the areas marked B_4C cover only the surface of the absorber pellets and therefore contain pure boron carbide. The pin cladding, the bonding sodium and the spacing wires were 'smeared' with the cooling sodium between the pins. A side investigation in which the absorbing regions of the model were based on the outer pin dimension and an accordingly mixed composition rather than on the pellet diameter, produced very similar final results.

The steel filling pins, the cylindrical inner guide tube and the outer hexagonal subassembly sheath were treated as separate regions and were not smeared with the adjacent sodium.

In the case of the sodium follower, the whole contents of the rod located within the hexagonal element sheath was replaced by pure sodium. The sheath itself remained unchanged.

The different cross sections needed to describe the internal absorber components in the DOT-IV calculations of BN (B_4C, sodium/steel mixture, pure sodium and pure steel) were as usual based on the 26 energy group library KFKINR001 and were processed by KAPER4. All cross sections were obtained from supercell runs were the composition in question was - as usual - immersed in a cylindrical 'fuel sea' with 'white' outer boundary condition. The cross sections used in DOT-IV for the SCP sodium follower and those used for the fuel annulus surrounding the SCP follower/absorber were the same as those used in the preceding analysis calculations (see Sec. III.2.1).

The *reference rod worth* obtained for SCP was 6900pcm.

SAC control rods and their sodium follower:

The models employed in the KfK/GRS TWODANT reference calculations for the two types of SAC absorbers are shown in the lower part of Figure 13. In this case, the models were surrounded by a core annulus of about 110 cm thickness and a global buckling of 8.62 m^{-2} was imposed to shift k_{eff} close to unity. The azimuthal symmetry of the SAC absorbers allowed to reduce the calculations to a 45° sector. Supplementary calculations in which the relatively crude RΘ segment models of Figure 13b were replaced by the refined models shown in Figure 14, where the circular surface of the absorber pins was more closely approximated, showed very little change in rod worth predictions of the order of 1%.

In the case of the SAC absorbers, the absorbing regions were not modelled according to the pellet size, but extended over the whole pin diameter, and therefore contained a mixture of B_4C, steel pin clad and bonding sodium. As for the SCP rods, the hexagonal element sheath was modelled as a separate region.

Although the same cross section library was used, the KfK/GRS cross section production for the SAC absorbers differed from the one used by BN for the SCP absorber in as far as the standard code for homogeneous cross section production GRUCAL was employed. This also applies to the SAC sodium follower for which consequently axial neutron leakage in the reference calculation was somewhat overestimated. This point will be further discussed in Sec. VI.4.

The *reference rod worths* obtained for the two types of SAC absorbers were:
Upper SAC : 1660 pcm , Lower SAC : 1289 pcm

VI.1.3 Homogeneous Cross Section production

As a next step, new KAPER4 supercell calculations were run for each absorber type. These differed from those that were used in the first analysis (Figure 8) in as far as the absorber containing regions were now reduced to cover only the areas, actually occupied by the totality of the absorber pins present in each type of absorber. (In the first analysis, the pin composition was mixed with the inter-pin sodium.)

For the SCP absorbers, this 'compacted' absorbing area formed, as in the first analysis, the innermost region of the supercell, but now with an outer radius of 6cm instead of the formerly used value of 7.47cm.

For the two SAC absorbers, the absorbing areas were now modelled as annuli of 14.86 and 34.68 cm thickness, positioned symmetrically to the absorber pin centres.

It should be mentioned that this reduction of the absorber containing areas to the physically meaningful minimum did not have any particular neutron physics reason, but had historically been the first step in the search for improved homogenized cross sections and in the attempt to reduce the absorber efficiency (see Sec. V.2).

The flux/volume averaged cross sections in 26 energy groups obtained from the KAPER4 runs were condensed to 4 energy groups using adequate flux spectra.

It is important to note that in the present approach, the 1D KAPER4 models used to describe the absorber heterogeneity have lost their decisive influence on the cross sections, as these KAPER4 runs solely serve for the production of first guess homogenized cross sections (see next section)! The homogeneous absorber cross sections could therefore be produced using any other cross section routine - even if it only homogenizes the cross sections by volume-weighting. The reason for using KAPER4 in the present investigation was simply in that all calculation models were readily available.

KAPER4 cross sections for the sodium follower were still available from the first analysis campaign. It is worth noting that unlike the 'first guess' homogeneous absorber cross sections described before, those used for the sodium follower had to prepared using KAPER4. This was necessary, as only the diffusion coefficients provided by this code guaranteed a satifactory treatment of axial neutron leakage through sodium channels in the subsequent 'Homogeneous' and later whole core analysis calculations (see Sec.III.2.3).

VI.1.4 The 'Homogeneous' Calculations

It is reminded that the essential point of these calculations was that they are performed on the same calculation level as the later envisaged whole core analysis calculations, i.e. in our case in diffusion theory, 4 energy groups and coarse meshes corresponding approximately to M1 (see Sec. III.1)

Similar to the *reference* calculations discussed above, these calculations were also performed for a macrocell model with a central sodium follower or control rod absorber embedded into a fuel region. Unlike the *reference* calculations, however, these insets were now treated as homogeneous regions for which the homogenized absorber and sodium follower cross sections in 4 energy groups described in the previous section were used. [7]

Rod worths emerging from these calculations were compared with those found with the reference calculations. In case of a disagreement, the KAPER4 run for the absorber in view was repeated as described in the previous section, but using a changed boron carbide density in the absorber region/s until agreement was achieved.

Supplementary studies in which only the ^{10}B enrichment was reduced instead of the total boron carbide density produced very similar results.

At BN, two different types of *homogeneous calculations*, were run using alternatively the coarse mesh code DEGEN / 34 / and the standard finite difference code D3E; both in 2D plane geometry. Axial neutron loss was simulated by using the same buckling of 5.8 m^{-2} as in the *reference* calculations. DEGEN-adjusted cross sections were later employed by BN for whole core DEGEN calculations, D3E-adjusted cross sections were transmitted to KfK. Using DEGEN it was found that the B_4C density in KAPER4 had to be reduced to 75% of its original value to bring *homogeneous* and *reference* rod worth into agreement, using D3E the fraction was 56.5%. The fact that different 'dilution' factors have to be applied for the two codes originates from the automatic mesh correction made in DEGEN.

At KfK, the *homogeneous* calculations were run using the code D3E in 3D geometry with the SPX-1 core height of 1m. B_4C dilution factors for the upper and lower SAC absorbers were found as 48% and 62%, respectively.

It is underlined that in the present approach only the absorber cross sections were modified to reach agreement of reference and homogeneous rod worths. The sodium follower cross sections remained unchanged, as with the use of modified diffusion coefficients (see Sec. III.2.3) their reactivity effect could be assumed to be calculated with sufficient accuracy.

---

[7] It is noted that the homogenisation also concerns the sodium-follower, since in the *reference* calculation the sodium content and the hexagonal subassembly sheath were represented separately.

VI.2 Rod worth predictions obtained with the new absorber cross sections

The SPX-1 analysis was partially repeated using D3E calculations in 4 energy groups and with M1 mesh size (7 points per subassembly cross section). The revised rod worth predictions obtained from these calculations without applying any a-posteriori corrections, and a comparison with the measured results is shown in Tables 17 through 20.

Configuration	3D Diffusion 4 groups, M1		Rod worths relative to $SCP^{\uparrow}$ $SAC^{\uparrow}$	Resulting SAC or single rod worth
	k_{eff}	$\rho[pcm]$	$\Delta\rho^{calc.}[pcm]$	$\Delta\rho^{calc.}_{SAC}[pcm]$
$SCP^{\uparrow}$ $SAC^{\uparrow}$	1.04594	+4392.1		
SCP^{542} $SAC^{\uparrow}$	1.00717	+712.3	-3679.8	1049.5^{SAC}
SCP^{542} $SAC^{\downarrow}$	0.99664	-337.2	-4729.3	
SCP^{520} $SAC^{\uparrow}$	1.00444	+441.8		
SCP^{520} $SAC^{\uparrow}$ $B4^{\uparrow}$	1.00736	+730.8	-3661.3	501.1^{B4}
SCP^{520} $SAC^{\uparrow}$ $B4^{\downarrow}$	1.00230	+229.7	4162.4	
$SCP^{\downarrow}$ $SAC^{\uparrow}$	0.96424	-3709.1	-8101.2	1164.2^{SAC}
$SCP^{\downarrow}$ $SAC^{\downarrow}$	0.95353	-4873.3	-9265.4	
$SCP^{\downarrow}$ $B12^{\uparrow}$ $SAC^{\uparrow}$	0.97422	-2645.7	-7037.8	1063.4^{B12}

Table 17. Third KfK analysis of CMP. 3D calculations, 4 groups, mesh M1

Control rod group	Insertion state of the remaining rods	Rod worths [pcm]		C/E
		$\Delta\rho^{calc.}$	$\Delta\rho^{meas.}$	
$SCP^{\uparrow\rightarrow 542}$	$SAC^{\uparrow}$	3679.8	3732.0	0.986
$SCP^{542\rightarrow\downarrow}$	$SAC^{\uparrow}$	4421.4	4381.0	1.009
$SCP^{\uparrow\rightarrow\downarrow}$	$SAC^{\uparrow}$	8101.2	8113.0	0.998
$SAC^{\uparrow\rightarrow\downarrow}$	SCP^{542}	1049.5	1039.0	1.010
$SAC^{\uparrow\rightarrow\downarrow}$	$SCP^{\downarrow}$	1164.2	1191.0	0.977
$SCP^{542\rightarrow\downarrow}$ $SAC^{\uparrow\rightarrow\downarrow}$	-	5585.6	5572.6	1.002
$SCP^{\uparrow\rightarrow\downarrow}$ $SAC^{\uparrow\rightarrow\downarrow}$	-	9265.4	9304.0	0.996
$B4^{\uparrow\rightarrow\downarrow}$	SCP^{520} $SAC^{\uparrow}$	501.1	478.5	1.047
$B12^{\uparrow\rightarrow\downarrow}$	$SCP^{\downarrow}$ $SAC^{\uparrow}$	1063.4	1051.5	1.011

Table 18. Third KfK analysis of CMP: Comparison of calculated and measured rod worths.

One observes that the prediction of control rod worths is substantially improved, although only relatively simple calculations (4 energy groups, M1 mesh) were used! The C/E ratios, now located close to unity and showing a much smaller dispersion than in the initial analysis, are in satisfactory agreement with the results obtained in the analyses of earlier experiments in critical assemblies and with the SPX-1 analysis performed at IA where the same cross section library but a MONTE CARLO code was used.

For completeness it should be mentioned that very similar results were found at BN, where the coarse mesh diffusion theory code DEGEN with its associated homogeneous cross sections had been used for the whole core calculations.

Configuration	3D Diffusion 4 groups, M1		Rod worths relative to $SCP^{\uparrow}$ $SAC^{\uparrow}$ $\Delta\rho^{calc.}[pcm]$	Resulting SAC worth $\Delta\rho^{calc.}_{SAC}[pcm]$
	k_{eff}	$\rho[pcm]$		
$SCP^{\uparrow}$ $SAC^{\uparrow}$	1.00541	+537.8		
SCP^{929} $SAC^{\uparrow}$	1.00230	+229.5	-308.3	972.4
SCP^{929} $SAC^{\downarrow}$	0.99263	-742.9	-1280.7	
$SCP^{\downarrow}$ $SAC^{\uparrow}$	0.92610	-7979.7	-8517.5	783.8
$SCP^{\downarrow}$ $SAC^{\downarrow}$	0.91943	-8763.5	-9301.3	

Table 19. Third KfK analysis of C1D. 3D calculations, 4 groups, mesh M1

Control rod group	Insertion state of the remaining rods	Rod worths [pcm]		C/E
		$\Delta\rho^{calc.}$	$\Delta\rho^{meas.}$	
$SCP^{\uparrow\rightarrow 929}$	$SAC^{\uparrow}$	308.3	321.8	0.958
$SCP^{929\rightarrow\downarrow}$	$SAC^{\uparrow}$	8209.2	7747.0	1.060
$SCP^{\uparrow\rightarrow\downarrow}$	$SAC^{\uparrow}$	8517.5	8068.8	1.056
$SAC^{\uparrow\rightarrow\downarrow}$	SCP^{929}	972.4	895.0	1.086
$SAC^{\uparrow\rightarrow\downarrow}$	$SCP^{\downarrow}$	783.8	705.0	1.112
$SCP^{929\rightarrow\downarrow}$ $SAC^{\uparrow\rightarrow\downarrow}$	-	8993.0	8452.0	1.064
$SCP^{\uparrow\rightarrow\downarrow}$ $SAC^{\uparrow\rightarrow\downarrow}$	-	9301.3	8773.8	1.060

Table 20. Third KfK analysis of C1D: Comparison of calculated and measured rod worths.

VI.3 Core excess reactivity and criticality prediction for CMP and C1D

Tables 21 and 22 show the core excess reactivity and criticality predictions for the core loading versions CMP and C1D as obtained with the new cross sections.

It is important to note that both, mesh and condensation corrections quoted in Tables 21 and 22 are related exclusively to the core itself, without the presence of the control rods. Corrections originating from the presence of inserted control rod absorbers are implicitely contained in the absorber cross sections.

Both, mesh and condensation corrections were taken from the second phase of the KfK analysis calculations:

Mesh corrections were obtained from the results of the supplementary calculations quoted in Tables A5.1 and A5.2 of Appendix 5 (see there for details).

Condensation corrections are based on the calculations performed at BN as indicated in Sec. IV.2.2.

Conf.	Basic Calc.	Corrections [pcm]			Final $\rho^{calc.}$	$\rho^{meas.}$	C-E
	3D Diff 4gr M1	CM^{rad}	CM^{ax}	Aging			
	ρ^{basic}[pcm]				[pcm]	[pcm]	[pcm]
$SCP^{\uparrow}$ $SAC^{\uparrow}$	+4392.1	+169	-224	-21	+4316	+3732	+584
SCP^{542} $SAC^{\uparrow}$	+712.3	+169	-224	-21	+636	0	+636

Table 21. **Third KfK analysis of CMP.:** Reactivity predictions for the core with all rods fully raised and for the critical core and comparison with the associated measured reactivities

Conf.	Basic Calc.	Corrections [pcm]			Final $\rho^{calc.}$	$\rho^{meas.}$	C-E
	3D Diff 4gr M1	CM^{rad}	CM^{ax}	Aging			
	ρ^{basic}[pcm]				[pcm]	[pcm]	[pcm]
$SCP^{\uparrow}$ $SAC^{\uparrow}$	+537.8	+290	-224	-5	+599	+322	+277
SCP^{929} $SAC^{\uparrow}$	+229.5	+290	-224	-5	+290	0	+290

Table 22. **Third KfK analysis of C1D.:** For comments see Table 21

The (C-E) results of Tables 21 and 22 show that as could be expected, the more accurate prediction of control rod worths also leads to a substantial improvement of the k_{eff} prediction for the critical core configurations. The (C-E) values for the critical configurations are now only marginally different from those for the configurations with all rods fully raised, both being well located within the range of uncertainty of the expected core reactivity overprediction of $+370\pm520$ pcm. As was mentioned before, the difference in (C-E) values of about 300 pcm, observed for CMP and C1D is caused by the poor prediction of the FAUXCOMB (dummy fuel) elements, present only in C1D. This problem has still not yet been solved.

VI.4 Supplementary investigations concerning the reliability of the 'Reference' transport theory calculations in plane RΘ-geometry

As was described in Sec. VI.1.2, the KfK/GRS *reference* calculations for the SAC absorbers and their sodium follower were run using 2D plane geometry with axial neutron leakage represented by the standard leakage term DB^2_{ax}, in which D was the standard diffusion coefficient $1/3\Sigma_{tr}$ from the homogeneous cross section routine GRUCAL and B^2_{ax} had been chosen as $8.62m^{-2}$. Recent investigations at GRS, in which the adequacy of the use of this type of leakage term was reconsidered, have come to the following conclusion:

For the two *reference* calculations containing the SAC absorbers, this approach could be considered sufficiently accurate and no further modifications were necessary to the original calculations. This conclusion is based on the fact that in an absorbing medium the principal contribution to neutron loss originates from the absorbtion term and that therefore a potential inaccurate assessment of axial leakage plays a subordinate role.

In the case of a central sodium follower, however, the use of the standard leakage term leads to a significant overestimation of the axial neutron leakage and thus to a k_{eff} value for the follower case which is too low.[8] Consequently the reactivity differences between the follower and the two absorber cases representing the *reference* rod worths are also calculated too low. To improve the reliability of the *reference* calculations, the sodium follower case was therefore re-run using an improved axial leakage term $D_{ax}B^2_{ax}$ with D_{ax} taken from a KAPER4 supercell calculation of a sodium follower embedded into the centre of a cylindrical fuel region. The latter was the same routine that served to produce sodium follower cross sections for the whole core calculations.

The *reference rod worths* now obtained for the SAC absorbers were 1819pcm (upper SAC) and 1411pcm (lower SAC) instead of the earlier quoted values of 1660 and 1289pcm respectively. Accordingly, the absorber concentrations used in the homogeneous calculations had now to be raised from the original fractions of 48% and 62% to 62% and 75%, respectively, to produce homogeneous rod worths that match the new *reference worths*. Using the homogenized cross sections based on these new, increased absorber concentrations in whole core analysis calculations, one finds that C/E ratios for SAC absorbers are now comprised between 1.06 and 1.10, depending on the insertion state of the SCP rods. Although this result somewhat deteriorates the consistency with the C/E ratios found for the SCP-rods, one has to see that the layout of the SAC-rods is much more complicated. In the case of the SAC-rods, the different approximations introduced in the present method might therefore well have a more severe impact on the reliability of the results.

Furthermore one finds that even the increased SAC C/E ratios still fit very well into the range of earlier observed C/E ratios between 1.0 and 1.1; in particular since large cores always showed a trend towards the upper end of this range.

The influence of the revised homogenized SAC cross sections on the prediction of the core excess reactivity and criticality (previous section) is insignificant, as in both cases the SAC absorbers are fully raised.

---

[8] This deficiency of the standard diffusion coefficients is obviously well known from problems encountered with their use in diffusion theory calculations (see Sec. III.2.3). Since in the present context only transport theory calculations were involved, it was initially believed that these would be less sensitive to errors in the diffusion coefficients.

VII Conclusions

Using standard data and cross section production methods, diffusion theory calculations of SPX-1 control rod worths performed at KfK and BN produced C/E ratios for rod bank insertions in the fully loaded power core CMP in the range of 1.2. Even higher ratios were found for an individual rod insertion and for experiments in the first critical core C1D. While the aggravation of the worth overprediction in the case of single rod worths could be explained as a superposition of errors on the worth of that rod on one hand and on the worth of the partially inserted control bank on the other, the situation in the case of the first critical core is still not very clear. Indications exist, however, that the C/E ratios in C1D are deteriorated by the use of inadequate cross sections for the dummy fuel assemblies.

As a consequence of the poor rod worth predictions, the criticality prediction for the two core loading versions CMP and C1D were accordingly inaccurate. (The same applies to the prediction of power distributions, a point that was not treated in the present report.)

Although a number of errors were later discovered in the initially used composition and geometry data, the correction of these did not significantly improve the rod worth prediction, but only rendered the prediction of the core excess reactivity more consistent with earlier experience.

A comparison with the analysis performed at IA where the same basic cross section library was used (KFKINR001) but rod worths predictions were based on MONTE CARLO calculations, showed that there C/E ratios were located close to unity and differed only relatively little from the analyses of earlier experiments. Since transport effects were found to account for only 5% within the 20% difference in C/E ratios, the remaining discrepancy had to be attributed to the method employed by KfK/BN to produce homogenized absorber cross sections. This method is based on flux averaging of the subregion cross sections of a simplified cylindrical model of a given absorber. Neutron fluxes are taken from a 'supercell' calculation in which the absorber in question is immersed in a clean fuel ambient.

The question arising at this point was obviously why the KfK/BN cross section production and calculation strategy should just in the case of SPX-1 lead to aberrant results, while the results of experiments in various critical facilities seemed rather consistent and largely agreed with those found by IA. So far, no ultimate answer can be given to this question, but a possible explanation is the following:

SPX-1 control rod absorbers have a more heterogeneous structure than most of those used in the critical facilities, which means that the average neutron cord lengths in the absorbing parts of SPX-1 control rods measured in mean free paths largely exceed those of the earlier experiments. In the case of SPX-1, the ringwise homogenization of the internal absorber structures for the cross section production will therefore have a more deteriorating influence on the treatment of neutron propagation and thus on the neutron flux shape within and in the neighbourhood of absorbers than in cases where the absorbers actually have a rather homogeneous structure. In these cases, the homogeneous modelling is obviously less unrealistic and the supercell neutron fluxes used for the cross section weighting will be more adequate.

Apart from these more basic considerations it is important to see that the choice of the cylindrical absorber model and in particular of the volume over which the absorber pins are mixed with their environment is obviously subject to some degree of arbitrariness. This point is particularly important for absorbers with highly enriched absorber pins - as in SPX-1. Test calculations have shown that apparently insignificant changes in the dilution of the absorbing material when setting up the

1D model can significantly alter its neutronic blackness leading to erroneous flux distributions and thus to wrong weighting functions for the cross section averaging.

Looking for possible ways to continue and improve the KfK/BN analysis, a comparison was also made with the analysis strategies used at CEA and AEA. Both groups use finite difference codes for rod worth predictions and are therefore also forced to produce homogenized absorber cross sections. Other than at KfK/BN, however, these groups use a variational method developed by J.Rowlands which is based on a $\Phi\Phi^+$ wheighting of the absorber subregion cross sections and preserves the worth of the heterogeneous control rod when using the resulting homogeneous cross sections. As the adjoint flux has to be taken from a calculation containing the homogeneous absorber, whose cross sections are a-priori unknown, the method uses an iterative procedure. Volume averaged cross sections are used as a first guess and are then iteratively improved through recursive calculation of the adjoint flux distribution. Despite the obvious merit of the rod worth preservation, this method shares the principal disadvantage of the KfK/BN method: The heterogeneous description of the absorber is also limited to a 1D(radial) representation. Apart from this basic disadvantage, a use of the 'Rowlands'-method at KfK or BN was not directly possible as the special computer modules were not available.

As more advanced methods like pin-cluster codes which allow a twodimensional description of an absorber geometry were also unavailable at KfK and BN, it was finally decided to use a completely different approach for the production of homogenized absorber cross sections. This novel method, basically similar to the MONSTRE method developed at CEA, was based on imposing agreement of the reactivity worth of a given absorber with respect to a sodium follower in two types of calculations:

(i) a reference calculation using transport theory in 26 energy groups with a detailed description of the absorber structure in RΘ geometry and

(ii) a simplified calculation on the level of standard analysis calculations in 4 energy groups and with homogeneous absorber cross sections. The adjustment of these cross sections to reproduce the absorber worth of the reference calculation was made by tuning of the absorber density. An alternative modification of the ^{10}B enrichment was shown to yield nearly the same results.

Tentative use of the new, properly tuned cross sections for the SPX-1 analysis in relatively simple diffusion theory calculations in 4 energy groups and with coarse meshes (only 7 points per subassembly) has given C/E ratios for control rods close to unity and significantly improved predictions of the critical mass and of ^{239}Pu fission rate distributions (this latter point was not treated in the present report). The results now show a much better consistency with those obtained earlier for corresponding experiments in critical facilities.

It should nevertheless be noted that in spite of the discussed merits of the presently chosen approach, the reference calculations in RΘ geometry, which have a decisive influence on the cross section production have certain deficiencies:

While allowing a detailed description of the radial and azimuthal structure of the absorber, this description is limited to just one horizontal plane. In the case of the SCP control rods this deficiency is presumed to be largely irrelevant as their absorbers have a uniform structure over their total axial height of 115 cm. The layout represented in the RΘ model is therefore really representative for the whole active height of the absorber (apart from the axial blanket and reflector regions, which have little importance).

For the SAC control rods with their axially articulated different absorber units, however, the 2D RΘ modelling is obviously less satisfying as it does not account for the presence of other structures or absorbers above or below the one described in the calculation. At present, this particular problem cannot be solved satisfactorily, as it would essentially require a reference transport theory calculation allowing an appropriate 3D modelling of the control rod, e.g. in RΘ-Z geometry, which is presently unavailable at BN and KfK.

Further, it should be remembered that in the reference calculations, the absorbers in question are embedded into the centre of a clean fuel region without any spectral perturbations from other control rods or zone boundaries and without a global flux gradient to which off-centre rods in a real reactor are exposed. Obviously, even existing advanced methods suffer from this shortcoming! The question therefore arises, how well parameters like neutronic 'albedo' and 'transparency' in differently distorted flux spectra and profiles can really be represented by the homogenized cross sections of a simple supercell model and what the role of compensating errors might be.

Finally, the present method assumes the correctness of the sodium follower cross sections and subjects therefore only the absorber cross sections to an adjustment procedure. Although the use of adequately modified diffusion coefficients for the sodium followers does indeed justify this assumption to a large extent, residual errors in particular in the treatment of follower neutron leakage will persist in the whole core calculations. These residual errors, however, are expected to be small and the fact that they are 'tuned' into the absorber cross sections is unlikely to have a severe impact on the present results.

The described procedure is thus not yet fully matured and will doubtlessly not be able to fully compete with the performance of 2D collision probability codes or more advanced schemes. Nevertheless, it seems to provide a useful and simple tool for the production of homogenized cross sections for control absorbers in those cases where only 1D codes are available --- as is presently the case at BN and KfK.
This is an important aspect in the context of the current campaign of control rod worth predictions for the European Fast Reactor EFR.

Acknowledgements

The author is deeply indepted to Drs. F. Helm and R. Böhme for their critical and patient reviewing of this report.

The majority of the calculations of the first KfK analysis campaign was run by D. Thiem whose effort is gratefully acknowledged.

Thanks are due also to Dr. W. Zwermann of the *Gesellschaft für Reaktorsicherheit / Munich, FRG /* who performed all calculations serving for the production of homogeneous equivalent SAC cross sections in the course of the third KfK analysis campaign.

References:

/ 1 / H.GIESE
'KfK Analysis of the SUPER-PHENIX-1 Control Rod Experiments
Part 1: The experimental Results'.
KfK-Report KfK-4653 (Kernforschungszentrum Karlsruhe 1991)

/ 2 / R. DE WOUTERS
Unpublished BN report (Dec. 1986)

/ 3 / G. BUCKEL, R. de WOUTERS and S. PILATE
Atomkernenergie, **30**, 82 (1977)

/ 4 / E. KIEFHABER
'The KFKINR-Set of Group Constants , Nuclear Data Basis, and
First Results of its Application to the Recalculation of
Fast Zero-Power Reactors'.
KfK-Report KFK-1572 (Kernforschungszentrum Karlsruhe 1972)

/ 5 / B. STEHLE
'D3D und D3E Zweige eines Fortran Programmes zur Lösung der
stationären dreidimensionalen Multigruppenneutronendiffusionsgleichungen
in Rechteck-, Zylinder- und Dreieckgeometrie'.
KfK-Report KfK-4764 (Kernforschungszentrum Karlsruhe 1991)

/ 6 / J.C. CABRILLAT et al.
'SUPER-PHENIX-1 Critical Mass Evaluation Intercomparison'.
Tagungsbericht der Reaktortagung des deutschen Atomforums,
Travemünde, West Germany, May 17-19, 1988, p. 27-30

/ 7 / U.K. WEHMANN, H. GIESE
'Methods for Shutdown Worth Calculations in Fast Reactors
and Their Validation With Help of SPX-1 Absorber Experiment
Evaluations'.
Proc. of the IAEA/IWGFR Specialists' Meeting on Methods for
Reactor Physics Calculations for Control Rods in Fast Reactors,
Winfrith, UK, December 6-8, 1988, p. 341-353.

/ 8 / H. GIESE, S. PILATE, J.M. STEVENSON
'Worths and Interactions of Simulated Fast Breeder Reactor
Rods in ZEBRA and SNEAK Assemblies'.
Nucl. Sci. Eng., **87**, 262-282 (1984)

/ 9 / H.GIESE
Unpublished KfK report (May 1984)

/ 10 / R. de WOUTERS and H. GIESE
Unpublished BN report (March 1989)

/ 11 / J.L. ROWLANDS, C.R. EATON
'The spatial averaging of cross sections for use in transport theory reactor calculations, with an application to control rod fine structure homogenisation'.
Proc. of the Specialists' Meeting on Homogenisation Methods in Reactor Physics, Lugano, Switzerland, November 13-15, 1978, p. 261-268.

/ 12 / G. PALMIOTTI
'A method to obtain new cross sections transport equivalent'.
Proc. of the IAEA/IWGFR Specialists' Meeting on Methods for Reactor Physics Calculations for Control Rods in Fast Reactors, Winfrith, UK, December 6-8, 1988, p. 33-56.

/ 13 / J.C. CABRILLAT, et al.
'Application of transport equivalent cross sections obtained by the MONSTRE-method to SPX-1 case'.
Proc. of the IAEA/IWGFR Specialists' Meeting on Methods for Reactor Physics Calculations for Control Rods in Fast Reactors, Winfrith, UK, December 6-8, 1988, p. 263-285.

/ 14 / T. TAKEDA and N. UTO
'Comparison of cell homogenization methods considering interaction effects between fuel cells and control rod cells'.
Proc. of the IAEA/IWGFR Specialists' Meeting on Methods for Reactor Physics Calculations for Control Rods in Fast Reactors, Winfrith, UK, December 6-8, 1988, p. 57-83.

/ 15 / M.P. FONTAINE, and R. de WOUTERS
Unpublished BN report (June 1989)

/ 16 / M.P. FONTAINE
Unpublished BN report (Oct. 1989)

/ 17 / H. GIESE, E. KIEFHABER, R. de WOUTERS and M.P. FONTAINE
'A Novel Approach for the Production of Homogenized Control Rod Absorber Cross Sections and its Application to the Analysis of the SUPER-PHENIX-1 Experiments',
Proc. Int. Conf. on the Physics of Reactors: Operation, Design, and Computation,
Marseille, France, April 23-27, 1990, Vol.2, p. X-35 - X-47

/ 18 / J.C. CABRILLAT et al.
'Common Lessons Drawn from Different Laboratories Analyses of SUPER-PHENIX Start-up Experiments',
Proc. Int. Conf. on the Physics of Reactors: Operation, Design, and Computation,
Marseille, France, April 23-27, 1990, Vol.1, p. VII-10 - VII-20

/ 19 / J. HOMMET et al.
Unpublished CEA report (Oct. 1985)

/ 20 / D WOLL
'GRUCAL, ein Programmsystem zur Berechnung makroskopischer Gruppenkonstanten'.
KfK-Report KfK-2108 (Kernforschungszentrum Karlsruhe 1975)

/ 21 / R. BÖHME and E.A. FISCHER
'The fast reactor cell code KAPER4'.
KfK-Report KfK-4435 (Kernforschungszentrum Karlsruhe 1988)

/ 22 / J.C. GAUTHIER et al.
'Measurement and Prediction of Control Rod Worth'.
Nucl. Sci. Eng., **106**, 18-29 (1990)

/ 23 / E.A. FISCHER
'Neutron Streaming in Fast Reactor Slab Lattices and in Cylindrical Channels'.
Nucl. Sci. Eng., **78**, 227-238 (1981)

/ 24 / H. GIESE
Unpublished CEA report (Sept. 1986)

/ 25 / R. de WOUTERS and K. PRESCHER
Unpublished IA/BN report (Feb. 1985)

/ 26 / T. NEWTON
'The Treatment of Absorber Rod Heterogeneity Effects Using Homogeneous Equivalent Cross-Sections and Their Application in Large Fast Reactors',
Proc. of the IAEA/IWGFR Specialists' Meeting on Methods for Reactor Physics Calculations for Control Rods in Fast Reactors, Winfrith, UK, December 6-8, 1988, p. 313-339

/ 27 / T. NEWTON
'An Evaluation of SUPER PHENIX 1 Core Reactivity Levels Using Cross-Section Adjustment Techniques in Diffusion Theory and a Comparison with Measurement',
Proc. Int. Conf. on the Physics of Reactors: Operation, Design, and Computation,
Marseille, France, April 23-27, 1990, Vol.S, p. SII-13 - SII-23

/ 28 / M. SALVATORES
'CEA Data and Methods for Control Rod Calculations',
Proc. of the IAEA/IWGFR Specialists' Meeting on Methods for Reactor Physics Calculations for Control Rods in Fast Reactors, Winfrith, UK, December 6-8, 1988, p. 287-312

/ 29 / G. HUMBERT et al.
'Parametric Studies on Heterogeneous Cores for Fast Breeder Reactors: The Pre-Racine and Racine Experimental Programs',
Nucl. Sci. Eng., **87**, 233-251 (1984)

/ 30 / H. GIESE, C. CAVAREC, G. GRANGET, G. PALMIOTTI
'The Racine-1E Critical Experiments for Control Rod Method and Data Validation - Experimental and Calculation Results',
Proc. Top. Meet. on Reactor Physics and Safety,
Saratoga Springs, NY, USA, September 17-19, 1986, p. 430-444

/ 31 / W. ZWERMANN, S. LANGENBUCH, H. GIESE, E. KIEFHABER
'An Improved Method for Calculating Control Rod Reactivity Worths in Fast Sodium Cooled Reactors',
KfK/GRS-Report to be published

/ 32 / W.A. RHOADES et al.
'The DOT-IV Two Dimensional, Discrete-Ordinates Transport Code with Space-Dependent Mesh and Quadrature',
ORNL/TM-6529, Oak Ridge National Laboratory (1978)

/ 33 / R.E. ALCOUFFE et al.
'Users' Guide for TWODANT: A Code Package for Twodimensional, Diffusion-Accelerated, Neutral Particle Transport',
LA 10049-M, Los Alamos National Laboratory (1984)

/ 34 / H. LUKAS et al.
'A Fast Two and Three-Dimensional One-Group Coarse-Mesh Diffusion Program in Hexagonal Geometry',
Proc. Int. Top. Mtg. on Advances in Mathematical Methods for the Solution of Nuclear Engineering Problems,
Munich, West Germany, April 27-29, 1981, Vol.I, p. 299-313

/ 35 / J.C. CABRILLAT
Unpublished CEA report (Oct. 1987)

/ 36 / G. GIACOMETTI, M. HÜSKEN, M. PIPAUD
Unpublished CEA report (Aug. 1983)

/ 37 / G.BUCKEL, K.KÜFNER, B.STEHLE
'Benchmark Calculations for a Sodium-Cooled Breeder Reactor by Two- and Three-Dimensional Diffusion Methods'.
Nucl. Sci. Eng., **64**, 75-89 (1977)

/ 38 / J.C. CABRILLAT et al.
'Methods and Data Development from the Super-Phenix Start-Up Experiments Analysis',
Proc. Int. Reactor Physics Conference,
Jackson Hole, Wyoming, USA, September 18-21, 1988, p. II.13-II.24

Appendix 1

This Appendix describes the revised cross section production for dummy fuel sub-assemblies 'FAUXCOMB' and SAC control rod absorbers.

General remarks

Two errors were discovered in the basic data and geometrical models used by BN for the first cross section preparation:

The first concerned the dummy fuel elements, 33 of which were present in the loading of the first critical core 'C1D'. These elements, referred to as 'FAUXCOMB' (= faux combustible) in french documentation, only consist of the outer hexagonal element sheath and a cylindrical inner steel tube with a wall thickness of 3.51 cm. The outer diameter of this tube is 16.04 cm, both dimensions referring to a temperature of 180°C.

At the time of the first BN analysis it was believed that both the hexagonal subassembly sheath and the inner steel tube were fabricated from molybdenum steel. Revised CEA documentation of 1987 (/ 35 /) then stated that only the steel used for the element sheath contained molybdenum, while that of the internal tube did not (for reasons of the relatively short residence time of these elements in the reactor).

The second error concerned the geometry and composition of the different absorber units of the secondary shut down rods SAC. This error occurred as the updated specification of these rods had not been available to BN at the time of the first cross section production. BN had therefore extracted the necessary information from an earlier CEA note quoting preliminary data / 36 /.

The data and models used at KfK for the revised cross section preparation will be described hereafter. Isotopic densities are always given in units of $10^{24}/cm^3$ and refer to a temperature of 180°C.

As usual in KfK/BN cross section productions, the contents of Mn was multiplied by a factor of 1.15 and added to Cu.

FAUXCOMB-elements

Homogenized cross sections for the 'FAUXCOMB'-subassemblies were produced using the supercell option of KAPER4. The cylindrical model of 'FAUXCOMB' used for this purpose is shown in Figure A1.1. The model comprises 3 regions with the following isotopic concentrations:

Isotope	Region 1	Region 2	Region 3	Average
Fe	0.00000E-0	0.59493E-1	0.18934E-1	0.34683E-1
Cr	0.00000E-0	0.16443E-1	0.54487E-2	0.96453E-2
Ni	0.00000E-0	0.72813E-2	0.39740E-2	0.47011E-2
Mo	0.00000E-0	0.00000E-0	0.47769E-3	0.13156E-3
Na	0.23860E-1	0.00000E-0	0.15488E-1	0.97357E-2
Ti	0.00000E-0	0.39665E-3	0.13916E-3	0.23480E-3
Cu	0.00000E-0	0.17530E-2	0.61507E-3	0.10377E-2
Si	0.00000E-0	0.13529E-2	0.32635E-3	0.76001E-3

Table A1.1 Isotopic densities of 'FAUXCOMB' subassemblies

SAC control rods

The cylindrical models used in the KAPER4 supercell runs for the different parts of the SAC control rods are also shown in Figure A1.1.

The model for the upper/central absorber unit comprises 2 radial zones, that of the lower absorber unit 3 radial zones.

The upper and lower articulations were treated as one homogeneous zone without radial subdivisions.

The isotopic concentrations used in these models are given in the Tables hereafter.

Isotope	Region 1	Region 2
Fe	0.40690E-2	0.97299E-2
Cr	0.11709E-2	0.27999E-2
Ni	0.85402E-3	0.20422E-2
Mo	0.10266E-3	0.24548E-3
Na	0.93722E-2	0.19558E-1
Ti	0.29907E-4	0.71515E-4
Cu	0.13218E-3	0.31608E-3
Si	0.70133E-4	0.16770E-3
B-10	0.50148E-1	0.00000E-0
B-11	0.55720E-2	0.00000E-0
C	0.13930E-1	0.00000E-0

Table A1.2 Isotopic densities of the upper/central SAC absorber unit

Isotope	Region 1	Region 2	Region 3
Fe	0.00000E-0	0.57041E-2	0.84347E-2
Cr	0.00000E-0	0.16415E-2	0.24272E-2
Ni	0.00000E-0	0.11972E-2	0.17704E-2
Mo	0.00000E-0	0.14391E-3	0.21280E-3
Na	0.23860E-1	0.10966E-1	0.20131E-1
Ti	0.00000E-0	0.41926E-4	0.61996E-4
Cu	0.00000E-0	0.18529E-3	0.27399E-3
Si	0.00000E-0	0.98319E-4	0.14538E-3
B-10	0.00000E-0	0.40991E-1	0.00000E-0
B-11	0.00000E-0	0.45546E-2	0.00000E-0
C	0.00000E-0	0.11387E-1	0.00000E-0

Table A1.3 Isotopic densities of the lower SAC absorber unit

Isotope	Upper articulation	Lower articulation
Fe	0.19546E-1	0.17074E-1
Cr	0.56248E-2	0.49135E-2
Ni	0.41025E-2	0.35837E-2
Mo	0.49313E-3	0.43077E-3
Na	0.15218E-1	0.16311E-1
Ti	0.14367E-3	0.12550E-3
Cu	0.63495E-3	0.55466E-3
Si	0.33690E-3	0.29430E-3

Table A1.4 Isotopic densities of the SAC articulations

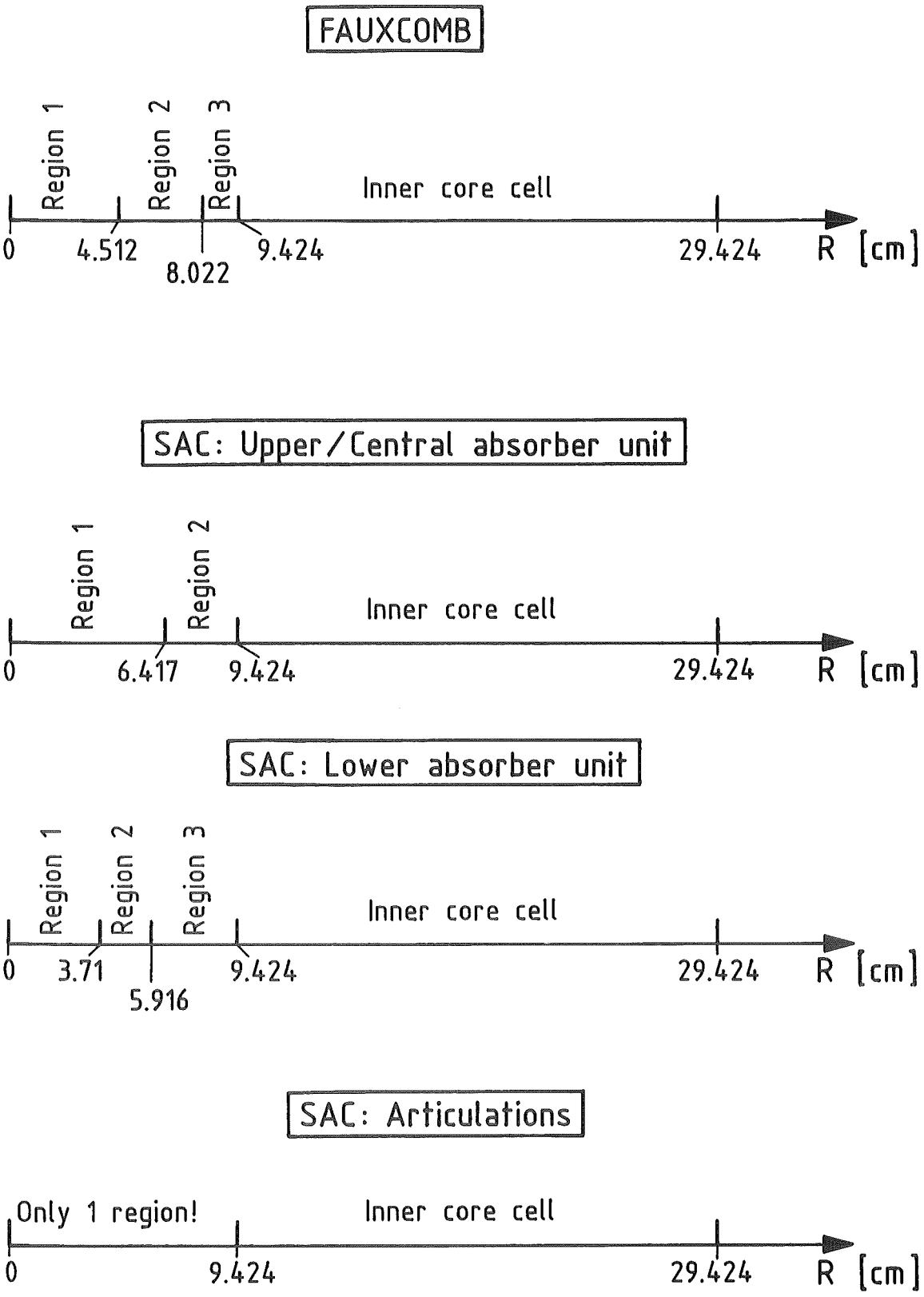

Figure A 1.1 Cylindrical models of "FAUXCOMB" and SAC used for KAPER 4 supercell calculations

Appendix 2

This Appendix describes the strategy used in the first KfK analysis phase to derive a dilution- insertion-equivalence-relationship for SCP control rods.

The dilution-insertion-equivalence model

The law of equivalence between an actual absorber insertion and the diluted absorber cross sections employed to simulate this insertion in a 2D center plane calculation was established in the following way:

SCP absorber cross sections in 26 energy groups, the production of which was described in the section III.2.2, were mixed with those of the SCP sodium follower in the subsequent relative proportions:

2.5% SCP absorber and 97.5% sodium follower
5.0% " " 95.0% " "
7.5% " " 92.5% " "

and so forth in steps of 2.5% to

97.5% SCP absorber and 2.5% sodium follower

The resulting 39 diluted absorber cross sections were coupled to the original cross section block and the resulting ensemble was condensed to 4 energy groups.

Two series of calculations were run:

- The first series used RZ geometry with the control rod rings cylindricalised to thin rings (Figure A2.1). The volume of these rings corresponded to the actual volume of the control rods, i.e. the rods where not smeared with the core material located between them but their volume was preserved. Axial meshes were 5 cm over the fissile height and 10 cm in the adjacent axial blankets and shields. Radial meshes ranged from below 1 cm in the control rod rings to about 5 cm in the clean core regions. Within this series of calculations, the inner and outer SCP absorber rings were inserted synchroneously in steps of 5 cm from the fully raised to the fully inserted state.

- The second series of calculations used 1D (radial) geometry employing the same radial core model as the RZ calculations above. In this second series of calculations, an initial sodium follower in the control rod positions was progressively replaced by the 39 diluted *and* also by the non-diluted absorber cross sections.

The results of the 2 series of calculations are shown in Tables A2.1 and A2.2 and in Figures A2.2 and A2.3.

It should be mentioned that for simplicity the RZ calculations only considered SCP insertions starting at the upper core/blanket and ending at the lower core/blanket interface. In reality, a fully raised SCP absorber has its lower end about 2 mm above the upper core/ blanket interface, a fully inserted absorber about 14 mm below the lower core/blanket interface (see Figure 6 of the main part of this report). In the present context, however, these small inaccuracies can be considered negligible.

SCP Insertion Depth [cm]	k_{eff}	$\rho[pcm]$	$\Delta\rho$	Fraction of full insertion worth [%]
0	1.03874	+3729.		
5	1.03659	+3530.	-199.	1.68
10	1.03350	+3241.	-488.	4.13
15	1.02950	+2865.	-864.	7.30
20	1.02462	+2403.	-1326.	11.21
25	1.01889	+1854.	-1875.	15.85
30	1.01235	+1220.	-2509.	21.21
35	1.00507	+ 504.	-3225.	27.27
40	0.99714	- 287.	-4016.	33.95
45	0.98869	-1144.	-4873.	41.20
50	0.97989	-2052.	-5781.	48.88
55	0.97096	-2991.	-6720.	56.81
60	0.96220	-3928.	-7657.	64.74
65	0.95390	-4833.	-8562.	72.39
70	0.94641	-5662.	-9391.	79.40
75	0.93998	-6385.	-10114.	85.51
80	0.93478	-6977.	-10706.	90.51
85	0.93082	-7432.	-11161.	94.36
90	0.92802	-7756.	-11485.	97.10
95	0.92618	-7970.	-11699.	98.91
100	0.92508	-8099.	-11828.	100.00

Table A2.1 First KfK analysis of CMP. RZ calculations. 4 energy groups

Absorber fraction in diluted SCP cross sections [%]	k_{eff}	$\rho[pcm]$	$\Delta\rho$	Fraction of full insertion worth [%]
0	1.04440	+4251.		
2.5	1.03753	+3617.	-634.	5.40
5.0	1.03070	+2979.	-1272.	10.83
7.5	1.02443	+2385.	-1866.	15.88
10.0	1.01865	+1831.	-2420.	20.60
12.5	1.01329	+1312.	-2939.	25.02
15.0	1.00831	+824.	-3427.	29.17
17.5	1.00366	+365.	-3886.	33.08
20.0	0.99931	-69.	-4320.	36.77
22.5	0.99522	-480.	-4731.	40.27
25.0	0.99137	-870.	-5121.	43.59
27.5	0.98774	-1241.	-5492.	46.75
30.0	0.98431	-1594.	-5845.	49.75
32.5	0.98106	-1931.	-6182.	52.62
35.0	0.97797	-2253.	-6504.	55.36
37.5	0.97504	-2560.	-6811.	57.98
40.0	0.97224	-2855.	-7106.	60.49
42.5	0.96958	-3137.	-7388.	62.89
45.0	0.96704	-3408.	-7659.	65.19
47.5	0.96461	-3669.	-7920.	67.42
50.0	0.96228	-3920.	-8171.	69.55
52.5	0.96005	-4161.	-8412.	71.60
55.0	0.95791	-4394.	-8645.	73.59
57.5	0.95586	-4618.	-8869.	75.49
60.0	0.95389	-4834.	-9085.	77.33
62.5	0.95199	-5043.	-9294.	79.11
65.0	0.95017	-5244.	-9495.	80.82
67.5	0.94841	-5440.	-9691.	82.49
70.0	0.94672	-5628.	-9879.	84.09
72.5	0.94508	-5811.	-10062.	85.65
75.0	0.94350	-5988.	-10239.	87.16
77.5	0.94198	-6159.	-10410.	88.61
80.0	0.94050	-6326.	-10577.	90.03
82.5	0.93908	-6487.	-10738.	91.40
85.0	0.93770	-6644.	-10895.	92.74
87.5	0.93636	-6796.	-11047.	94.03
90.0	0.93506	-6945.	-11196.	95.30
92.5	0.93381	-7088.	-11339.	96.52
95.0	0.93259	-7228.	-11479.	97.71
97.5	0.93141	-7364.	-11615.	98.87
100.0	0.93026	-7497.	-11748.	100.00

Table A2.2 **First KfK analysis of CMP. 1D calculations. 4 energy groups**
All calculations used an axial buckling of $B^2 = 5.41m^{-2}$.

The equivalence relationship between control rod ring insertion and the degree of dilution of the absorber cross sections that should be used in a horizontal plane calculation to simulate this insertion, could not be established directly on the basis of the calculated SCP reactivity worths $\Delta\rho$ as the full insertion worths are found to be somewhat different in the RZ and 1D calculations. The relationship had therefore to be based on a comparison of the relative fractions of the full insertion worths obtained with the different absorber insertions and diluted cross sections, respectively. The result of this comparison is shown in Figure A2.4.

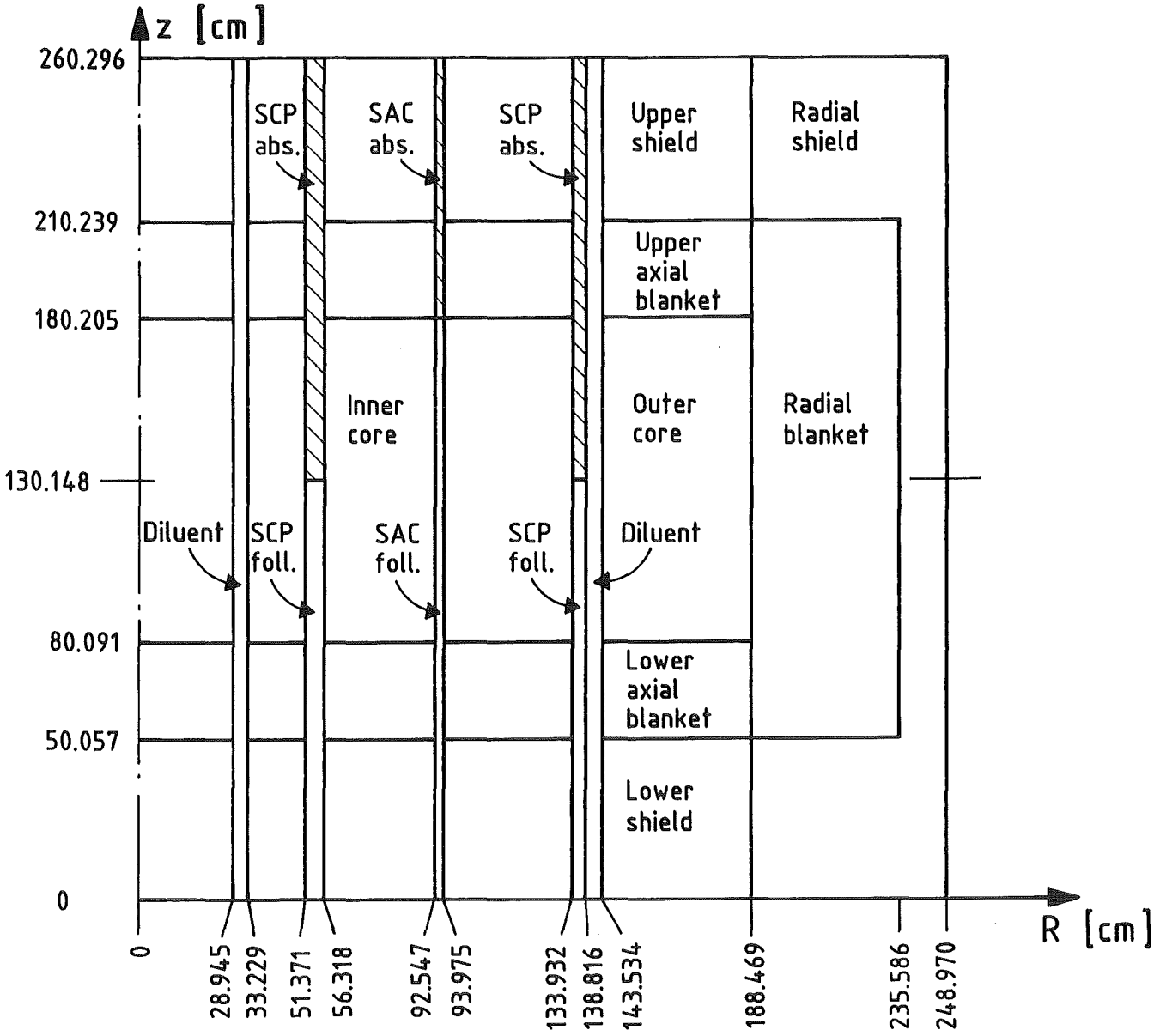

Figure A 2.1 RZ model of SPX-1

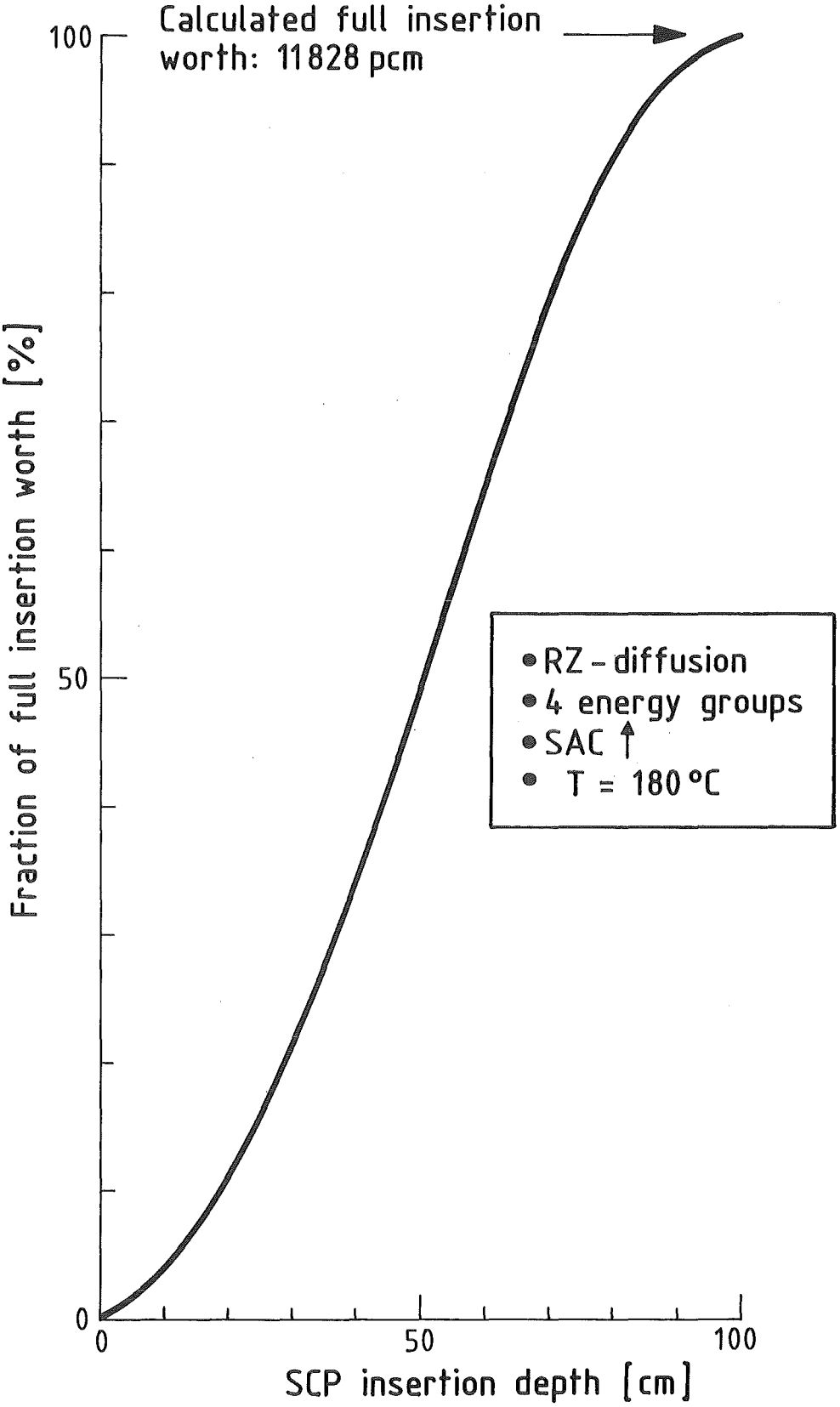

Figure A 2.2 SCP bank worth variation with insertion depth

RZ - calculation

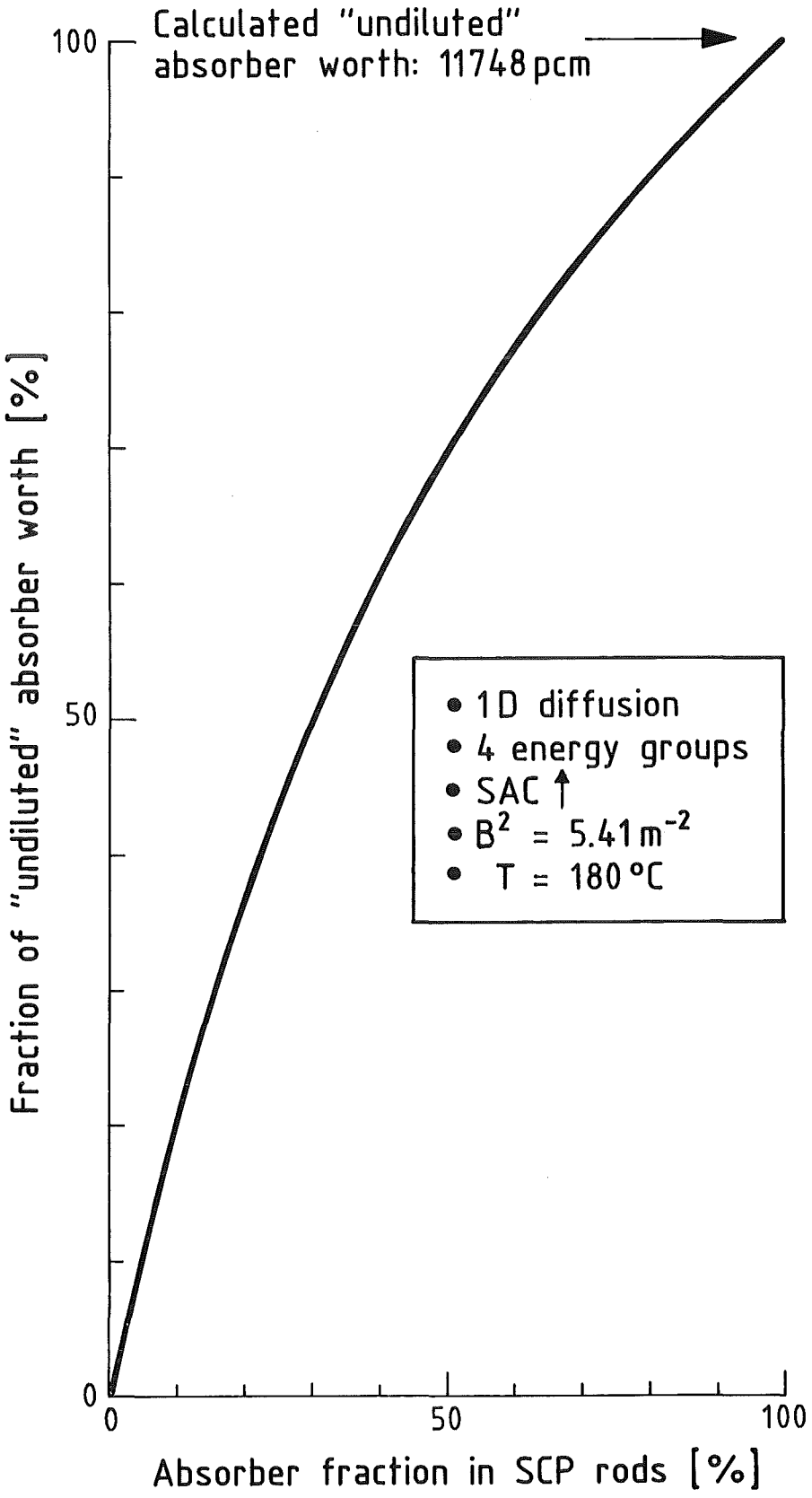

Figure A 2.3 SCP bank worth variation with absorber "dilution"

1D calculation

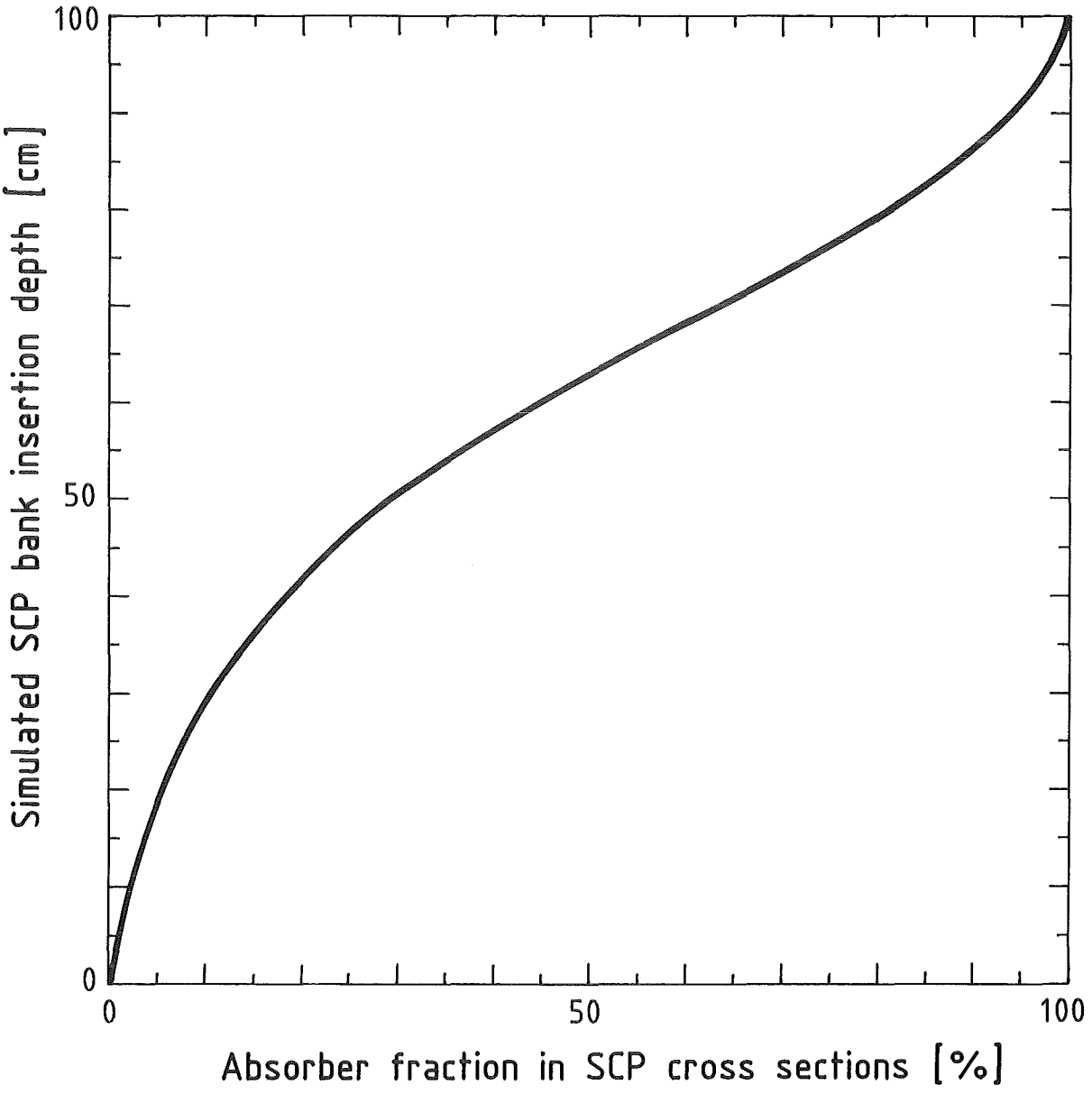

Figure A 2.4 Dilution - insertion - equivalence curve

Appendix 3

This Appendix summarizes the results of the supplementary diffusion theory calculations in 2D centre plane, in RZ and in 1D(radial) geometry, performed as part of the first KfK analysis to assess condensation and mesh size corrections.

Condensation and mesh corrections

As part of the first analysis phase, numerous calculations were run to assess condensation and mesh corrections and to check the mutual dependence of the two. The present Appendix quotes the results of these calculations, the majority of which did not serve a particular purpose but helped to arrive at a better understanding of the dependence of these corrections on control rod configurations and to see wether 3D corrections could be reliably synthesized from 2D and 1D calculations. Tables A3.3 through A3.14 refer to calculations in 2D centreplane geometry, Tables A3.15 and A3.16 to those in RZ and 1D(radial) geometry. 2D calculations were always run in both, 26 and 4 energy groups and with alternatively a radial mesh M1 and M2.

Comparing the condensation corrections 'CC' of Tables A3.7 and A3.8 with those of Tables A3.9 and A3.10, one finds that these depend only very weakly on the radial mesh grid. Similarly it is found that mesh corrections change very little when passing from calculations in 26 to 4 energy groups (Tables A3.11 through A3.14)

A comparison of condensation corrections found by combination of the results of 2D and 1D calculations with those observed in 3D calculations is presented in Table A3.1. For the 5 configurations selected here, the synthesis procedure is found to reproduce the 3D results within about 0.9%.

Configuration	CC^{rad} [%]	CC^{RZ} [%]	CC^{1D} [%]	CC^{ax} [%]	CC^{synth} [%]	CC^{3D} [%]
$SCP^{\uparrow}\ SAC^{\downarrow}$	-2.53	-1.63	-1.51	-0.12	-2.65	-3.01
$SCP^{540}\ SAC^{\uparrow}$	+1.88	-2.07	+3.03	-5.10	-3.22	-2.34
$SCP^{540}\ SAC^{\downarrow}$	+1.22	-1.65	+2.00	-3.65	-2.43	-2.29
$SCP^{\downarrow}\ SAC^{\uparrow}$	-2.40	-1.86	-1.67	-0.19	-2.59	-2.58
$SCP^{\downarrow}\ SAC^{\downarrow}$	-2.21	-1.47	-1.29	-0.18	-2.39	-2.42

Table A3.1 First KfK analysis of CMP. Condensation corrections to rod worths.
Axial condensation corrections were obtained from the difference of the corrections found in RZ and in 1D geometry.
Condensation corrections for the critical insertion level of SCP ('$SCP^{540'}$ which in the later analysis phases was corrected to '$SCP^{542'}$) were obtained by forming the mean value of the corrections found for the 'frame values'; i.e. '$SCP^{567'}$ and '$SCP^{517'}$ in RZ geometry and '$SCP^{550'}$ and '$SCP^{530'}$ in 1D geometry, respectively.

Radial mesh corrections used for the core excess reactivity and criticality prediction of the first analysis phase (see Sec.III.6.3) were derived from Tables A3.3 to A3.6. Using the results of the calculations in 26 energy groups and alternatively a radial mesh M1 or M2, application of the extrapolation formula discussed in Sec. III.5 ($k_{eff}^{M\infty} = (4k_{eff}^{M2} - k_{eff}^{M1})/3$) led to the corrections summarized in Table A3.2 below.

Control rod configuration	k_{eff}^{M1}	k_{eff}^{M2}	$k_{eff}^{M_\infty}$	Mesh correction $CM^{M2 \rightarrow M_\infty}$ [pcm]
Note: C1D results:				
$SCP^{\uparrow}$, $SAC^{\uparrow}$	1.00273	1.00430	1.00482	+52
SCP^{894}, $SAC^{\uparrow}$	0.99468	0.99622	0.99673	+51
SCP^{929}, $SAC^{\uparrow}$				+52
Note: CMP results:				
$SCP^{\uparrow}$, $SAC^{\uparrow}$	1.04323	1.04402	1.04428	+26
SCP^{530}, $SAC^{\uparrow}$	0.98786	0.99079	0.99177	+98
SCP^{550}, $SAC^{\uparrow}$	0.99112	0.99381	0.99471	+90
SCP^{540}, $SAC^{\uparrow}$				+94

Table A3.2 First KfK analysis of CMP. Radial mesh corrections for CMP and C1D.

The calculations that served to produce these corrections were run using SCP absorber dilutions which showed, according to the insertion-dilution equivalence model developed in Appendix 1, the closest correspondence to the actual absorber insertions. The final corrections were then obtained by simple linear interpolation.

The presentation of the detailed results of the calculations starts on the following page. This blank page was inserted to allow the presentation of results obtained with M1 and M2 radial mesh on opposing pages and thus to facilitate their comparison. The same applies to the results obtained in 4 and 26 energy groups and in RZ and 1D(radial) geometry, respectively.

Configuration	2D Diffusion 26 energy groups, M1		2D Diffusion 4 energy groups, M1	
	k_{eff}	$\rho[pcm]$	k_{eff}	$\rho[pcm]$
$SCP^{\uparrow}$ $SAC^{\uparrow}$	1.04323	+4143.5	1.04429	+4241.3
$SCP^{\uparrow}$ $SAC^{\downarrow ul}$	1.02843	+2764.4	1.02898	+2816.3
$SCP^{\uparrow}$ $SAC^{\downarrow ll}$	1.03205	+3105.9	1.03290	+3185.7
$SCP^{\uparrow}$ $SAC^{\downarrow av}$	1.03047	+2956.5	1.03119	+3024.7
SCP^{550} $SAC^{\uparrow}$	0.99112	-895.4	0.99311	-693.7
SCP^{550} $SAC^{\downarrow ul}$	0.97622	-2435.4	0.97784	-2266.0
SCP^{550} $SAC^{\downarrow ll}$	0.97972	-2069.7	0.98160	-1874.9
SCP^{550} $SAC^{\downarrow av}$	0.97817	-2231.4	0.97994	-2047.0
SCP^{530} $SAC^{\uparrow}$	0.98786	-1229.0	0.98969	-1041.4
SCP^{530} $SAC^{\downarrow ul}$	0.97297	-2778.4	0.97444	-2622.8
SCP^{530} $SAC^{\downarrow ll}$	0.97645	-2411.8	0.97818	-2230.9
SCP^{530} $SAC^{\downarrow av}$	0.97491	-2574.0	0.97653	-2403.4
$SCP^{\downarrow}$ $SAC^{\uparrow}$	0.93710	-6712.7	0.93579	-6861.6
$SCP^{\downarrow}$ $SAC^{\downarrow ul}$	0.92276	-8370.2	0.92127	-8545.3
$SCP^{\downarrow}$ $SAC^{\downarrow ll}$	0.92586	-8007.6	0.92454	-8161.8
$SCP^{\downarrow}$ $SAC^{\downarrow av}$	0.92446	-8170.9	0.92307	-8333.7
SCP^{512} $SAC^{\uparrow}$	0.98479	-1544.7	0.98647	-1371.7
SCP^{530} $B4^{\uparrow}$ $SAC^{\uparrow}$	0.99216	-789.8	0.99393	-610.9
SCP^{530} $B4^{\downarrow}$ $SAC^{\uparrow}$	0.98552	-1469.0	0.98720	-1296.6
SCP^{512} $B4^{\uparrow}$ $SAC^{\uparrow}$	0.98940	-1071.6	0.99102	-906.5
SCP^{512} $B4^{\downarrow}$ $SAC^{\uparrow}$	0.98258	-1772.5	0.98411	-1614.2

Table A3.3 First KfK analysis of CMP. 2D calculations, radial mesh M1

For configurations where SAC was inserted, three calculations were run: One using the upper/central link absorber ('ul'), one using the lower link absorber ('ll') and one using axially volume averaged cross sections ('av'). Partial SCP insertion was approached using two different sets of diluted SCP absorber cross sections, which according to the dilution-insertion-equivalence model 'framed' the real insertion level. The axial buckling was $B^2 = 5.41m^{-2}$

Configuration	2D Diffusion 26 energy groups, M1		2D Diffusion 4 energy groups, M1	
	k_{eff}	$\rho[pcm]$	k_{eff}	$\rho[pcm]$
$SCP^{\uparrow}$ $SAC^{\uparrow}$	1.00273	+272.6	1.00280	+279.4
SCP^{894} $SAC^{\uparrow}$	0.99468	-534.4	0.99590	-412.0

Table A3.4 First KfK analysis of C1D. 2D calculations, radial mesh M1

Configuration	2D Diffusion 26 energy groups, M2		2D Diffusion 4 energy groups, M2	
	k_{eff}	$\rho[pcm]$	k_{eff}	$\rho[pcm]$
$SCP^{\uparrow}\ SAC^{\uparrow}$	1.04402	+4216.4	1.04506	+4311.7
$SCP^{\uparrow}\ SAC^{\downarrow ul}$	1.03008	+2920.4	1.03063	+2971.7
$SCP^{\uparrow}\ SAC^{\downarrow ll}$	1.03340	+3232.0	1.03422	+3309.2
$SCP^{\uparrow}\ SAC^{\downarrow av}$	1.03193	+3093.8	1.03264	+3160.5
$SCP^{550}\ SAC^{\uparrow}$	0.99381	-623.2	0.99574	-427.7
$SCP^{550}\ SAC^{\downarrow ul}$	0.97977	-2065.0	0.98135	-1900.0
$SCP^{550}\ SAC^{\downarrow ll}$	0.98298	-1731.1	0.98481	-1542.8
$SCP^{550}\ SAC^{\downarrow av}$	0.98154	-1880.5	0.98327	-1701.6
$SCP^{530}\ SAC^{\uparrow}$	0.99079	-929.5	0.99256	-749.8
$SCP^{530}\ SAC^{\downarrow ul}$	0.97676	-2379.5	0.97819	-2229.9
$SCP^{530}\ SAC^{\downarrow ll}$	0.97996	-2044.8	0.98162	-1871.9
$SCP^{530}\ SAC^{\downarrow av}$	0.97852	-2194.6	0.98009	-2031.1
$SCP^{\downarrow}\ SAC^{\uparrow}$	0.94542	-5772.8	0.94409	-5922.3
$SCP^{\downarrow}\ SAC^{\downarrow ul}$	0.93178	-7321.7	0.93029	-7493.5
$SCP^{\downarrow}\ SAC^{\downarrow ll}$	0.93470	-6986.5	0.93336	-7139.4
$SCP^{\downarrow}\ SAC^{\downarrow av}$	0.93337	-7138.7	0.93198	-7299.0
$SCP^{512}\ SAC^{\uparrow}$	0.98797	-1218.0	0.98956	-1054.5
$SCP^{530}\ B4^{\uparrow}\ SAC^{\uparrow}$	0.99484	-518.3	0.99654	-346.9
$SCP^{530}\ B4^{\downarrow}\ SAC^{\uparrow}$	0.98867	-1145.8	0.99029	-980.8
$SCP^{512}\ B4^{\uparrow}\ SAC^{\uparrow}$	0.99229	-777.0	0.99383	-620.7
$SCP^{512}\ B4^{\downarrow}\ SAC^{\uparrow}$	0.98597	-1422.9	0.98743	-1273.3

Table A3.5 **First KfK analysis of CMP. 2D calculations, radial mesh M2**
For comments see previous table.

Configuration	2D Diffusion 26 energy groups, M2		2D Diffusion 4 energy groups, M2	
	k_{eff}	$\rho[pcm]$	k_{eff}	$\rho[pcm]$
$SCP^{\uparrow}\ SAC^{\uparrow}$	1.00430	+428.6	1.00435	+433.2
$SCP^{894}\ SAC^{\uparrow}$	0.99622	-378.9	0.99751	-250.0

Table A3.6 **First KfK analysis of C1D. 2D calculations, radial mesh M2**

Configuration	Calculated rod worths relative to $SCP^{\uparrow}$ $SAC^{\uparrow}$ $\Delta\rho^{calc.}[pcm]$		CC^{M1} [%]	Resulting SAC or B4 worth $\Delta\rho^{calc.}_{SAC}$ or $\Delta\rho^{calc.}_{B4}$ [pcm]		CC^{M1} [%] (SAC)
	26 groups	4 groups		26 gr.	4 gr.	
$SCP^{\uparrow}$ $SAC^{\uparrow}$	0	0		1379.1^{ul}	1425.0^{ul}	-3.22^{ul}
$SCP^{\uparrow}$ $SAC^{\downarrow ul}$	-1379.1	-1425.0	-3.22	1037.6^{ll}	1055.6^{ll}	-1.71^{ll}
$SCP^{\uparrow}$ $SAC^{\downarrow ll}$	-1037.6	-1055.6	-1.71	1187.0^{av}	1216.6^{av}	-2.43^{av}
$SCP^{\uparrow}$ $SAC^{\downarrow av}$	-1187.0	-1216.6	-2.43			
SCP^{550} $SAC^{\uparrow}$	-5038.9	-4935.0	+2.11	1540.0^{ul}	1572.3^{ul}	-2.05^{ul}
SCP^{550} $SAC^{\downarrow ul}$	-6578.9	-6507.3	+1.10	1174.3^{ll}	1181.2^{ll}	-0.58^{ll}
SCP^{550} $SAC^{\downarrow ll}$	-6213.2	-6116.2	+1.59	1336.0^{av}	1353.3^{av}	-1.28^{av}
SCP^{550} $SAC^{\downarrow av}$	-6374.9	-6288.3	+1.38			
SCP^{530} $SAC^{\uparrow}$	-5372.5	-5282.7	+1.70	1549.4^{ul}	1581.4^{ul}	-2.02^{ul}
SCP^{530} $SAC^{\downarrow ul}$	-6921.9	-6864.1	+0.84	1182.8^{ll}	1189.5^{ll}	-0.56^{ll}
SCP^{530} $SAC^{\downarrow ll}$	-6555.3	-6472.2	+1.28	1345.0^{av}	1362.0^{av}	-1.25^{av}
SCP^{530} $SAC^{\downarrow av}$	-6717.5	-6644.7	+1.10			
$SCP^{\downarrow}$ $SAC^{\uparrow}$	-10856.2	-11102.9	-2.22	1657.5^{ul}	1683.7^{ul}	-1.56^{ul}
$SCP^{\downarrow}$ $SAC^{\downarrow ul}$	-12513.7	-12786.6	-2.13	1294.9^{ll}	1300.2^{ll}	-0.41^{ll}
$SCP^{\downarrow}$ $SAC^{\downarrow ll}$	-12151.1	-12403.1	-2.03	1458.2^{av}	1472.1^{av}	-0.94^{av}
$SCP^{\downarrow}$ $SAC^{\downarrow av}$	-12314.4	-12575.0	-2.07			
SCP^{512} $SAC^{\uparrow}$	-5688.2	-5613.0	+1.34			
SCP^{530} $B4^{\uparrow}$ $SAC^{\uparrow}$	-4933.3	-4852.2	+1.67	679.2	685.7	-0.95
SCP^{530} $B4^{\downarrow}$ $SAC^{\uparrow}$	-5612.5	-5537.9	+1.35			
SCP^{512} $B4^{\uparrow}$ $SAC^{\uparrow}$	-5215.1	-5147.8	+1.31	700.9	707.7	-0.96
SCP^{512} $B4^{\downarrow}$ $SAC^{\uparrow}$	-5916.0	-5855.5	+1.03			

Table A3.7 First KfK analysis of CMP. 2D calculations, radial mesh M1

Configuration	Calculated rod worths relative to $SCP^{\uparrow}$ $SAC^{\uparrow}$ $\Delta\rho^{calc.}[pcm]$		CC^{M1} [%]
	26 groups	4 groups	
$SCP^{\uparrow}$ $SAC^{\uparrow}$	0.	0.	
SCP^{894} $SAC^{\uparrow}$	-807.0	-691.4	+16.72

Table A3.8 First KfK analysis of C1D. 2D calculations, radial mesh M1

Configuration	Calculated rod worths relative to $SCP^{\uparrow}$ $SAC^{\uparrow}$ $\Delta\rho^{calc.}[pcm]$		CC^{M2} [%]	Resulting SAC or B4 worth $\Delta\rho^{calc.}_{SAC}$ or $\Delta\rho^{calc.}_{B4}$ [pcm]		CC^{M2} [%] (SAC)
	26 groups	4 groups		26 gr.	4 gr.	
$SCP^{\uparrow}$ $SAC^{\uparrow}$	0	0		1295.6^{ul}	1340.1^{ul}	-3.32^{ul}
$SCP^{\uparrow}$ $SAC^{\downarrow ul}$	-1295.6	-1340.1	-3.32	984.0^{ll}	1002.6^{ll}	-1.86^{ll}
$SCP^{\uparrow}$ $SAC^{\downarrow ll}$	-984.0	-1002.6	-1.86	1122.2^{av}	1151.3^{av}	-2.53^{av}
$SCP^{\uparrow}$ $SAC^{\downarrow av}$	-1122.2	-1151.3	-2.53			
SCP^{550} $SAC^{\uparrow}$	-4839.2	-4739.5	+2.10	1441.8^{ul}	1472.3^{ul}	-2.07^{ul}
SCP^{550} $SAC^{\downarrow ul}$	-6281.0	-6211.8	+1.11	1107.9^{ll}	1115.1^{ll}	-0.65^{ll}
SCP^{550} $SAC^{\downarrow ll}$	-5947.1	-5854.6	+1.58	1257.3^{av}	1273.9^{av}	-1.30^{av}
SCP^{550} $SAC^{\downarrow av}$	-6096.5	-6013.4	+1.38			
SCP^{530} $SAC^{\uparrow}$	-5145.5	-5061.6	+1.66	1450.0^{ul}	1480.1^{ul}	-2.03^{ul}
SCP^{530} $SAC^{\downarrow ul}$	-6595.5	-6541.7	+0.82	1115.3^{ll}	1122.1^{ll}	-0.61^{ll}
SCP^{530} $SAC^{\downarrow ll}$	-6260.8	-6183.7	+1.25	1265.1^{av}	1281.3^{av}	-1.26^{av}
SCP^{530} $SAC^{\downarrow av}$	-6410.6	-6342.9	+1.07			
$SCP^{\downarrow}$ $SAC^{\uparrow}$	-9988.8	-10234.1	-2.40	1548.9^{ul}	1571.2^{ul}	-1.42^{ul}
$SCP^{\downarrow}$ $SAC^{\downarrow ul}$	-11537.7	-11805.3	-2.27	1213.7^{ll}	1217.1^{ll}	-0.28^{ll}
$SCP^{\downarrow}$ $SAC^{\downarrow ll}$	-11202.5	-11451.2	-2.17	1365.9^{av}	1376.7^{av}	-0.78^{av}
$SCP^{\downarrow}$ $SAC^{\downarrow av}$	-11354.7	-11610.8	-2.21			
SCP^{512} $SAC^{\uparrow}$	-5434.0	-5366.3	+1.26			
SCP^{530} $B4^{\uparrow}$ $SAC^{\uparrow}$	-4734.3	-4658.7	+1.62	627.5	633.9	-1.01
SCP^{530} $B4^{\downarrow}$ $SAC^{\uparrow}$	-5361.8	-5292.6	+1.31			
SCP^{512} $B4^{\uparrow}$ $SAC^{\uparrow}$	-4993.0	-4932.5	+1.23	645.9	652.6	-1.03
SCP^{512} $B4^{\downarrow}$ $SAC^{\uparrow}$	-5638.9	-5585.1	+0.96			

Table A3.9 First KfK analysis of CMP. 2D calculations, radial mesh M2

Configuration	Calculated rod worths relative to $SCP^{\uparrow}$ $SAC^{\uparrow}$ $\Delta\rho^{calc.}[pcm]$		CC^{M2} [%]
	26 groups	4 groups	
$SCP^{\uparrow}$ $SAC^{\uparrow}$	0.	0.	
SCP^{894} $SAC^{\uparrow}$	-807.5	-683.2	+18.19

Table A3.10 First KfK analysis of C1D. 2D calculations, radial mesh M2

Configuration	Calculated rod worths relative to $SCP^{\uparrow}$ $SAC^{\uparrow}$ $\Delta\rho^{calc.}[pcm]$			$CM^{M1\rightarrow M_\infty}$ [%]	$CM^{M2\rightarrow M_\infty}$ [%]
	M1	M2	M∞		
$SCP^{\uparrow}$ $SAC^{\uparrow}$	0	0	0		
$SCP^{\uparrow}$ $SAC^{\downarrow ul}$	-1425.0	-1340.1	-1311.9	-7.94	-2.10
$SCP^{\uparrow}$ $SAC^{\downarrow ll}$	-1055.6	-1002.6	-984.9	-6.70	-1.77
$SCP^{\uparrow}$ $SAC^{\downarrow av}$	-1216.6	-1151.3	-1129.5	-7.16	-1.89
SCP^{550} $SAC^{\uparrow}$	-4935.0	-4739.5	-4674.6	-5.28	-1.37
SCP^{550} $SAC^{\downarrow ul}$	-6507.3	-6211.8	-6113.8	-6.05	-1.58
SCP^{550} $SAC^{\downarrow ll}$	-6116.2	-5854.6	-5767.8	-5.70	-1.48
SCP^{550} $SAC^{\downarrow av}$	-6288.3	-6013.4	-5922.3	-5.82	-1.51
SCP^{530} $SAC^{\uparrow}$	-5282.7	-5061.6	-4988.2	-5.57	-1.45
SCP^{530} $SAC^{\downarrow ul}$	-6864.1	-6541.7	-6434.9	-6.25	-1.63
SCP^{530} $SAC^{\downarrow ll}$	-6472.2	-6183.7	-6088.1	-5.93	-1.55
SCP^{530} $SAC^{\downarrow av}$	-6644.7	-6342.9	-6242.9	-6.05	-1.58
$SCP^{\downarrow}$ $SAC^{\uparrow}$	-11102.9	-10234.1	-9948.1	-10.40	-2.79
$SCP^{\downarrow}$ $SAC^{\downarrow ul}$	-12786.6	-11805.3	-11482.7	-10.20	-2.73
$SCP^{\downarrow}$ $SAC^{\downarrow ll}$	-12403.1	-11451.2	-11138.2	-10.20	-2.73
$SCP^{\downarrow}$ $SAC^{\downarrow av}$	-12575.0	-11610.8	-11293.8	-10.20	-2.73
SCP^{512} $SAC^{\uparrow}$	-5613.0	-5366.3	-5284.5	-5.85	-1.52
SCP^{530} $B4^{\uparrow}$ $SAC^{\uparrow}$	-4852.2	-4658.7	-4594.5	-5.31	-1.38
SCP^{530} $B4^{\downarrow}$ $SAC^{\uparrow}$	-5537.9	-5292.6	-5211.2	-5.90	-1.54
SCP^{512} $B4^{\uparrow}$ $SAC^{\uparrow}$	-5147.8	-4932.5	-4861.2	-5.57	-1.45
SCP^{512} $B4^{\downarrow}$ $SAC^{\uparrow}$	-5855.5	-5585.1	-5495.5	-6.15	-1.60

Table A3.11 First KfK analysis of CMP. 2D calculations, 4 energy groups

Configuration	Calculated rod worths relative to $SCP^{\uparrow}$ $SAC^{\uparrow}$ $\Delta\rho^{calc.}[pcm]$			$CM^{M1\rightarrow M_\infty}$ [%]	$CM^{M2\rightarrow M_\infty}$ [%]
	M1	M2	M∞		
$SCP^{\uparrow}$ $SAC^{\uparrow}$	0	0	0		
SCP^{894} $SAC^{\uparrow}$	-691.4	-683.2	-680.6	-1.56	-0.38

Table A3.12 First KfK analysis of C1D. 2D calculations, 4 energy groups

Configuration	Calculated rod worths relative to $SCP^{\uparrow}$ $SAC^{\uparrow}$ $\Delta\rho^{calc.}[pcm]$			$CM^{M1\rightarrow M_\infty}$ [%]	$CM^{M2\rightarrow M_\infty}$ [%]
	M1	M2	M∞		
$SCP^{\uparrow}$ $SAC^{\uparrow}$	0	0	0		
$SCP^{\uparrow}$ $SAC^{\downarrow ul}$	-1379.1	-1295.6	-1268.0	-8.06	-2.13
$SCP^{\uparrow}$ $SAC^{\downarrow ll}$	-1037.6	-984.0	-966.3	-6.87	-1.80
$SCP^{\uparrow}$ $SAC^{\downarrow av}$	-1187.0	-1122.2	-1100.7	-7.27	-1.92
SCP^{S50} $SAC^{\uparrow}$	-5038.9	-4839.2	-4773.0	-5.28	-1.37
SCP^{S50} $SAC^{\downarrow ul}$	-6578.9	-6281.0	-6182.3	-6.03	-1.57
SCP^{S50} $SAC^{\downarrow ll}$	-6213.2	-5947.1	-5859.0	-5.70	-1.48
SCP^{S50} $SAC^{\downarrow av}$	-6374.9	-6096.5	-6004.3	-5.81	-1.51
SCP^{S30} $SAC^{\uparrow}$	-5372.5	-5145.5	-5070.2	-5.63	-1.46
SCP^{S30} $SAC^{\downarrow ul}$	-6921.9	-6595.5	-6487.4	-6.28	-1.64
SCP^{S30} $SAC^{\downarrow ll}$	-6555.3	-6260.8	-6163.2	-5.98	-1.56
SCP^{S30} $SAC^{\downarrow av}$	-6717.5	-6410.6	-6309.0	-6.08	-1.58
$SCP^{\downarrow}$ $SAC^{\uparrow}$	-10856.2	-9988.8	-9703.4	-10.62	-2.86
$SCP^{\downarrow}$ $SAC^{\downarrow ul}$	-12513.7	-11537.7	-11216.9	-10.36	-2.78
$SCP^{\downarrow}$ $SAC^{\downarrow ll}$	-12151.1	-11202.5	-10890.6	-10.37	-2.78
$SCP^{\downarrow}$ $SAC^{\downarrow av}$	-12314.4	-11354.7	-11039.2	-10.36	-2.78
SCP^{S12} $SAC^{\uparrow}$	-5688.2	-5434.0	-5349.8	-5.95	-1.52
SCP^{S30} $B4^{\uparrow}$ $SAC^{\uparrow}$	-4933.3	-4734.3	-4668.4	-5.37	-1.39
SCP^{S30} $B4^{\downarrow}$ $SAC^{\uparrow}$	-5612.5	-5361.8	-5278.7	-5.95	-1.55
SCP^{S12} $B4^{\uparrow}$ $SAC^{\uparrow}$	-5215.1	-4993.0	-4919.4	-5.67	-1.47
SCP^{S12} $B4^{\downarrow}$ $SAC^{\uparrow}$	-5916.0	-5638.9	-5547.1	-6.24	-1.63

Table A3.13 First KfK analysis of CMP. 2D calculations, 26 energy groups

Configuration	Calculated rod worths relative to $SCP^{\uparrow}$ $SAC^{\uparrow}$ $\Delta\rho^{calc.}[pcm]$			$CM^{M1\rightarrow M_\infty}$ [%]	$CM^{M2\rightarrow M_\infty}$ [%]
	M1	M2	M∞		
$SCP^{\uparrow}$ $SAC^{\uparrow}$	0	0	0		
SCP^{894} $SAC^{\uparrow}$	-807.0	-807.5	-807.6	+0.07	+0.01

Table A3.14 First KfK analysis of C1D. 2D calculations, 26 energy groups

Configuration	k_{eff}	$\rho[pcm]$	$\Delta\rho[pcm]$	$CC^{RZ}[\%]$
Note: Calculations in 26 energy groups				
$SCP^{\uparrow}\ SAC^{\uparrow}$	1.03759	+3623.0		
$SCP^{\uparrow}\ SAC^{\downarrow}$	1.01491	+1468.7	-2154.3	
$SCP^{567}\ SAC^{\uparrow}$	0.98908	-1104.2	-4727.2	
$SCP^{567}\ SAC^{\downarrow}$	0.96751	-3357.9	-6980.9	
$SCP^{517}\ SAC^{\uparrow}$	0.98052	-1986.3	-5609.3	
$SCP^{517}\ SAC^{\downarrow}$	0.95930	-4243.0	-7866.0	
$SCP^{\downarrow}\ SAC^{\uparrow}$	0.92697	-7877.9	-11500.9	
$SCP^{\downarrow}\ SAC^{\downarrow}$	0.91016	-9871.0	-13494.0	
Note: Calculations in 4 energy groups				
$SCP^{\uparrow}\ SAC^{\uparrow}$	1.03867	+3723.2		
$SCP^{\uparrow}\ SAC^{\downarrow}$	1.01557	+1533.1	-2190.1	-1.63
$SCP^{567}\ SAC^{\uparrow}$	0.98908	-1104.5	-4827.7	-2.08
$SCP^{567}\ SAC^{\downarrow}$	0.96735	-3375.3	-7098.5	-1.66
$SCP^{517}\ SAC^{\uparrow}$	0.98035	-2004.4	-5727.6	-2.07
$SCP^{517}\ SAC^{\downarrow}$	0.95901	-4274.5	-7997.7	-1.65
$SCP^{\downarrow}\ SAC^{\uparrow}$	0.92597	-7995.2	-11718.4	-1.86
$SCP^{\downarrow}\ SAC^{\downarrow}$	0.90932	-9972.0	-13695.2	-1.47

Table A3.15 First KfK analysis of CMP. RZ calculations. 26, 4 energy groups

As usual, condensation corrections, given in the last column as CC^{RZ} indicate the percentage by which rod worths $\Delta\rho$ obtained in 4 energy groups have to be reduced to obtain the results in 26 energy groups.

The 4 group results differ to some extent from those found in the assessment of the dilution-insertion-equivalence model (Appendix 2, Table A2.1) as somewhat different condensation spectra were used in the two sets of calculations.

Configuration	k_{eff}	$\rho[pcm]$	$\Delta\rho[pcm]$	$CC^{1D}[\%]$
Note: Calculations in 26 energy groups				
$SCP^{\uparrow}\ SAC^{\uparrow}$	1.04316	+4137.4		
$SCP^{\uparrow}\ SAC^{\downarrow av}$	1.02010	+1970.9	-2166.5	
$SCP^{S50}\ SAC^{\uparrow}$	0.98929	-1082.6	-5220.0	
$SCP^{S50}\ SAC^{\downarrow av}$	0.96759	-3349.6	-7487.0	
$SCP^{S30}\ SAC^{\uparrow}$	0.98581	-1439.4	-5576.8	
$SCP^{S30}\ SAC^{\downarrow av}$	0.96428	-3704.0	-7841.4	
$SCP^{\downarrow}\ SAC^{\uparrow}$	0.93190	-7307.7	-11445.1	
$SCP^{\downarrow}\ SAC^{\downarrow av}$	0.91514	-9272.8	-13410.2	
Note: Calculations in 4 energy groups				
$SCP^{\uparrow}\ SAC^{\uparrow}$	1.04422	+4234.7		
$SCP^{\uparrow}\ SAC^{\downarrow av}$	1.02077	+2035.0	-2199.7	-1.51
$SCP^{S50}\ SAC^{\uparrow}$	0.99185	-821.7	-5056.4	+3.24
$SCP^{S50}\ SAC^{\downarrow av}$	0.96996	-3097.2	-7331.9	+2.12
$SCP^{S30}\ SAC^{\uparrow}$	0.98825	-1189.0	-5423.7	+2.82
$SCP^{S30}\ SAC^{\downarrow av}$	0.96654	-3462.3	-7697.0	+1.88
$SCP^{\downarrow}\ SAC^{\uparrow}$	0.93106	-7404.5	-11639.2	-1.67
$SCP^{\downarrow}\ SAC^{\downarrow av}$	0.91449	-9350.2	-13584.9	-1.29

Table A3.16 First KfK analysis of CMP. 1D calculations. 26 and 4 energy groups
All calculations used an axial buckling of $B^2 = 5.41m^{-2}$. Partial SCP bank insertions (levels '550' and '530') were simulated by the use of adequately diluted absorbers. For cases with inserted SAC, the axially volume averaged cross sections of SAC were used.
For further comments see previous table.

Appendix 4

On the influence of SCP bank insertion on single rod worths

On the influence of SCP bank insertion on single rod worths

With the objective to clarify the origin of the enhanced overestimation of an individual rod worth (C/E = 1.28) found in the first KfK analysis, a number of calculations was run that served to estimate the influence of a bankwise insertion of the complete SCP system less one control rod on the worth of that residual rod. Chosen for the individual rod were the inner ring rod B4 and the outer ring rod B12 respectively; the latter only for reasons of general interest rather than for a specific analysis.
All calculations were run in 4 energy groups, mesh M1 and 2D centre-plane geometry with an axial buckling of 5.67 m^{-2}

The investigations were organized in the following way:
In a first step, the reactivity worth of the control rod in question was determined in the all-follower core, i.e. in the situation where all control rod absorbers are fully raised. In this case the core reactivity perturbation caused by the other rods of the SCP system was zero, and the reactivity difference between the all-follower core and the situation with one rod fully inserted gave the unperturbed worth of that individual rod. Subsequently, the initial sodium-follower composition of the other SCP rods was stepwise replaced by differently concentrated absorbers, which can be understood as a simulation of a stepwise insertion of SCP. Such absorber cross sections were available from the dilution-insertion-eqivalence model of Appendix 2. For each of the so created core reactivity perturbations, the worth of the individual rod, i.e. the reactivity difference between the states fully raised and fully inserted, was determined.
For the individual rods also, differently concentrated absorbers were used:
In the case of B4 :

1. The full concentration absorber ('100%') as obtained from the cross section production of Sec. III.2.2,

2. A cross section mixture of 72.5% of absorber and 27.5% sodium follower cross sections, giving a good reproduction of the B4 worth predicted in the first KfK analysis phase. See below for further details.

3. A mixture with a corresponding ratio of 45% / 55%, giving - in combination with the correct SCP-worth - a B4 worth of ≃475pcm, close to the measured value of 478.5pcm.

In the case of B12 :

1. The full concentration absorber ('100%'), and

2. An absorber/sodium-follower mixture of 45% / 55%.

The results obtained for rod B4 are listed in Tables A4.1 through A4.3 and in Figure A4.1. Those for B12 in Tables A4.4 and A4.5 and in Figure A4.2.

Passing from zero core perturbation to about 10000 pcm, the worth of B4 is found to be approximately tripled, that of B12 is even increased by approximately a factor of 10. Obviously, these calculations are run on too low a level to give very reliable answers, but for the present purpose they can be considered sufficiently accurate.

Going back to the results of Sec. III.6.1, we find that the final prediction for the reactivity difference between configuration $SCP^{520}\ B4^{\uparrow}$ and the all follower core was 4617.8 pcm and that the worth of B4 inserted from this situation was predicted to

be 615.1 pcm. This situation is well reproduced in Figure A4.1 when the 72.5% absorber curve is used for B4. It is very likely that the above reactivity difference of 4617.8 pcm is similarly overpredicted as the reactivity held down at critical (C/E = 1.23 in line 1 of Table 5). We therefore reduced the value of 4617.8 pcm by 23% and obtained a value of -3754 pcm. This value was also indicated in Figure A4.1 and a corresponding B4 worth of 560 pcm is found.[9] Comparing this latter value with the measured rod worth of 478.5 pcm, one obtains C/E = 1.17, which is 8.5% lower than the initially found C/E ratio of 1.28, and close to the C/E ratios found for bankwise insertions.

One concludes that the enhanced overprediction of the worth of the individual rod B4 was a consequence of the overprediction of the worth of the remaining SCP rods. A realistic prediction of the latter worth would have led to a C/E ratio much closer to those found for rod banks.

---

[9] Using the up to now most accurate absorber cross sections, the third phase of the KfK/BN analysis produced a value for the reactivity difference between the all-follower core and SCP^{520} $B4^{\uparrow}$ of 3661.3pcm (see Table 17 of Sec.VI.2). Using this value in Figure A4.1 would have given a B4 worth of ≃555pcm, i.e. very close to the value used above.

In these calculations a 100%(non-diluted) absorber was used for $B4^{\downarrow}$

Control rod configuration	k_{eff}	$\rho[pcm]$	Core reactivity perturbation due to SCP insertion $\Delta\rho[pcm]$	Worth of B4 insertion [pcm]
$SCP^{\uparrow}$, $B4^{\uparrow}$	1.03847	+3704.4	0	-437.0
$SCP^{\uparrow}$, $B4^{\downarrow}$	1.03378	+3267.4		
SCP5.0% *abs*, $B4^{\uparrow}$	1.02604	+2537.9	-1166.5	-482.1
SCP5.0% *abs*, $B4^{\downarrow}$	1.02099	+2055.8		
SCP10.0% *abs*, $B4^{\uparrow}$	1.01535	+1511.6	-2192.8	-527.4
SCP10.0% *abs*, $B4^{\downarrow}$	1.00994	+984.2		
SCP17.44% *abs*, $B4^{\uparrow}$	1.00278	+277.4	-3427.0	-591.7
SCP17.44% *abs*, $B4^{\downarrow}$	0.99687	-314.3		
SCP25.0% *abs*, $B4^{\uparrow}$	0.99187	-819.9	-4524.3	-660.2
SCP25.0% *abs*, $B4^{\downarrow}$	0.98541	-1480.1		
SCP97.5% *abs*, $B4^{\uparrow}$	0.94328	-6013.5	-9717.9	-1237.6
SCP97.5% *abs*, $B4^{\downarrow}$	0.93239	-7251.1		
SCP100.0% *abs*, $B4^{\uparrow}$	0.94238	-6114.4	-9818.8	-1255.0
SCP100.0% *abs*, $B4^{\downarrow}$	0.93136	-7369.4		

Table A4.1 The influence of SCP bank insertion on B4 worth.
Results of 2D calculations with partial SCP insertion simulated by diluted absorbers. $B^2 = 5.67m^{-2}$. SAC is always fully raised.

In these calculations a 72.5% absorber was used for B4$^{\downarrow}$

Control rod configuration	k_{eff}	$\rho[pcm]$	Core reactivity perturbation due to SCP insertion $\Delta\rho[pcm]$	Worth of B4 insertion [pcm]
SCP$^{\uparrow}$, B4$^{\uparrow}$	1.03847	+3704.4	0	-396.9
SCP$^{\uparrow}$, B4$^{\downarrow}$	1.03421	+3307.5		
SCP5.0% *abs*, B4$^{\uparrow}$	1.02604	+2537.9	-1166.5	-439.1
SCP5.0% *abs*, B4$^{\downarrow}$	1.02144	+2098.8		
SCP10.0% *abs*, B4$^{\uparrow}$	1.01535	+1511.6	-2192.8	-481.6
SCP10.0% *abs*, B4$^{\downarrow}$	1.01041	+1030.0		
SCP17.44% *abs*, B4$^{\uparrow}$	1.00278	+277.4	-3427.0	-542.0
SCP17.44% *abs*, B4$^{\downarrow}$	0.99736	-264.6		
SCP25.0% *abs*, B4$^{\uparrow}$	0.99187	-819.9	-4524.3	-606.4
SCP25.0% *abs*, B4$^{\downarrow}$	0.98594	-1426.3		
SCP97.5% *abs*, B4$^{\uparrow}$	0.94328	-6013.5	-9717.9	-1150.3
SCP97.5% *abs*, B4$^{\downarrow}$	0.93315	-7163.8		
SCP100.0% *abs*, B4$^{\uparrow}$	0.94238	-6114.4	-9818.8	-1166.7
SCP100.0% *abs*, B4$^{\downarrow}$	0.93213	-7281.1		

Table A4.2 The influence of SCP bank insertion on B4 worth.

In these calculations a 45% absorber was used for B4$^{\downarrow}$

Control rod configuration	k_{eff}	$\rho[pcm]$	Core reactivity perturbation due to SCP insertion $\Delta\rho[pcm]$	Worth of B4 insertion [pcm]
SCP$^{\uparrow}$, B4$^{\uparrow}$	1.03847	+3704.4	0	-331.4
SCP$^{\uparrow}$, B4$^{\downarrow}$	1.03491	+3373.0		
SCP5.0% *abs*, B4$^{\uparrow}$	1.02604	+2537.9	-1166.5	-368.2
SCP5.0% *abs*, B4$^{\downarrow}$	1.02218	+2169.7		
SCP10.0% *abs*, B4$^{\uparrow}$	1.01535	+1511.6	-2192.8	-405.4
SCP10.0% *abs*, B4$^{\downarrow}$	1.01119	+1106.2		
SCP17.44% *abs*, B4$^{\uparrow}$	1.00278	+277.4	-3427.0	-458.4
SCP17.44% *abs*, B4$^{\downarrow}$	0.99819	-181.0		
SCP25.0% *abs*, B4$^{\uparrow}$	0.99187	-819.9	-4524.3	-515.1
SCP25.0% *abs*, B4$^{\downarrow}$	0.98683	-1335.0		
SCP27.5% *abs*, B4$^{\uparrow}$	0.98881	-1131.6	-4836.0	-533.1
SCP27.5% *abs*, B4$^{\downarrow}$	0.98363	-1664.7		
SCP100.0% *abs*, B4$^{\uparrow}$	0.94238	-6114.4	-9818.8	-1008.0
SCP100.0% *abs*, B4$^{\downarrow}$	0.93351	-7122.4		

Table A4.3 The influence of SCP bank insertion on B4 worth.

In these calculations a 100%(non-diluted) absorber was used for B12$^{\downarrow}$

Control rod configuration	k_{eff}	$\rho[pcm]$	Core reactivity perturbation due to SCP insertion $\Delta\rho[pcm]$	Worth of B12 insertion [pcm]
SCP$^{\uparrow}$, B12$^{\uparrow}$	1.03847	+3704.4	0	-214.7
SCP$^{\uparrow}$, B12$^{\downarrow}$	1.03616	+3489.7		
SCP5.0% *abs*, B12$^{\uparrow}$	1.02575	+2510.8	-1193.6	-262.2
SCP5.0% *abs*, B12$^{\downarrow}$	1.02300	+2248.6		
SCP10.0% *abs*, B12$^{\uparrow}$	1.01491	+1468.8	-2235.6	-318.7
SCP10.0% *abs*, B12$^{\downarrow}$	1.01163	+1150.1		
SCP17.44% *abs*, B12$^{\uparrow}$	1.00235	+234.2	-3470.2	-415.2
SCP17.44% *abs*, B12$^{\downarrow}$	0.99819	-181.0		
SCP25.0% *abs*, B12$^{\uparrow}$	0.99173	-833.9	-4538.3	-541.6
SCP25.0% *abs*, B12$^{\downarrow}$	0.98643	-1375.5		
SCP27.5% *abs*, B12$^{\uparrow}$	0.98883	-1129.9	-4834.3	-587.1
SCP27.5% *abs*, B12$^{\downarrow}$	0.98312	-1717.0		
SCP100.0% *abs*, B12$^{\uparrow}$	0.95124	-5126.3	-8830.7	-2243.1
SCP100.0% *abs*, B12$^{\downarrow}$	0.93136	-7369.4		

Table A4.4 The influence of SCP bank insertion on B12 worth.

In these calculations a 45% absorber was used for B12$^{\downarrow}$

Control rod configuration	k_{eff}	$\rho[pcm]$	Core reactivity perturbation due to SCP insertion $\Delta\rho[pcm]$	Worth of B12 insertion [pcm]
SCP$^{\uparrow}$, B12$^{\uparrow}$	1.03847	+3704.4	0	-171.1
SCP$^{\uparrow}$, B12$^{\downarrow}$	1.03663	+3533.3		
SCP5.0% *abs*, B12$^{\uparrow}$	1.02575	+2510.8	-1193.6	-212.0
SCP5.0% *abs*, B12$^{\downarrow}$	1.02353	+2298.8		
SCP10.0% *abs*, B12$^{\uparrow}$	1.01491	+1468.8	-2235.6	-261.5
SCP10.0% *abs*, B12$^{\downarrow}$	1.01222	+1207.3		
SCP17.44% *abs*, B12$^{\uparrow}$	1.00235	+234.2	-3470.2	-347.0
SCP17.44% *abs*, B12$^{\downarrow}$	0.99887	-112.8		
SCP25.0% *abs*, B12$^{\uparrow}$	0.99173	-833.9	-4538.3	-460.4
SCP25.0% *abs*, B12$^{\downarrow}$	0.98722	-1294.3		
SCP27.5% *abs*, B12$^{\uparrow}$	0.98883	-1129.9	-4834.3	-501.4
SCP27.5% *abs*, B12$^{\downarrow}$	0.98395	-1631.3		
SCP100.0% *abs*, B12$^{\uparrow}$	0.95124	-5126.3	-8830.7	-1944.9
SCP100.0% *abs*, B12$^{\downarrow}$	0.93396	-7071.2		

Table A4.5 The influence of SCP bank insertion on B12 worth.

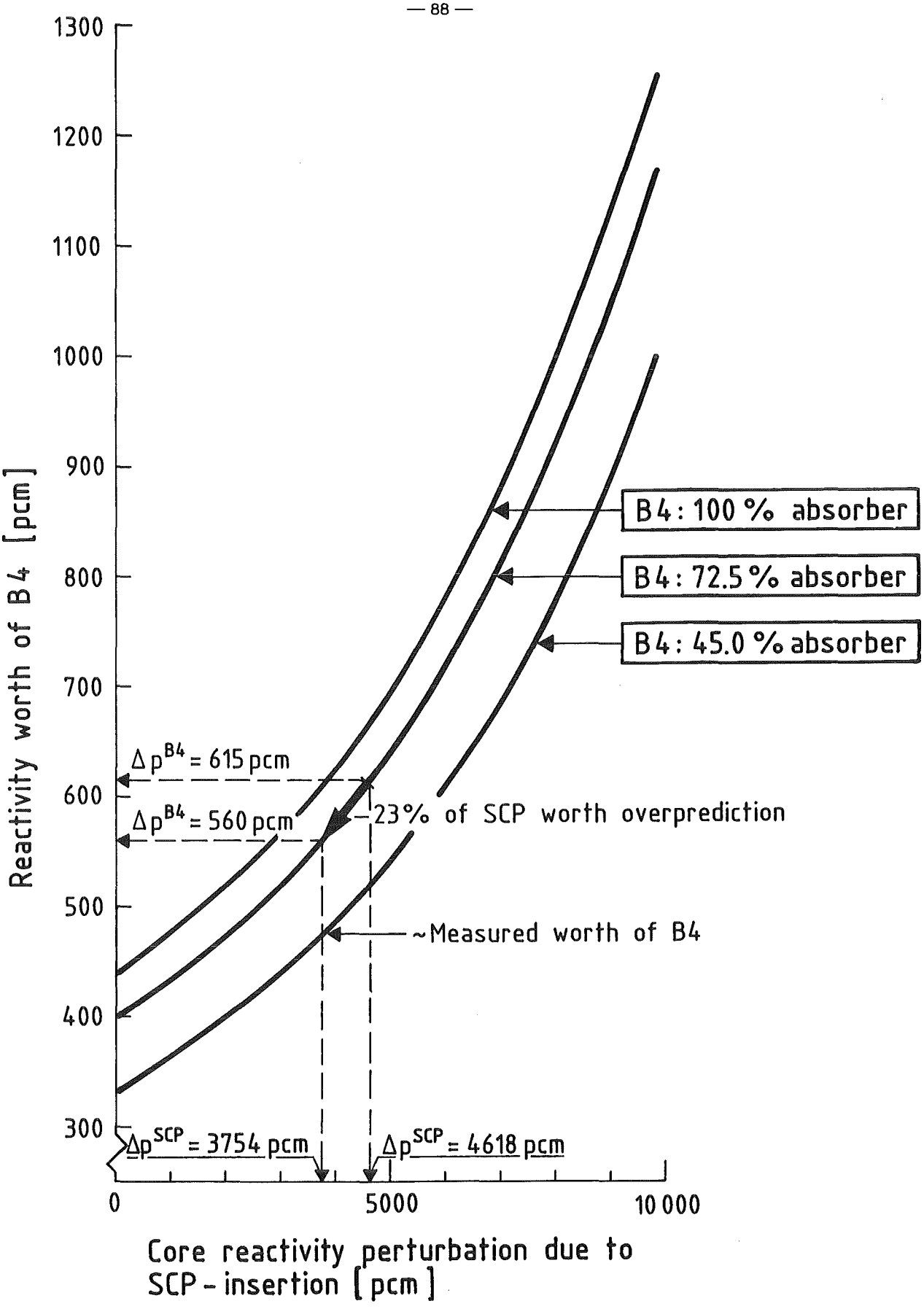

Figure A 4.1 The dependence of B4 worth on SCP insertion
Calculations: Diffusion, 2D, 4 groups, M1

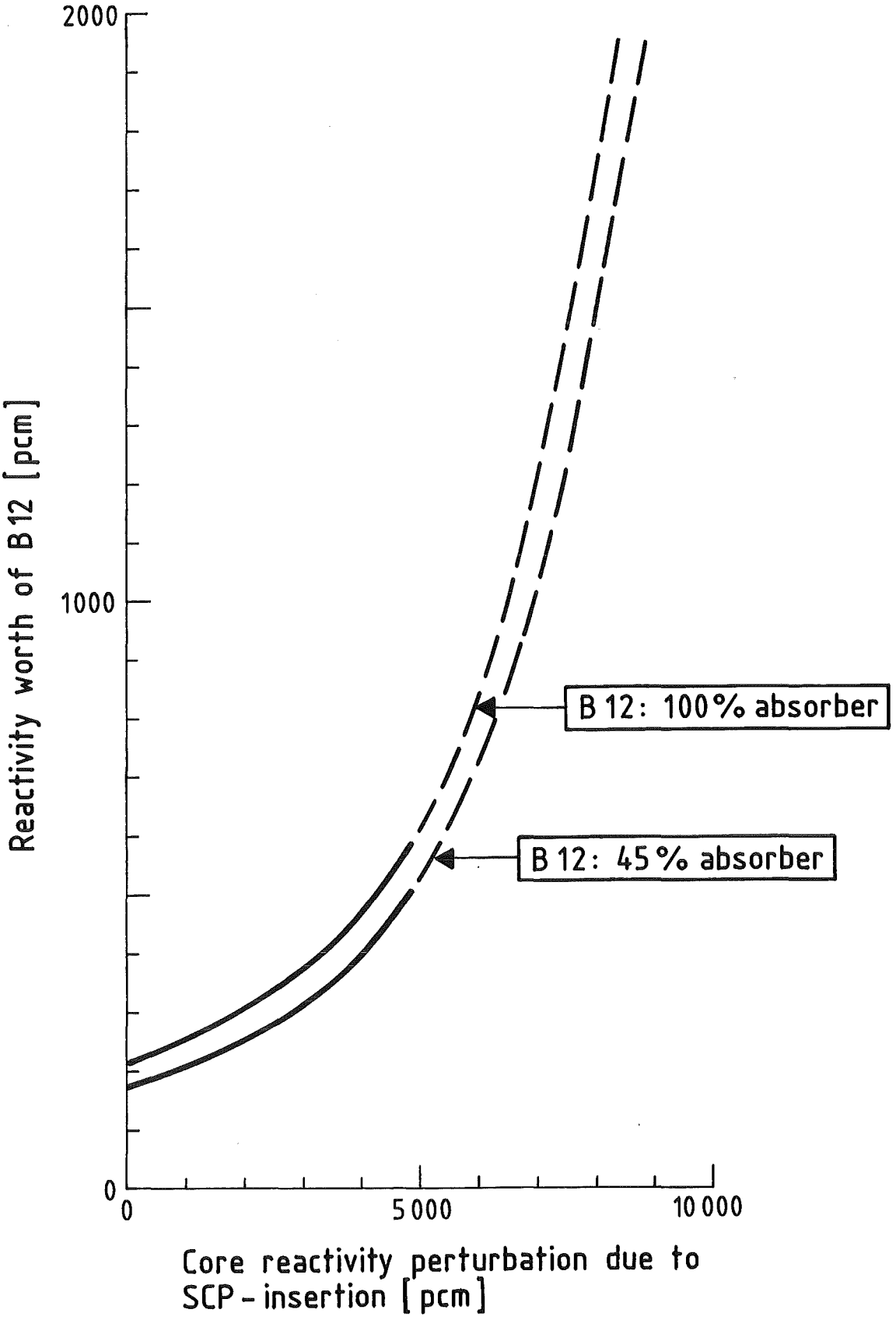

Figure A 4.2 The dependence of B12 worth on SCP insertion
Calculations: Diffusion, 2D, 4 groups, M1

Appendix 5

The production of mesh corrections for the prediction of core excess reactivity and criticality in the second analysis phase.

Mesh corrections of the second analysis phase

In the second phase of the KfK analysis mesh corrections were tentatively not derived separately for the radial and axial directions and later added to give the total correction, but were assessed directly as total corrections from a set of 3D calculations already available. This was done in the following way:

D3E calculations for a specified radial mesh and a certain number of axial planes are usually not directly performed by the code according to the user input specification but automatically run through a sequence of intermediate calculations with progressively refined axial and radial mesh widths. The objective of this stepwise solution of a given problem is to arrive at an optimized source guess for the final (specified) calculation. The following Tables show the results of these intermediate and of the final calculations in the case of the second KfK analysis phase of SPX-1. The final calculations (last two columns) are those that provided the basic k_{eff} values for Sec. IV.2.

Configuration	3D Diffusion, 4 energy groups					
	Radial mesh M1 39 axial planes		Radial mesh M1 63 axial planes		Radial mesh M2 63 axial planes	
	k_{eff}	ρ[pcm]	k_{eff}	ρ[pcm]	k_{eff}	ρ[pcm]
$SCP^{\uparrow}$ $SAC^{\uparrow}$	1.04381	+4197.0	1.04471	+4279.6	1.04576	+4376.1
SCP^{542} $SAC^{\uparrow}$	0.99124	-883.4	0.99231	-774.8	0.99646	-355.1

Table A5.1 Second KfK analysis of CMP. 3D calculations.

Configuration	3D Diffusion, 4 energy groups					
	Radial mesh M1 39 axial planes		Radial mesh M1 63 axial planes		Radial mesh M2 63 axial planes	
	k_{eff}	ρ[pcm]	k_{eff}	ρ[pcm]	k_{eff}	ρ[pcm]
$SCP^{\uparrow}$ $SAC^{\uparrow}$	1.00323	+321.8	1.00411	+409.7	1.00595	+591.9
SCP^{929} $SAC^{\uparrow}$	0.99878	-122.0	0.99971	-29.0	1.00181	+181.0

Table A5.2 Second KfK analysis of C1D. 3D calculations.

The two intermediate calculations used a radial mesh M1 (7 points per subassembly), the first of these only 39 axial planes. The final calculation used a radial mesh M2 (19 points per subassembly) and 63 axial planes.

The extrapolation of the results of these calculations to an infinitely small mesh is based on the fact that the k_{eff} value of such calculations increases linearly with the square of the average point distance. Tests have also shown that in a homogeneous reactor with the same mesh (point-distance) in all 3 coordinate directions, halving of the mesh in one direction produces exactly one third of the effect on k_{eff} obtained by halving the mesh in all three directions.

The difficulty encountered in the present case is that the variation of the mesh size (point-distance) from one calculation to the next is different for the radial and axial direction and that the reactor is not homogeneous so that the standard extrapolation laws do not apply exactly. The mesh corrections determined hereafter have therefore to be seen as approximate values.

The procedure is demonstrated for the first case of Table A5.1, i.e. configuration $SCP^{\uparrow}\ SAC^{\uparrow}$ of core version CMP. Only the first and the final calculation are used:

Taking the first calculation (M1, 39 ax. planes) as a reference, the transition from a radial mesh M1 to M2 corresponds to halving of the mesh size in the horizontal plane, i.e. in 2 coordinate directions; the transition from 39 to 63 axial planes corresponds to an average reduction of the axial mesh by a factor of 0.6129. The average mesh reduction for all three coordinate directions is thus obtained as:

$$\frac{2 \times 0.5 + 1 \times 0.6129}{3} = 0.5376$$

Sqaring of this result gives a value of 0.2890. We therefore have 2 points available from which we can extrapolate to the k_{eff} value belonging to an infinitely small mesh: P1(1.000/1.04381) and P2(0.289/1.04576). This extrapolation leads to $k_{eff} = 1.04656$, $\rho = +4448.9$ pcm. The difference between this result and that of the basic calculations ($\rho = +4376.1$ pcm) and hence the required mesh correction is +73 pcm.

A graphical demonstration of the linear extrapolation is given Figure A5.1.

Similarly, the extrapolated k_{eff} and reactivity values for the remaining 3 configurations $SCP^{542}\ SAC^{\uparrow}$ of CMP and $SCP^{\uparrow}\ SAC^{\uparrow}$ and $SCP^{929}\ SAC^{\uparrow}$ of C1D are obtained as 0.99852 ($\rho = -147.7$ pcm), 1.00705 ($\rho = +700.1$ pcm) and 1.00304 ($\rho = +303.1$ pcm). Comparing again the extrapolated reactivity values with the values quoted in the last column of Tables A5.1 and A5.2, one finds mesh corrections for the remaining three configurations of +207.4, +108.2 and +122.1 pcm.

The results of the supplementary calculations quoted in Tables A5.1 and A5.2 also served to assess mesh corrections for the core reactivity predictions of the third analysis phase. Calculations run for this latter purpose used a radial mesh M1 and 63 axial planes (see Sec. VI.3) and therefore employed the same geometrical resolution as the second block of calculations quoted in Tables A5.1 and A5.2. Since in the third analysis phase, mesh corrections related to control rod insertion were automatically accounted for in the cross section preparation for the control rod absorbers, only the core inherent corrections are of relevance in the present context. These can be easily extracted from the first lines of Tables A5.1 and A5.2: For CMP one compares the reactivity value of the calculation 'Radial mesh M1, 63 axial planes' (+4279.6 pcm) with the associated extrapolated value (+4448.9 pcm) and obtains a mesh correction of +169.3 pcm. The same type of comparison performed for C1D gives a correction of +290.4 pcm.

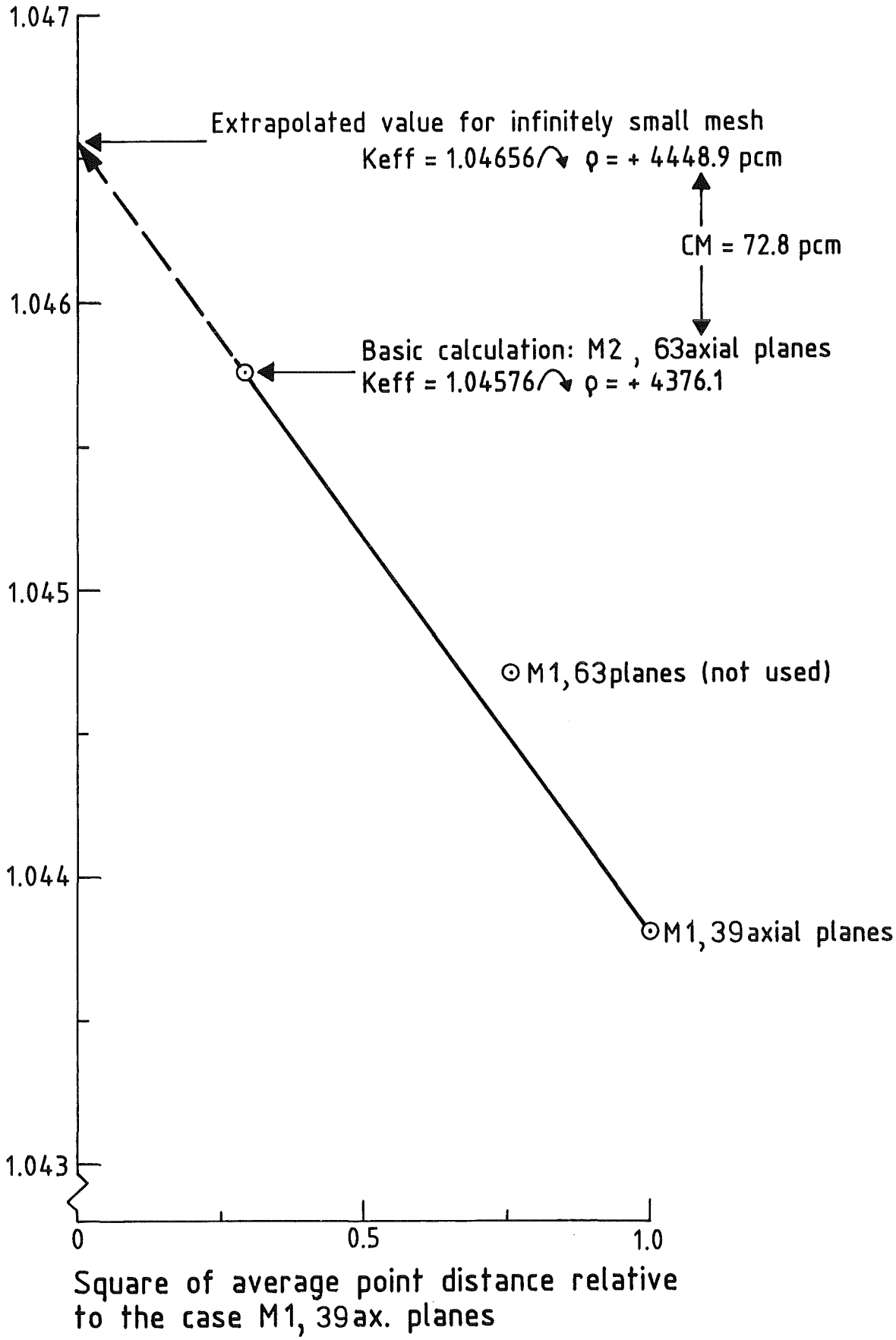

Figure A5.1 Mesh correction for configuration SCP↑ SAC↑
Core loading version CMP

Appendix 6

This Appendix discusses the alternative KAPER4 models tentatively used for the SCP absorbers to investigate the origin of the rod worth overprediction.

1. Generalities

The total volume fractions of the different constituants of SCP absorbers including their hexagonal wrapper are

Sodium: 41.72%, Steel: 26.60%, B_4C: 25.36%, Void: 6.32%

In KfK/BN cross section preparations, the void volume, located between the boroncarbide pellets and their claddings (0.5655 cm^2 per absorber pin), was simply added to the sodium volume. Tests have shown that this simplification has no significant influence on the results.

Another simplification, shared by all analysis groups concerned the steel filling pieces which complete the absorber pin matrix for better fit within the cylindrical guide tube. It was generally assumed that the total volume of these filling pieces would add up to 6 complete pins of 21 mm diameter, i.e. the same diameter as the absorber pins. A thourough assessment, however, shows that the bigger and smaller filling pieces do not add up to complete pins but only to $\simeq$90% of the volume of those. This means that in the volume fractions used in all analyses, there is too much steel and too little sodium. As the error is relatively small, it is not expected to have a major effect on the results. This point was not further investigated.

It is recalled that in the first analysis phase, the zone radii (@ 180°C) and volume fractions used for the cylindrical SCP absorber model were:

Inner zone: r_1 = 7.470 cm → Sodium: 30.95%, Steel: 28.69%, B_4C: 30.96%
Outer zone: r_2 = 9.423 cm → Sodium: 73.98%, Steel: 26.02%

2. The Unit-Cell-Model

The first of the two tentatively established cylindrical models for SCP was based on the unit-cell philosophy. Each of the 31 absorber pins was surrounded by the same fictous hexagonal unit cell with a side length chosen such that these cells formed a uniform pattern without any gaps. The arrangement of these unit cells and the resulting cylindrical model used in this first study are shown in Figure A6.1. The volume fractions used for the different cylindrical regions and the mesh divisions are given in Table A6.1 hereafter. All radii refer to a temperature of 180°C.

Region No.	Outer radius [cm]	Meshes [cm]	Volume fractions [%]
1	6.673	6 * 1.112	Sodium: 34.985 Steel: 14.446 B_4C: 50.569
2	7.269	2 * 0.298	Sodium: 19.398 Steel: 80.602
3	7.470	2 * 0.100	Steel: 100.0
4	9.423	4 * 0.488	Sodium: 77.100 Steel: 22.900

Table A6.1 Specification of the unit-cell-model.

To check the influence of small parameter variations, the cross section preparation for the unit cell model was repeated

- using the more realistic SCP volume fractions accounting for the void volume between the boroncarbide pellets and their steel cladding
- using the volume fractions on which the AEA analysis was based and which differ to some extent from those of the KfK/BN analysis. The AEA cross section preparation also accounted for the void volume.

3. The Envelope-Model

In the second model, a different - but apparently not less plausible than the first - criterion was used to define the area covered be the absorber. In this case, the choice of the outer radius of the absorbing zone was based on the area enclosed by a line following the circumference of the absorber pins and joining the absorber pins at the points of minimum distance. Figure A6.2 shows the position of this line and the resulting cylindrical model. The volume fractions used for the envelope model and the mesh divisions are given in Table A6.2:

Region No.	Outer radius [cm]	Meshes [cm]	Volume fractions [%]
1	6.370	4 * 1.592	Sodium: 28.591 Steel: 15.916 B_4C: 55.493
2	7.269	3 * 0.300	Sodium: 45.787 Steel: 54.213
3	7.470	2 * 0.100	Steel: 100.0
4	9.423	4 * 0.488	Sodium: 77.103 Steel: 22.897

Table A6.2 Specification of the 'envelope'-model.

4. Results obtained with the alternative SCP models

A series of diffusion theory calculations in 4 energy groups, was run to test the performance of the cross sections derived on the basis of the new cylindrical models. These calculations were run alternatively in 2D geometry with radial meshes M1 and M2, respectively, and in 3D geometry with a radial mesh M2.

The results of the 2D calculations are summarized in Table A6.3, those of the 3D calculations in Table A6.4. While 2D calculations were run only for the fully raised and fully inserted SCP bank, 3D calculations also covered the case of critical insertion (*SCP*[542]). In view of the exploratory character of these calculations, the latter case was not systematically treated with all different types of cross sections available.

The results of Tables A6.3 and A6.4 allow the following conclusions:

1. The finding of predominant importance is that the production of homogenized SCP cross sections on the basis of the alternative cylindrical absorber models, leads to a reduction of the SCP bank worth with respect to the first KFK/BN analysis of 9 to 10% (Last column: 'Worth reduction'). The reduction is somewhat more pronounced for the 'envelope' than for the 'unit-cell' model. C/E ratios of about 1.2, found in the initial phases of the KfK/BN analysis, would therefore be lowered to about 1.1, a value that would be much closer to those found in earlier analyses of critical assemblies.

2. In terms of heterogeneity factors F_{het} one finds that with the 'Old het. SCP cross sections', the SCP bank worth reduction with respect to homogeneous (volume averaged) cross sections was only about 9%, while with the alternative SCP models reductions of 17 to 19% are obtained.

3. Minor variations within the 'unit-cell' model, like accounting for the void volume between absorber pellets and claddings rather than replacing it by sodium, or an alternative use of the AEA volume fractions for the regions surrounding the central absorbing area have little influence on the SCP bank worth.

4. Practically the same worth reduction upon the use of the new absorber cross sections is seen for partial and for full SCP bank insertion.

5. As the cross sections of the SAC rod were not modified, the worth reductions observed in the cases SCP^{542}, $SAC^{\downarrow}$ and $SCP^{\downarrow}$, $SAC^{\downarrow}$ are somewhat smaller than in the cases where only SCP was inserted.

   It is interesting to see, however, that through mutual influence of the rod systems, the worth of SAC is reduced in parallel with the worth of SCP: From 1269 to 1260 pcm ($\simeq$0.75% rel.) for SCP at critical and from 1411 to 1395 pcm ($\simeq$1.1% rel.) when SCP is fully inserted. This was checked for the envelope model only.

6. 2D calculations with a radial mesh M1 (top part of Table A6.3) overestimate the heterogeneity factors and worth reductions by about 10% rel..

7. Concerning the k_{eff} and ρ values of Tables A6.3 and A6.4 it should be mentioned that the new prepared SCP cross were coupled to the cross section block of the first KfK analysis but that the geometrical model of the calculations had already been updated and thus corresponded to the second analysis phase.[10] This is the reason for the small differences observed e.g. between the present 3D results and those of Table 1 of the main part of this report, even in the case where the same SCP cross sections (Old het.) were used.

Encouraged by the successful use of the new SCP absorber cross sections in the CMP core, a small number of 3D calculations was subsequently run for the first critical core C1D. As, however, the rod worth reductions were similar to those observed for the CMP core in Tables A6.1 and A6.2, the results will not be given here explicitely.

---

[10] For reasons of consistency, it was considered prudent to condense the new SCP cross sections with the same spectra as used for the 'Old het. SCP' cross sections. Since the cross section block employed in the second analysis phase was provided by BN in condensed form, the associated spectra were not directly available and therefore those of the first analysis were employed.

Control rod configuration	k_{eff}	$\rho[pcm]$	SCP bank worth [pcm]	F_{het} [%]	Worth Reduction [%]
Note: Mesh M1:					
SCP↑, SAC↑	1.03847	+3704.4	0.0	-	-
SCP↓, SAC↑ Hom. SCP absorber	0.92039	-8649.0	-12353.4	-	-
SCP↓, SAC↑ Old Het SCP abs.	0.93136	-7369.4	-11073.8	-10.4	-
SCP↓, SAC↑ Unit-cell-model Void replaced by Na	0.94077	-6296.0	-10000.4	-19.0	-9.7
SCP↓, SAC↑ Unit-cell-model With void	0.94072	-6301.2	-10005.6	-19.0	-9.6
SCP↓, SAC↑ Unit-cell-model AEA	0.94034	-6344.9	-10049.3	-18.7	-9.3
SCP↓, SAC↑ Envelope-model	0.94261	-6088.9	-9793.3	-20.7	-11.6
Note: Mesh M2:					
SCP↑, SAC↑	1.03924	+3775.9	0.0	-	-
SCP↓, SAC↑ Hom. SCP absorber	0.93038	-7482.7	-11258.6	-	-
SCP↓, SAC↑ Old Het SCP abs.	0.93960	-6427.9	-10203.8	-9.4	-
SCP↓, SAC↑ Unit-cell-model Void replaced by Na	0.94758	-5531.9	-9307.8	-17.3	-8.8
SCP↓, SAC↑ Unit-cell-model With void	0.94752	-5538.2	-9314.1	-17.3	-8.7
SCP↓, SAC↑ Unit-cell-model AEA	0.94721	-5572.8	-9348.7	-17.0	-8.4
SCP↓, SAC↑ Envelope-model	0.94914	-5359.1	-9135.0	-18.9	-10.5

Table A6.3 The influence of the use of different KAPER4 models on SCP bank worth

Results of 2D calculations, 4 energy groups, mesh M1/M2, $B^2 = 5.67m^{-2}$. SAC is always fully raised.

F_{het} is the heterogeneity factor $(\Delta\rho_{het} - \Delta\rho_{hom})/\Delta\rho_{hom}[\%]$ that indicates the percentage reduction in calculated rod worth observed when homogeneous (i.e. volume weighted) cross sections are replaced by cross sections that account for the heterogeneous structure of the control rods.

The column 'Worth reduction' indicates the percentage by which the C/E ratio of the first KfK analysis using the 'Old heterogeneous SCP cross sections' would be reduced by the use of the newly prepared SCP cross sections.

Control rod configuration	k_{eff}	$\rho[pcm]$	SCP bank worth [pcm]	F_{het} [%]	Worth Reduction [%]
Note: Hom. GRUCAL cross sections used for SCP					
$SCP^{\uparrow}, SAC^{\uparrow}$	1.04110	+3947.7	0.0	-	-
$SCP^{\downarrow}, SAC^{\uparrow}$	0.93072	-7443.5	-11391.2	-	-
Note: Old het. cross sections used for SCP					
$SCP^{\uparrow}, SAC^{\uparrow}$	1.04165	+3998.7	0.0	-	-
$SCP^{542}, SAC^{\uparrow}$	0.99285	-719.7	-4718.4	-	-
$SCP^{542}, SAC^{\downarrow}$	0.98050	-1988.7	-5987.4	-	-
$SCP^{\downarrow}, SAC^{\uparrow}$	0.94025	-6354.9	-10353.6	-9.1	-
$SCP^{\downarrow}, SAC^{\downarrow}$	0.92794	-7765.9	-11764.6	-	-
Note: Unit-cell model cross sections used for SCP					
$SCP^{\uparrow}, SAC^{\uparrow}$	1.04206	+4036.1	0.0	-	-
$SCP^{\downarrow}, SAC^{\uparrow}$	0.94844	-5436.3	-9472.4	-16.8	-8.5
Note: Envelope model cross sections used for SCP					
$SCP^{\uparrow}, SAC^{\uparrow}$	1.04214	+4043.5	0.0	-	-
$SCP^{542}, SAC^{\uparrow}$	0.99817	-182.8	-4226.3	-	-10.4
$SCP^{542}, SAC^{\downarrow}$	0.98578	-1442.4	-5485.9	-	-8.4
$SCP^{\downarrow}, SAC^{\uparrow}$	0.95010	-5252.2	-9295.7	-18.4	-10.2
$SCP^{\downarrow}, SAC^{\downarrow}$	0.93767	-6647.7	-10691.2	-	-9.1

Table A6.4 The influence of the use of different KAPER4 models on SCP bank worth.
Results of 3D calculations, 4 energy groups, mesh M2. For further comments see Table A6.3.

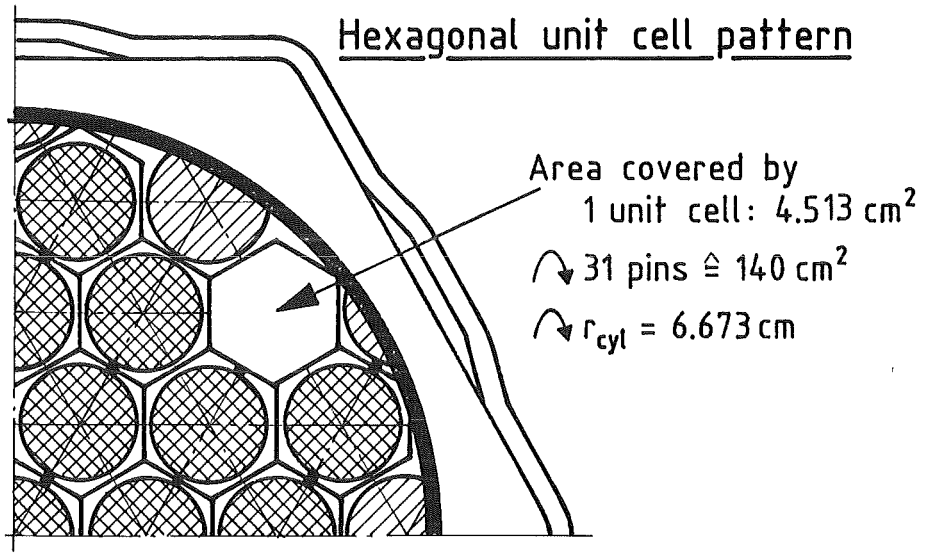

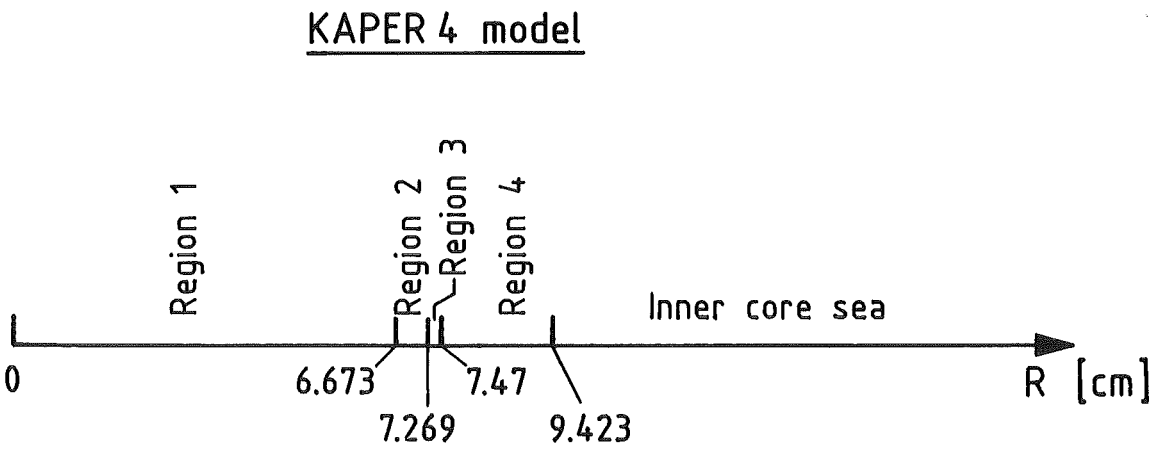

Figure A 6.1 The "unit-cell" model of SCP (180 °C)

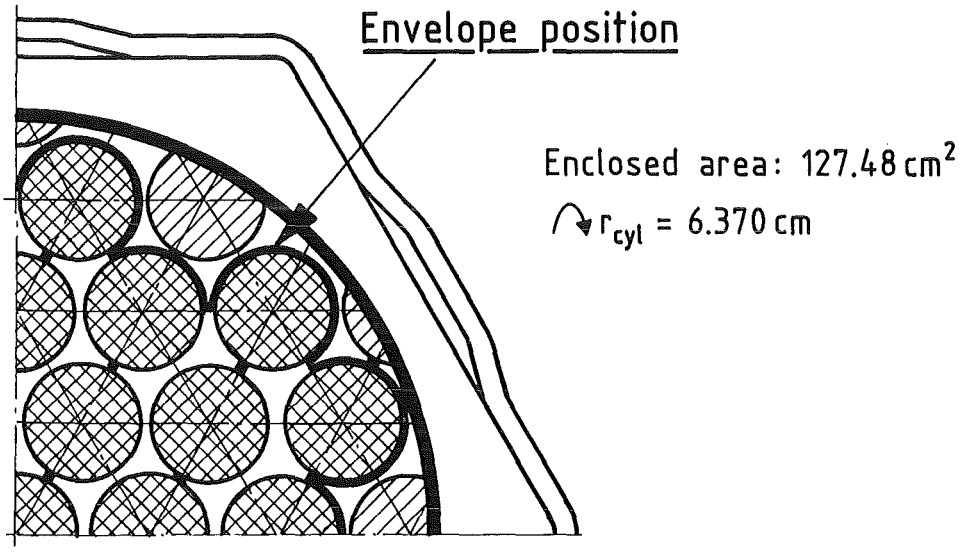

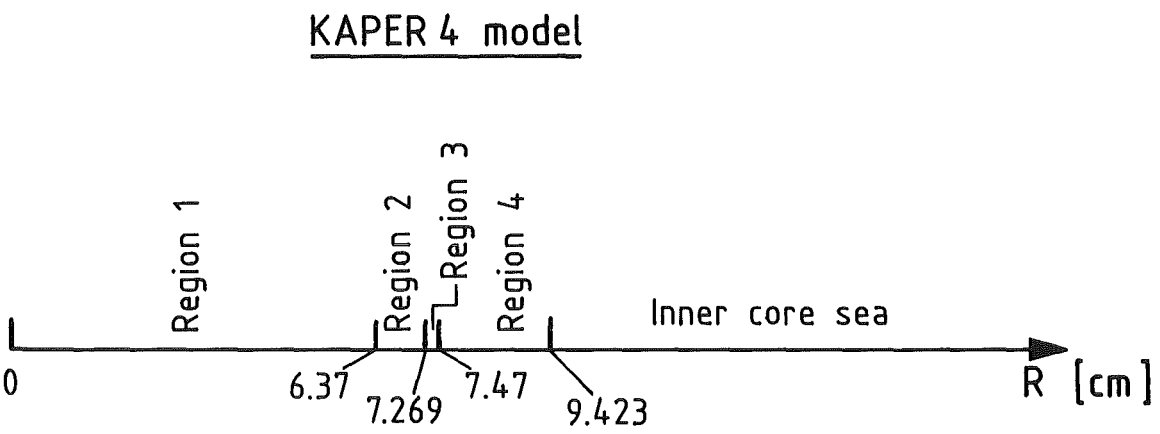

Figure A 6.2 The "envelope" model of SCP (180 °C)

Figures of the main part of this report

B1 ... B21 : Individual control rods of the SCP system
SAC1 ... SAC3 : Individual control rods of the SAC system
D : Diluent positions
B : BOUPHY position
F : Dummy fuel element positions
GDN : Neutron guide tube positions for under vessel reactor operation instrumentation

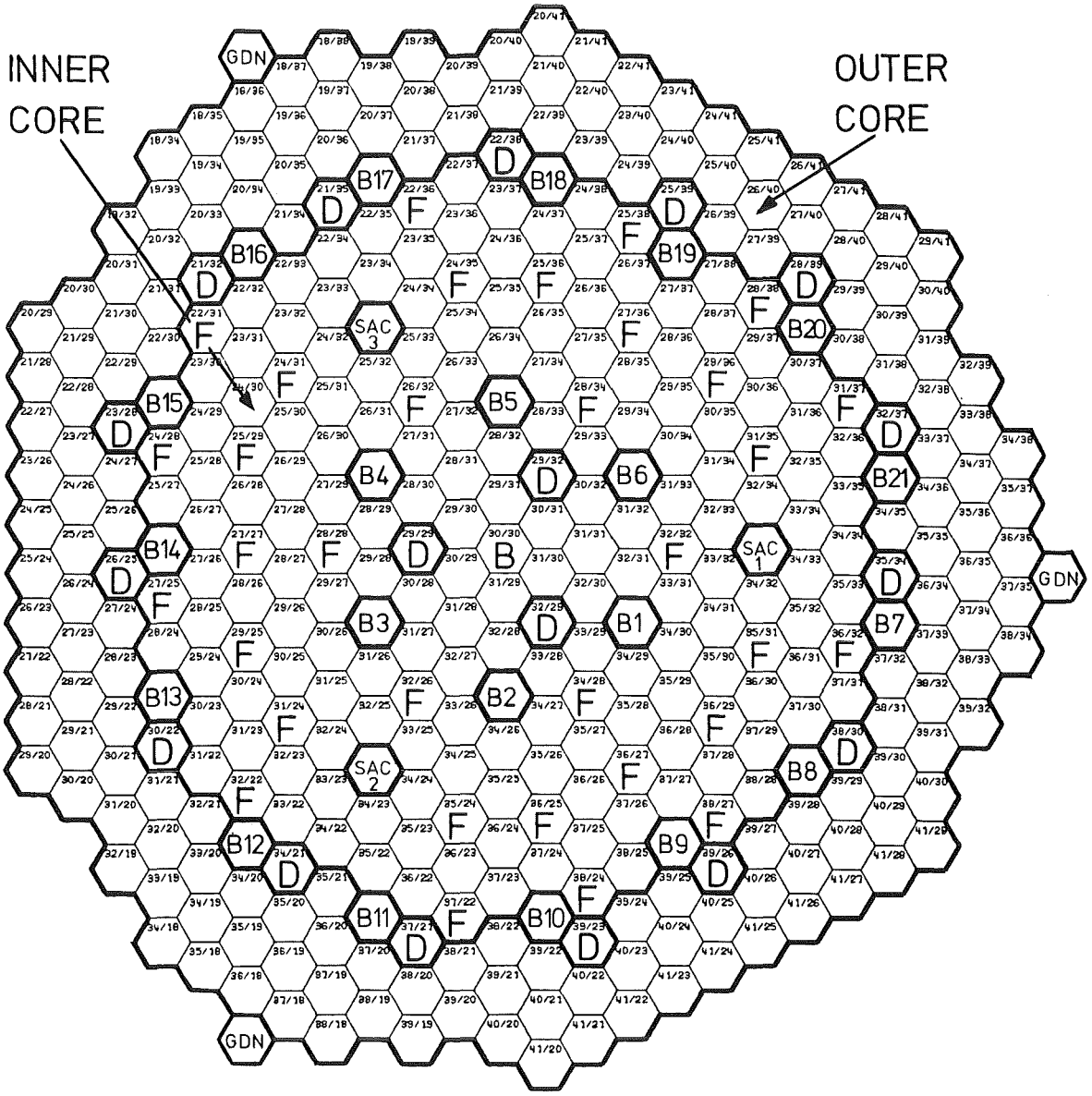

Figure 1 Core loading of SUPER-PHENIX-1
Core version C1D

B1 ... B21 : Individual control rods of the SCP system
SAC1 ... SAC3 : Individual control rods of the SAC system
D : Diluent positions
B : BOUPHY position
GDN : Neutron guide tube positions for under vessel reactor operation instrumentation

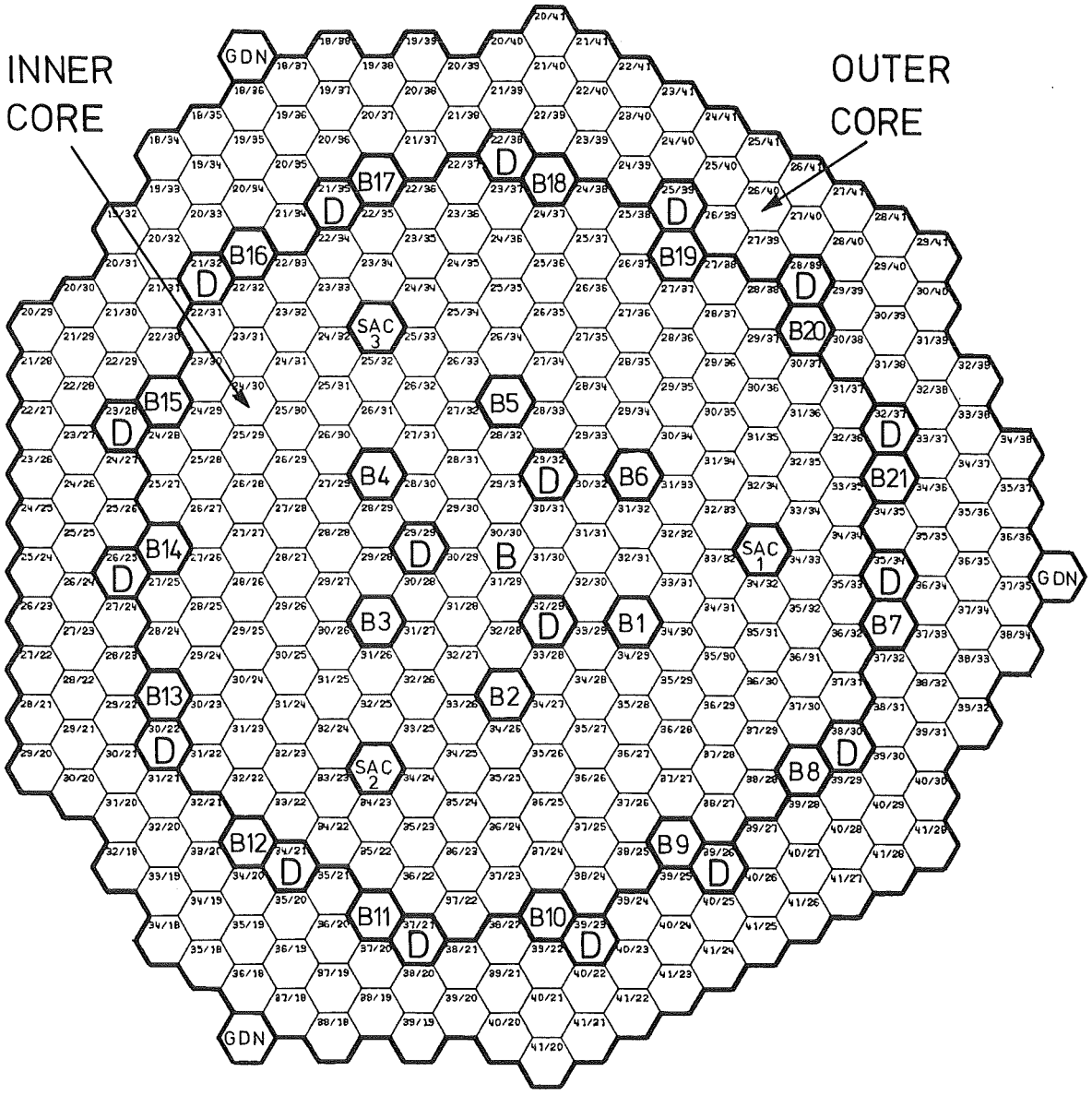

Figure 2 Core loading of SUPER-PHENIX-1
Core version CMP

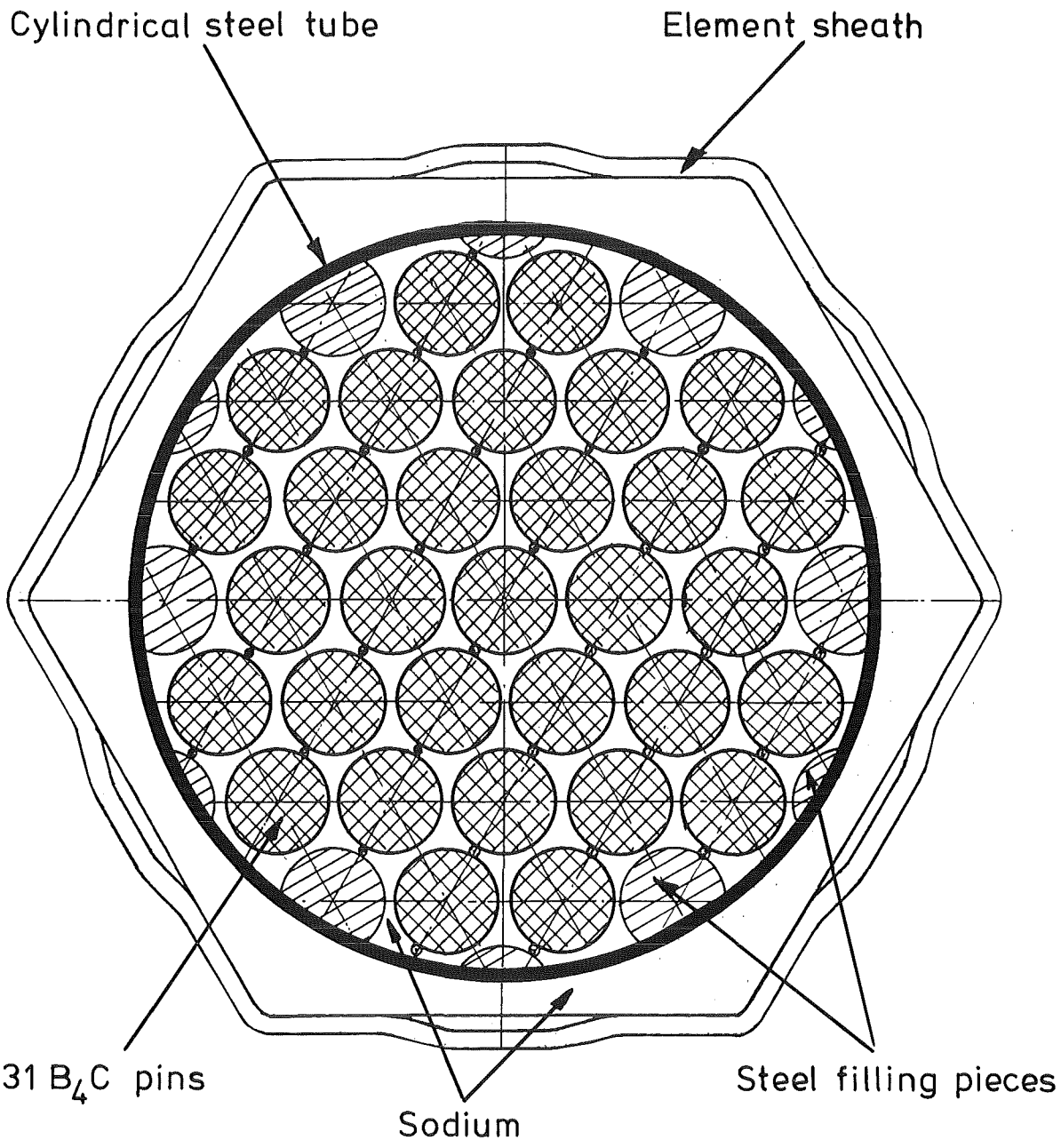

Figure 3 Layout of an SCP absorber

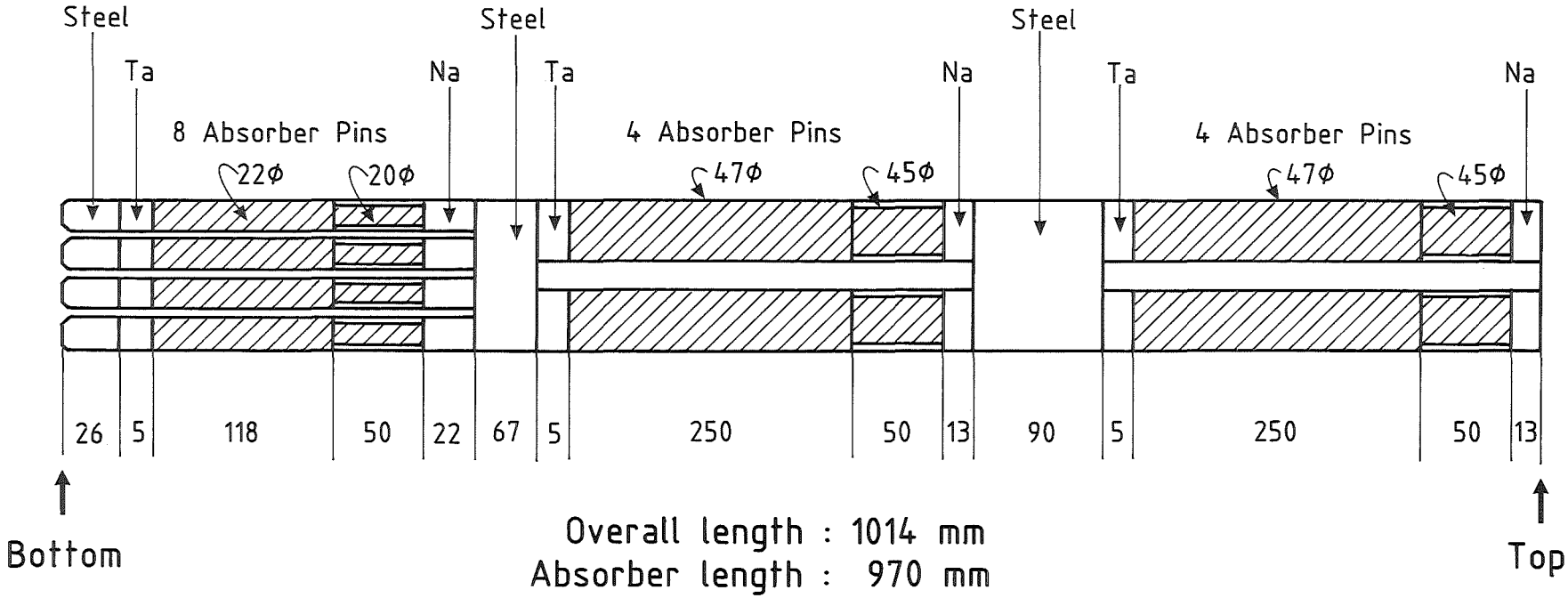

Figure 4 Schematic construction of a SAC absorber assembly

(All dimensions are given in [mm] and refer to T=20°C)

ATTENTION: DRAWING IS NOT TO SCALE!

Upper and central absorber unit

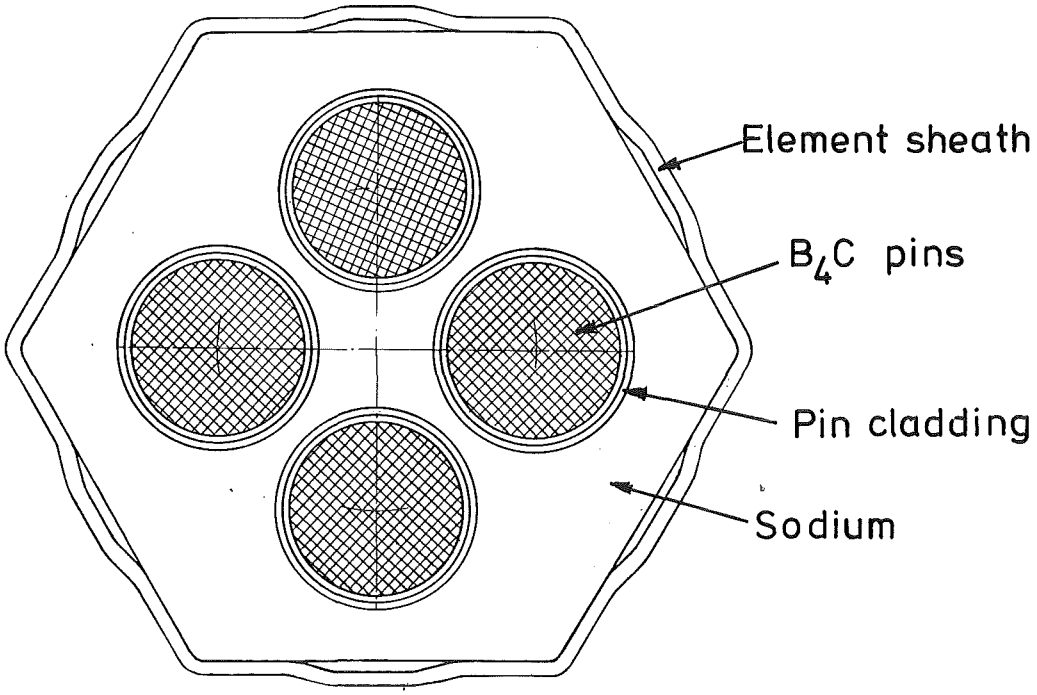

Lower absorber unit

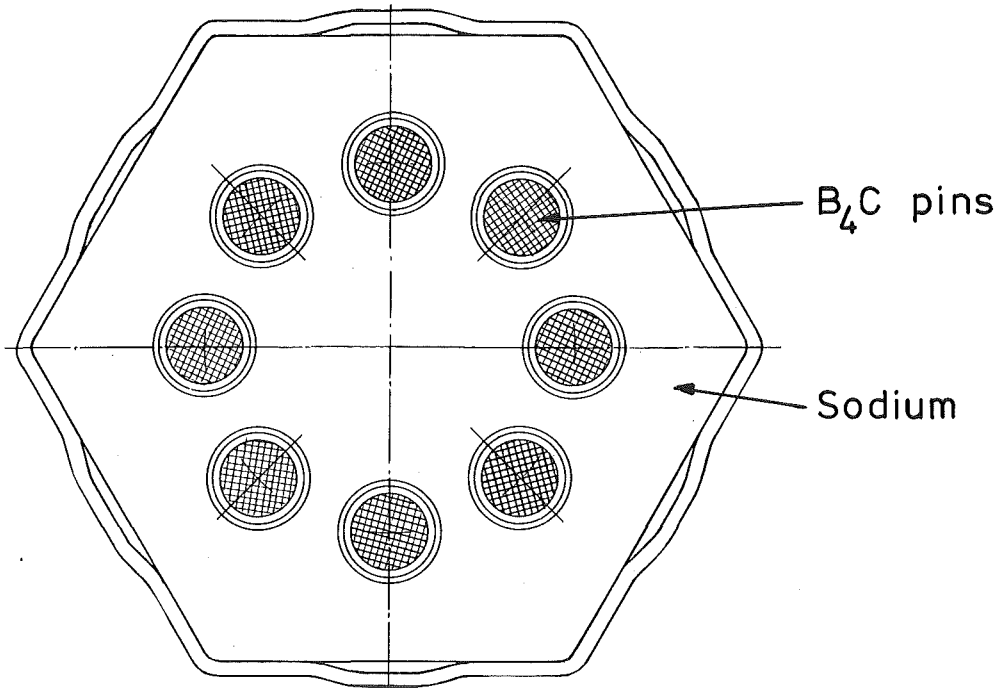

Figure 5 Layout of the SAC absorbers

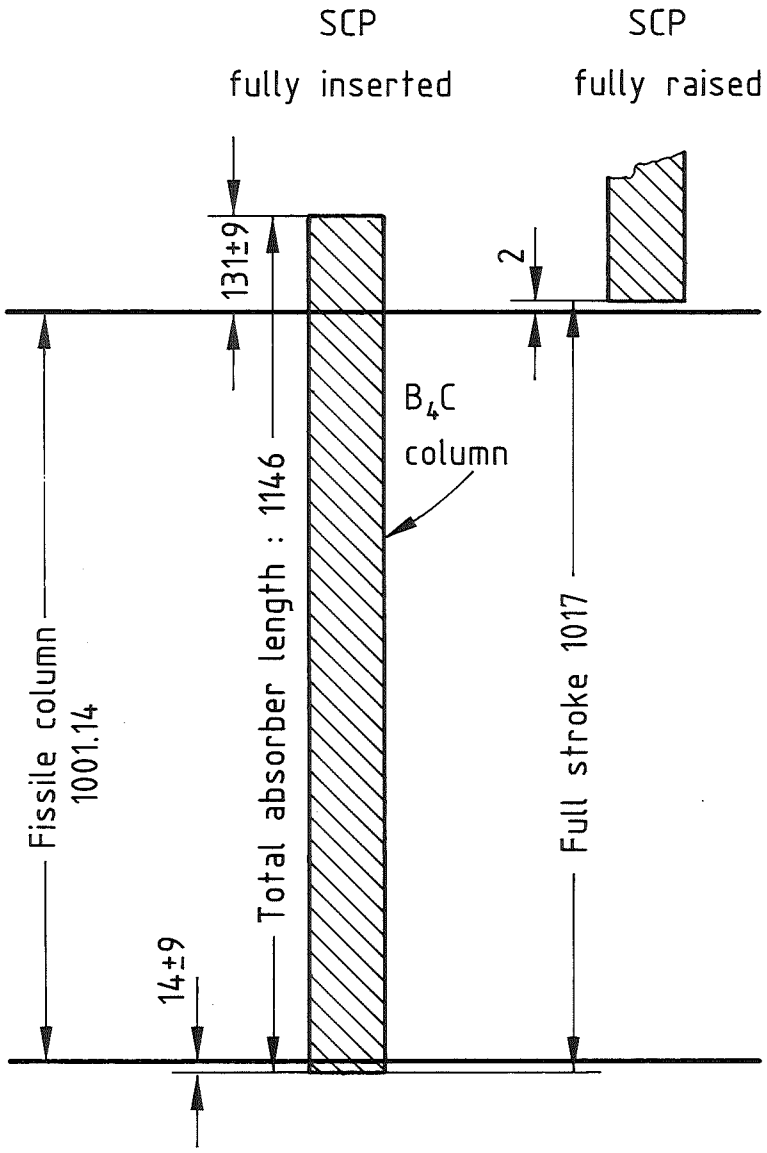

Figure 6
Axial position of the B_4C column of SCP control rods with respect to the fissile loading at 180°C

(Dimensions are in [mm])

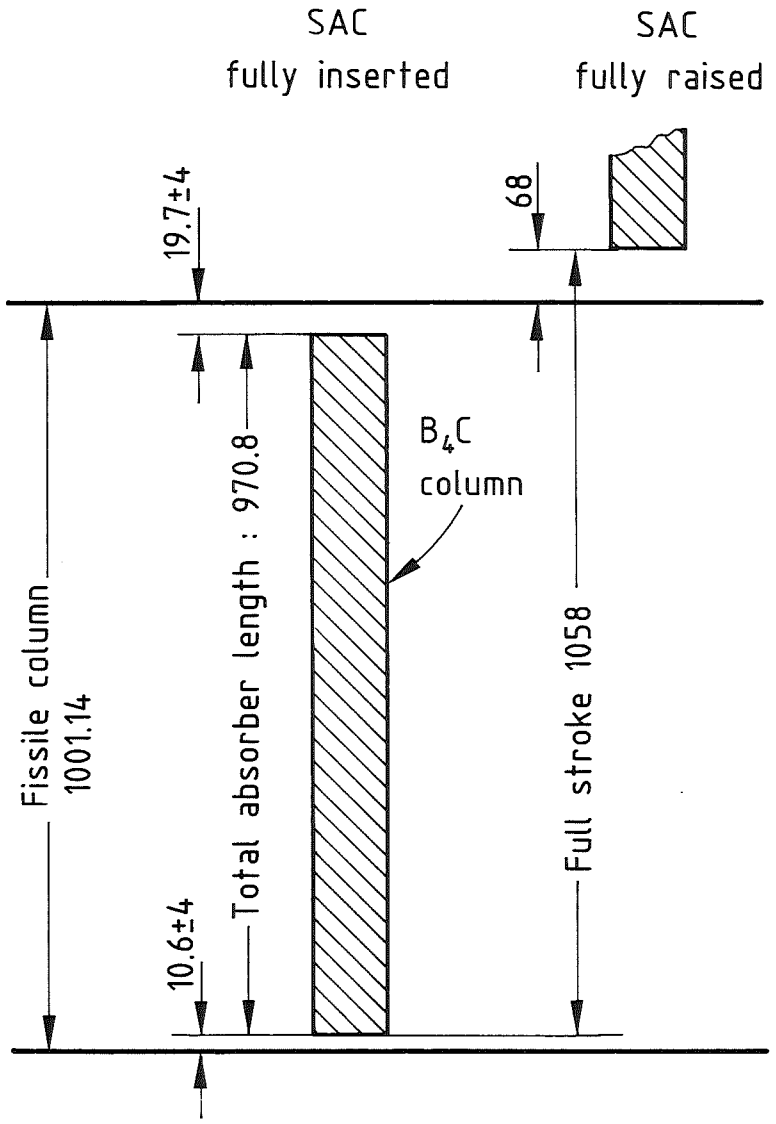

Figure 7
Axial position of the B_4C column of SAC control rods with respect to the fissile loading at 180°C
(Dimensions are in [mm])

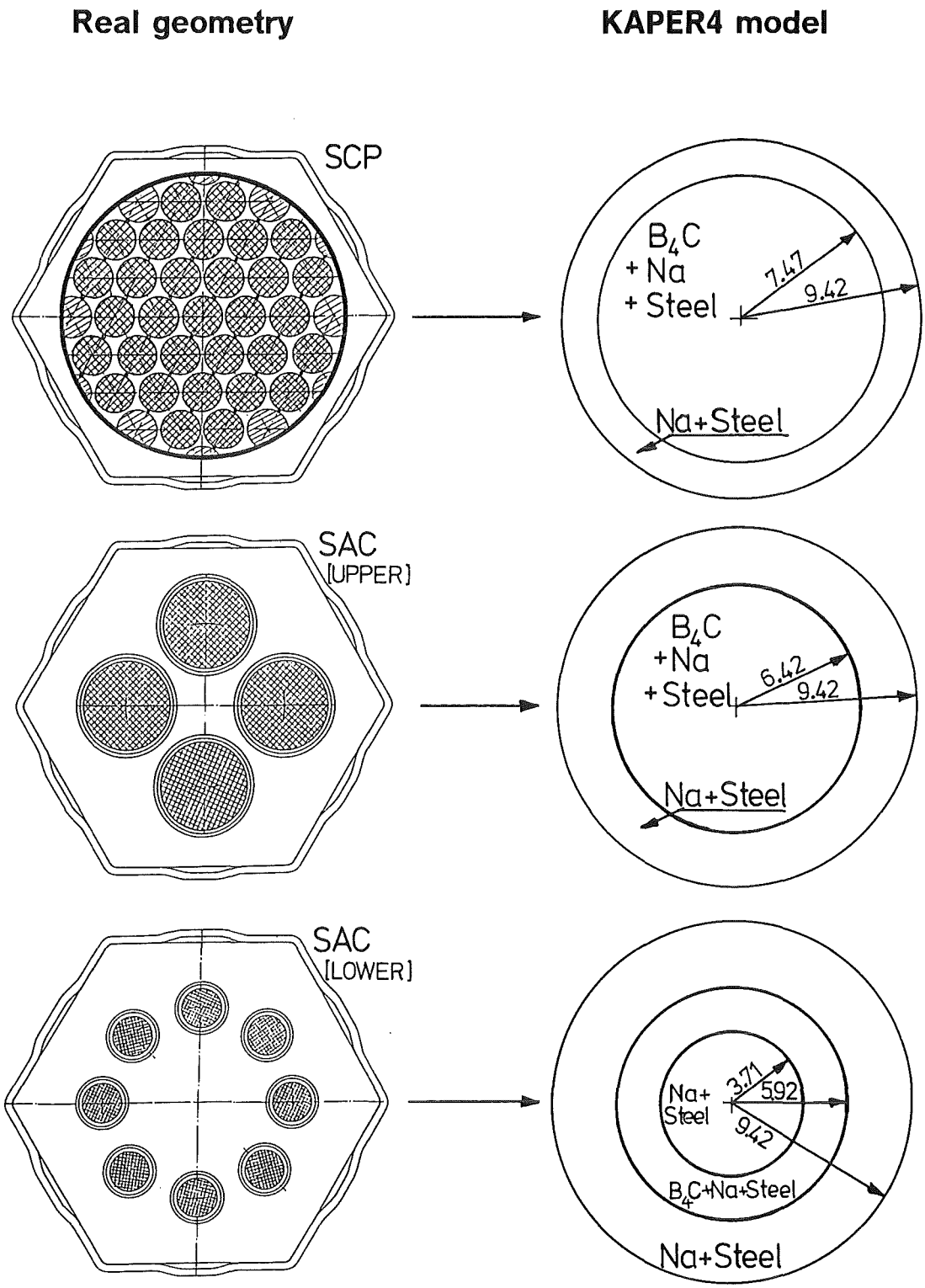

Figure 8
KAPER4 models used for the cross section production for SPX-1 control rod absorbers in the first BN/KfK analysis campaign. (T = 180°C).

(Dimensions are in [cm])

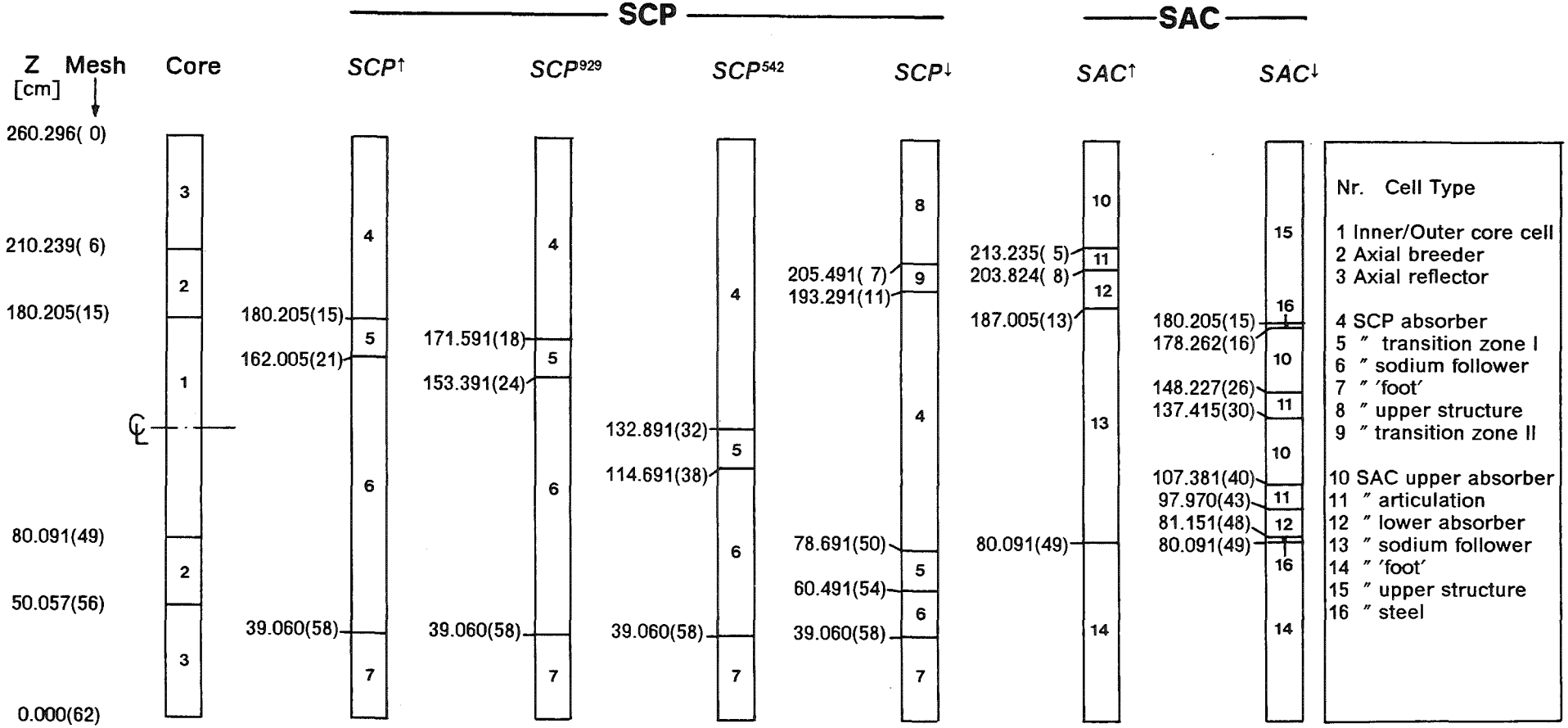

Numbers in elements indicate the cell type (see figure caption).

Figure 9 Axial models used for core and control elements in KfK D3E calculations (T = 180°C).

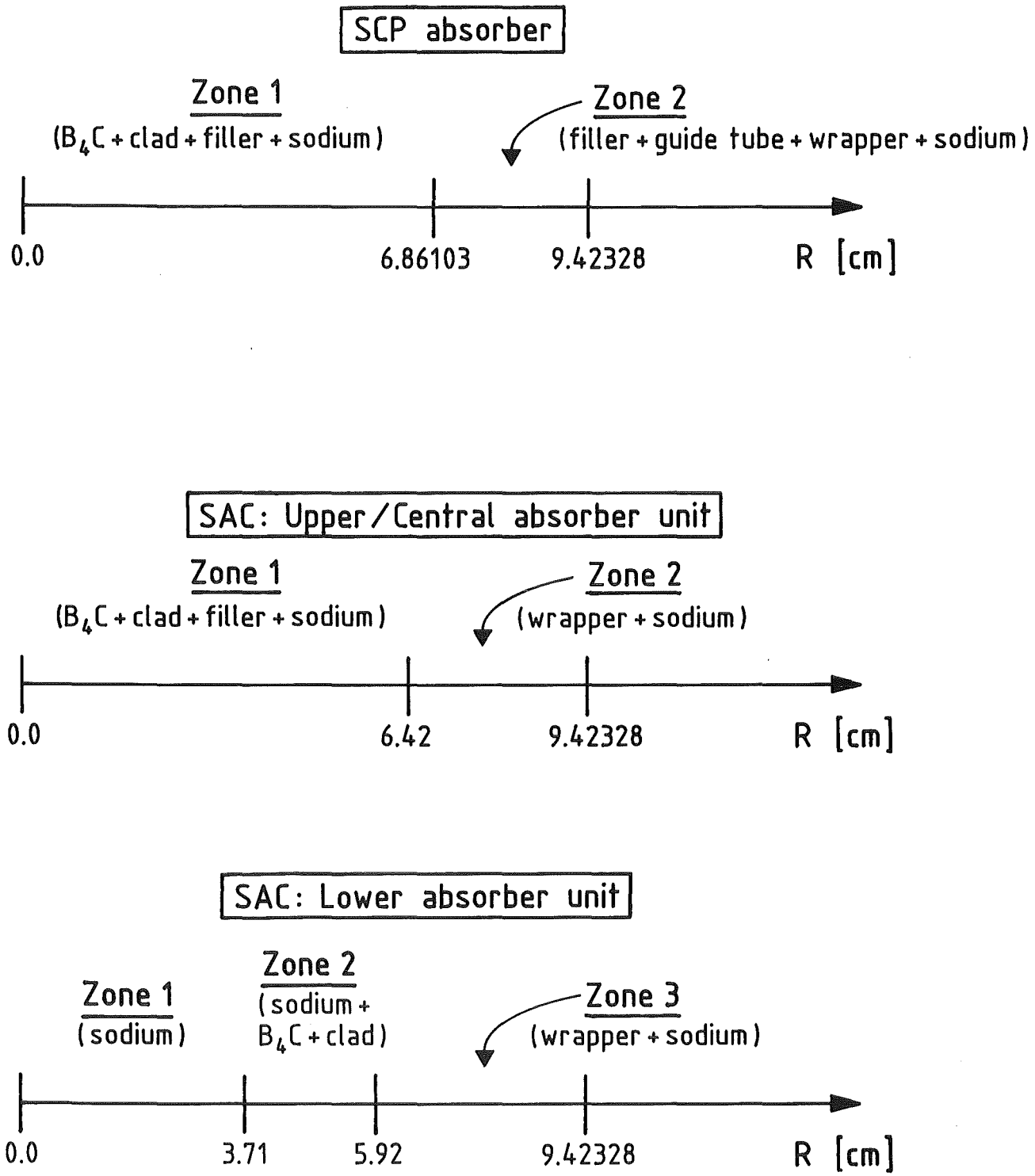

Figure 10 Cylindrical models of SPX-1 control rod absorbers as used in Interatom MONTE CARLO calculations (T = 180°C)

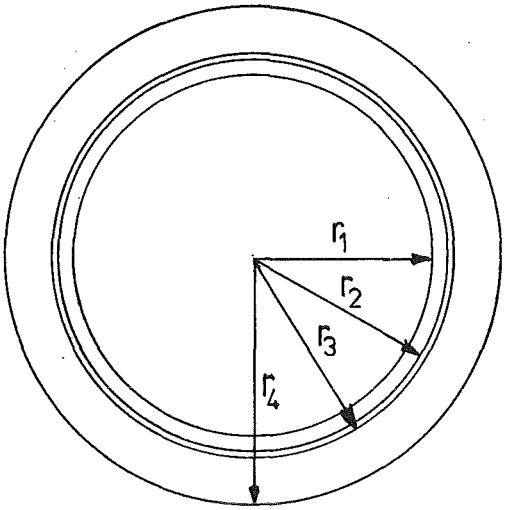

Heterogeneous control rod

Radii [cm] T=20°C	Number of meshes	Composition
r_1 = 6.66	19	Sodium 22.39% Steel 14.45% Void 12.59% B_4C 50.57%
r_2 = 7.25	2	Sodium 39.83% Steel 60.17%
r_3 = 7.45	1	Steel 100.00%
r_4 = 9.40	2	Sodium 73.97% Steel 26.03%

Homogeneous control rod

Radii [cm] T=20°C	Number of meshes	Composition
r = 9.40	24	Sodium 42.44% Steel 25.88% Void 6.32% B_4C 25.36%

Figure 11
Cylindricalized model of an SCP absorber as used in the AEA analysis (T = 20°C). From / 26 /.

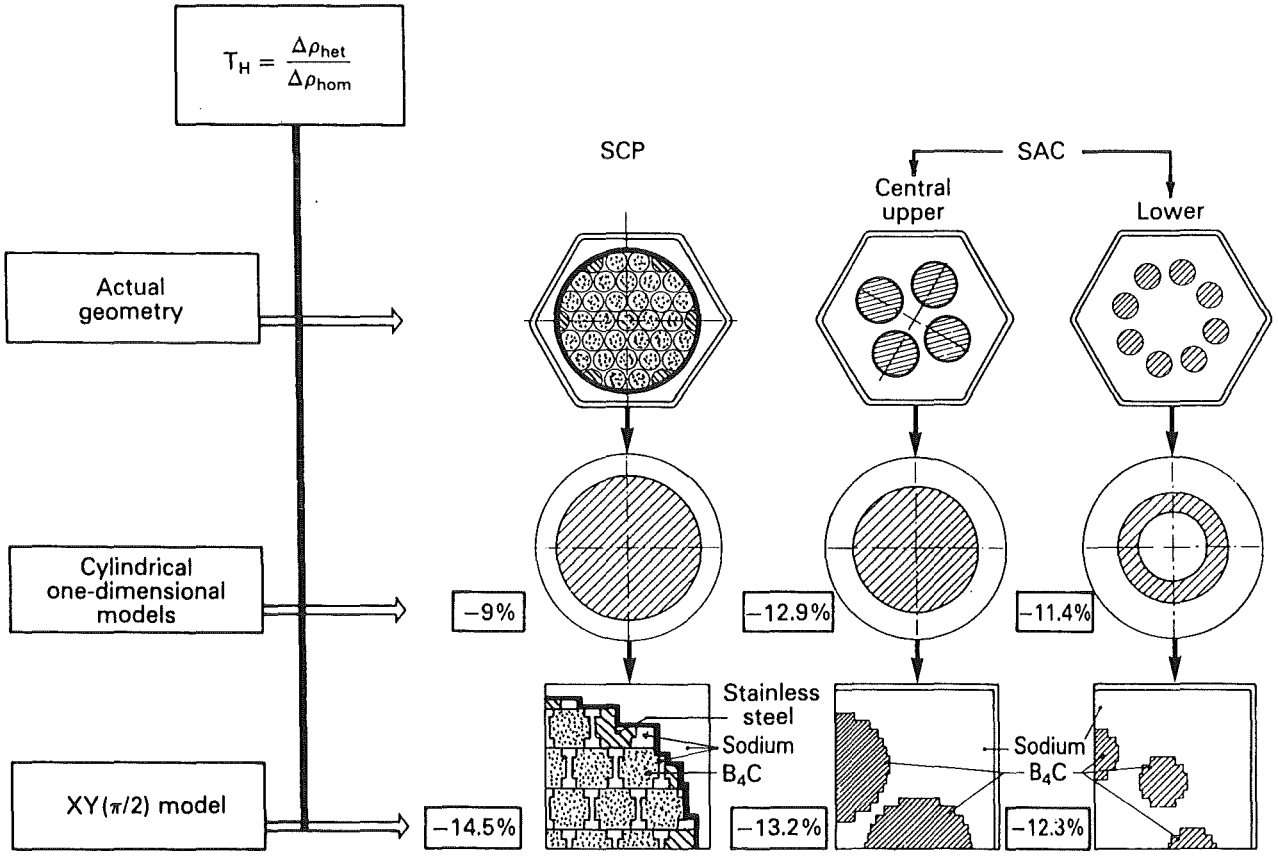

Figure 12
Cylindricalized and detailed XY-geometry models of SPX-1 control rod absorbers as used in the CEA analysis. T_H = Heterogeneity correction. From / 22 /.

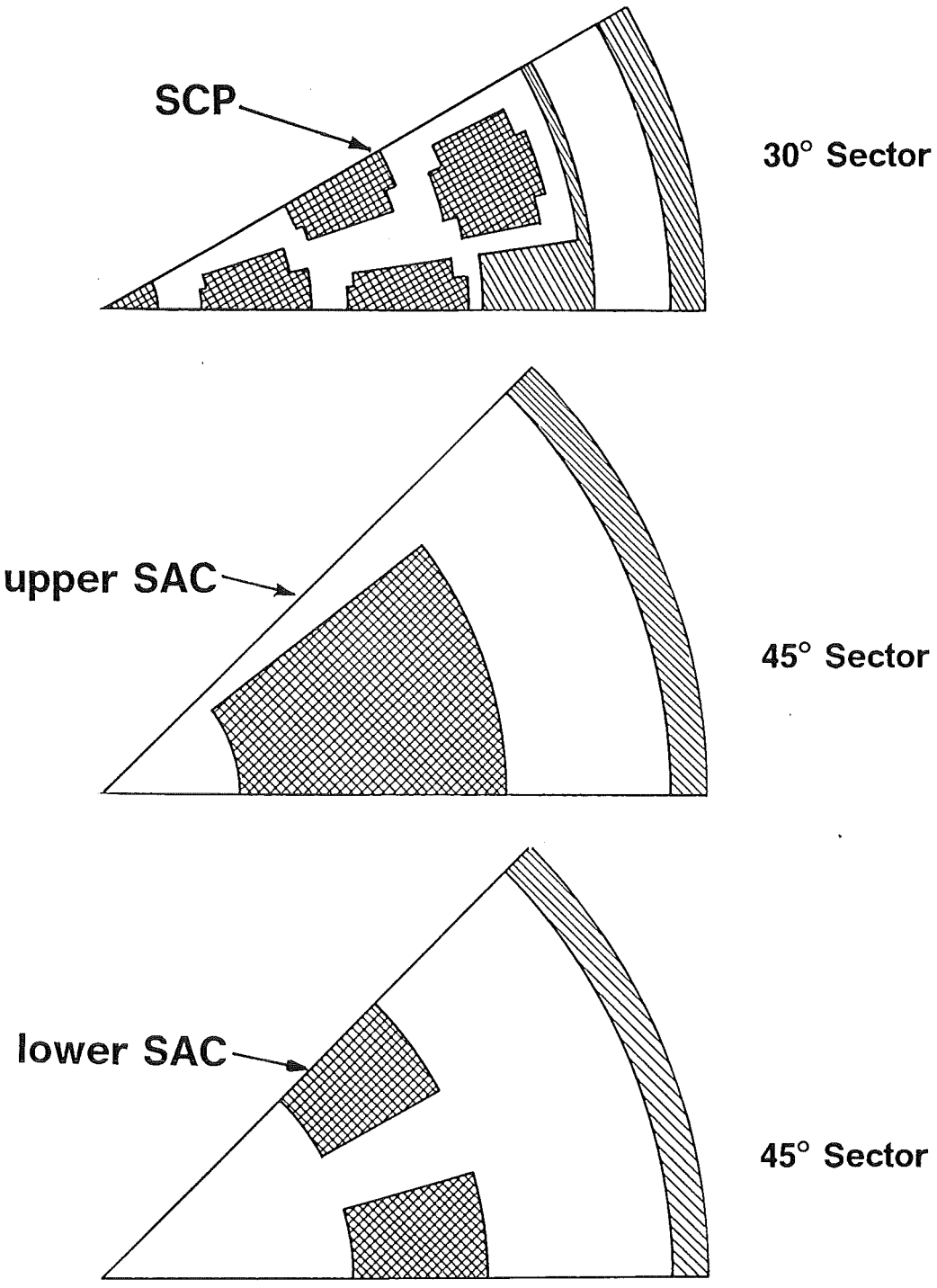

Figure 13
RΘ-models of SCP and SAC as used in the third BN/KfK analysis campaign. From / 15,31 /.

Lower SAC absorber

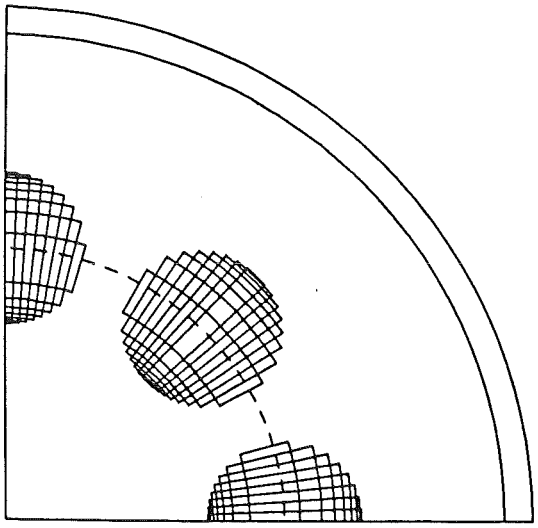

Upper SAC absorber

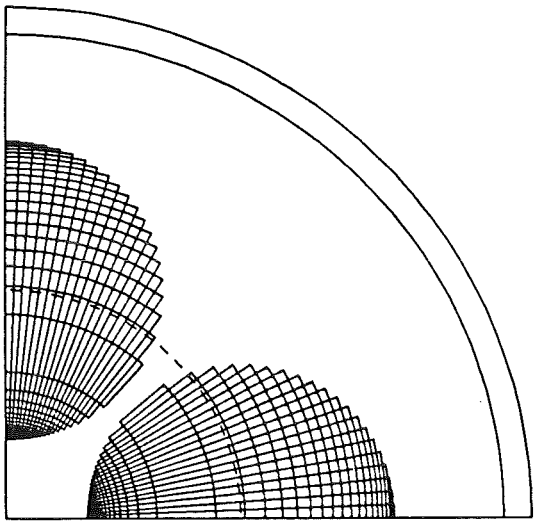

Figure 14
Refined RΘ-models of SAC absorbers. From / 31 /.